NANYANG TECHNOLOGICAL UNIVERSITY

Polymer Functionalized Nanostructures for Antibacterial Application

PU LU

School of Chemical and Biomedical Engineering

2017

Polymer Functionalized Nanostructures for Antibacterial Application

PU LU

School of Chemical and Biomedical Engineering

A thesis submitted to the Nanyang Technological University in fulfilment of the requirement for the degree of Doctor of Philosophy

2017

Acknowledgements

Firstly, I would like to deeply express my warm thanks to Assoc. Prof. Duan Hongwei for the opportunity to perform all my projects in his research group. During these years, he has helped me along the way, especially with project designing and academic writing skills. He has also brought me into the field of nanomaterials and polymers.

I would also like to extend my gratitude to Prof Mary B. Chan-Park for her patient guidance to help me think out solutions when facing experimental problems.

I really appreciate the guidance from Dr. Jibin Song, Dr. Yimin Sun, Dr. Jinbao Xu, Dr. Zheng Fang, Dr. Xiujuan Wang and Dr. Shucong Yu to help me in material preparation, material analysis and experimental problem discussions.

Additionally, I owe my genuine gratitude to all the other group members and friends with my experiments. They treat me like family members and always encourage me.

Specially, I would like to thank my family and boyfriend. Thanks for your love, support and encouragement.

Last but not least, thanks for the financial support by the Tier 3 project (MOE2013-T3-1-002) from Singapore Ministry of Education and thanks Nanyang Technological University for your comfortable and positive environment.

Table of Contents

List of Abbreviations

ATRP	Atom transfer radical polymerization
BHI	Brain heart infucion
CB	Conduction band
CDC	Centres for Disease Control and Prevention
CFU	Colony forming units
DMF	Dimethylformamide
DMSO	Dimethyl sulfoxide
DNA	Deoxyribonucleic acid
E. coli	*Escherichia coli*
E. faecalis	*Enterococcus faecalis*
FESEM	Field emission scanning electron microscopy
FTIR	Fourier-transform infrared spectroscopy
GO	Graphene oxide
GPC	Gel permeation chromatography
H	Field strength
HPLC	High performance liquid chromatography
LB	Luria Bertani broth
M	Magnetization

MIC	Minimum inhibitory concentration
M_n	Number-average molecular weight
MRSA	Methicillin-resistant *Staphylococcus aureus*
NADH	Nicotinamide adenine dinucleotide
NMR	Nuclear magnetic resonance
PBS	Phosphate-buffered saline
PDI	Polydispersity Index
PEG	Polyethylene glycol
QAS	Quaternary ammonium salts
Q-PVP	N-alkylated poly(4-vinylpyridine)
RNA	Ribonucleic acid
ROP	Ring opening polymerization
ROS	Reactive oxygen species
S. aureus	*Staphylococcus aureus*
SEM	Scanning electron microscopy
TEM	Transmission electron microscopy
TGA	Thermogravimetric analysis
THF	Tetrahydrofuran
VB	Valence band
XRD	X-ray powder diffraction

List of Figures

List of Tables

Summary

Polymer Functionalized Nanostructures for Antibacterial Application

Student: PU LU

Supervisor: Associate Professor Duan Hongwei

Research in this thesis is to take advantages of polymer-functionalized nanostructures for antibacterial applications. Due to dramatically enhanced surface area to volume ratio of nanomaterials, functionalized nanoparticles not only show superior antibacterial performance but also possess the ability to assemble into various structures. On one hand, nanomaterials serve as scaffolds for grafting abundant and distinct polymers to enlarge localized charge density of polymers, a critical factor in antibacterial material preparation, or to assemble into distinct structures for drug loading. On the other hand, intrinsic characteristics of nanomaterials may be employed into the killing system, such as hyperthermia effect and magnetic separation ability.

In the first project, polymer poly(4-vinylpyridine) grafted graphene oxide (GO) were synthesized through atom transfer radical polymerization (ATRP), which were subsequently quaternized with different alkyl chain lengths to improve water solubility. The composites displayed excellent antibacterial activity at low concentrations of 10 μg/ml. Their antibacterial effect varied with alkyl chain lengths with highest activity for alkyl chain length of four carbon. The polymer-grafted GO were further made into papers, which demonstrated

similar antibacterial effect. Polymer brushes quaternized with butyl chains demonstrated the highest toxicity up to 99.9% for both *E. coli* and *S. aureus* in paper form. All materials showed better activities against *S. aureus* (Gram-positive) than *E. coli* (Gram-negative). SEM observations confirm that the materials wrapped and penetrated through the cell membrane. Zeta potential measurement also proved the importance of higher charge density of materials for better antibacterial applications.

In the second project, biodegradable cationic polymers were synthesized by ring opening polymerization and decorated superparamagnetic nanoparticles $MnFe_2O_4$ through ligand exchange reaction. The material displayed synergistic antibacterial effect due to membrane destruction by cationic polymers and hyperthermia effect by the magnetic core. It exhibited antibacterial activity that was superior to polymers alone at about 1000 times due to higher charge density for polymers on nanoparticle surfaces. In alternating magnetic field, the superparamagnetic core leads to a hyperthermia effect to further improve the antimicrobial activity.

The third project focuses on developing a magnetic vesicle delivery system that is able to carry antibiotic payloads and release them in response to specific types of pathogens. More specifically, magnetic nanoparticles are grafted with mixed polymer brushes of hydrophilic PEG and hydrophobic PCL. The resultant amphiphilic nanoparticles self-assemble into vesicles with PCL forming the hydrophobic shell protected by PEG grafts. Thanks to the lipase-specific degradation of PCL, the magnetic vesicles can de destructed by lipase secreted by specific bacteria such as *S. aureus*. As a result, the antibiotic-loaded vesicles showed selective antibiotic release against lipase-secreting bacteria. In contrast,

this response is absent in low lipase-secreting bacteria. Moreover, antibody-conjugated vesicles could rapidly capture targeted specific bacteria and be collected by external magnetic field, which allowed for further reducing the MIC of the antibiotics.

Chapter 1. Introduction

1.1 Backgrounds

1.1.1 World of bacteria

Bacteria are microscopic and single cell organisms that exist everywhere and affect environment around us. Some strains are beneficial, even essential. For example, bacteria in the intestine of animals help digest nutrients, produce vitamins and generate growth factors.[1,2] Others may help with our immunity system, protecting ourselves from other harmful pathogens.[3] They also act as a source in medicine of antibiotics and vaccines.[4,5] However, some bacteria may cause damages. They accelerate spoilage and decomposition of foods, textiles and dwelling.[6-8] The harmful strains may also proliferate on or in our body, causing bacteria related infections, such as pneumonia, meningitis and food poisoning.[9-11]

Infections may be transmitted to us by contact, through a vehicle and from the animal and insects as illustrated in Figure 1.1. Diseases can be spread by direct contact between person-to-person, indirect contact between person and the utilities used by another person and air transmission such as coughing.[12] The food we eat, the water we drink and the cosmetics we use are also sources of bacterial infection.[13] Additionally, insects and animals are able to bring their diseases to us as well.[14,15]

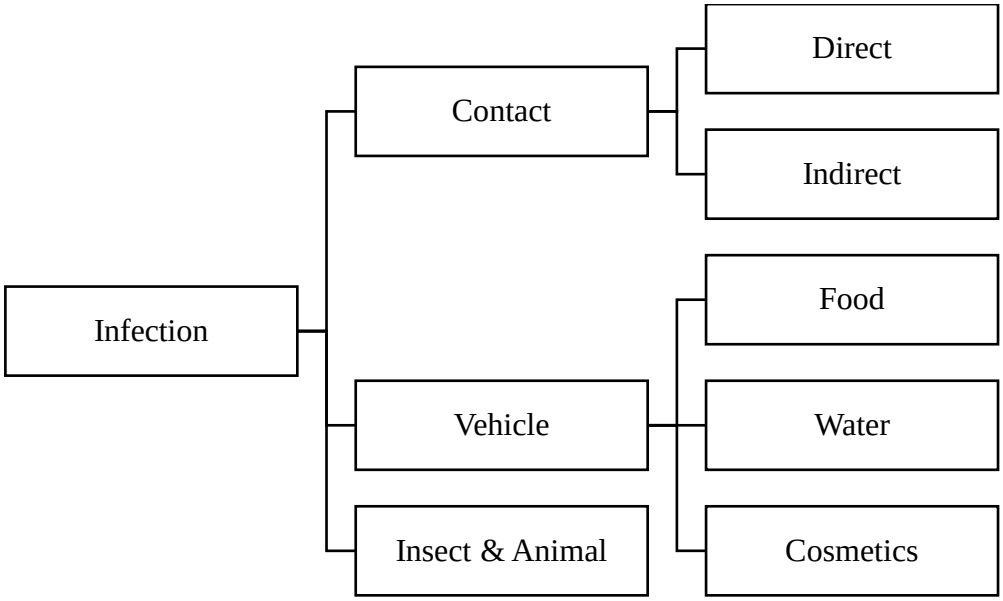

Figure 1.1 Sources of infection.[16]

In developing countries, where water and food are contaminated, waste are deposed unsanitarily, personal hygiene and sanitary conditions are lacked behind, and medical assistance are not accessible, infections become the first cause of mortality there in the occurrence of cholera, dysentery, malaria, etc.[17] On the contrary, morbidity and mortality by antibiotic-resistant pathogens increase in developed countries. According to Centres for Disease Control and Prevention (CDC) of USA, there are at least 2, 049,442 antibiotic resistant infections in 2013, with around 23000 direct deaths.[18] The antibiotic-resistant pathogens migrate easily to form new paths for microorganism to run into human hosts.[19,20] *S. aureus* is a typical representative of bacteria that has evolved from penicillin-resistant phenotypes into methicillin-resistant strain (MRSA) and been the main cause for surgical site infections.[21] Hence, it is of particular importance to develop new generation of antimicrobial agents with improved safety and efficiency to prevent and treat infections from all aspects.

1.1.2 Gram-positive and Gram-negative Bacteria

Bacteria are classified by Hans Christan Gram into two types based on their interaction with crystal violet dye: Gram-positive bacteria and Gram-negative bacteria.[22] Gram-positive bacteria retain violet dye after staining due to thick peptidoglycan layer while Gram-negative bacteria do not retain dye because of thinner peptidoglycan layer. The comparison of the two types of bacteria are summarized in Table 1.1.

Table 1.1 Comparison between Gram-negative and Gram-positive bacteria.[23]

Bacteria Type	Gram-negative	Gram-positive
Peptidoglycan layer	Single layer (1–7nm)	Multiple layers (20–80 nm)
Outer membrane	Present	Absent
Resistance to physical disruption	High	Low
Resistance to antibiotics	High	Low
Teichoic acid	Absent	Present

The main differences between Gram-negative bacteria and Gram-positive bacteria lie in their differences in outer membrane (Figure 1.2).[24] The Gram positive bacterial cell wall is composed of thick peptidoglycan layer between 20 and 40 layers thick, with abundant teichoic acid and lipoteichoic acids. These

acids are negatively charged due to the presence of phosphate in their structure. On the other hand, for Gram-negative bacteria, the peptidoglycan layer is thinner with only one or two layers. However, they possess an additional outer membrane which is absent in Gram-positive bacteria, contributing to higher resistance to antibacterial materials, for example, resistance to physical disruption and antibiotics. Their outer membrane is composed of phospholipids and lipopolysaccharides, which contribute to a strong negative charge to surface of Gram negative bacterial cells. Hence, both Gram-negative and Gram-positive bacteria display net negative charges.

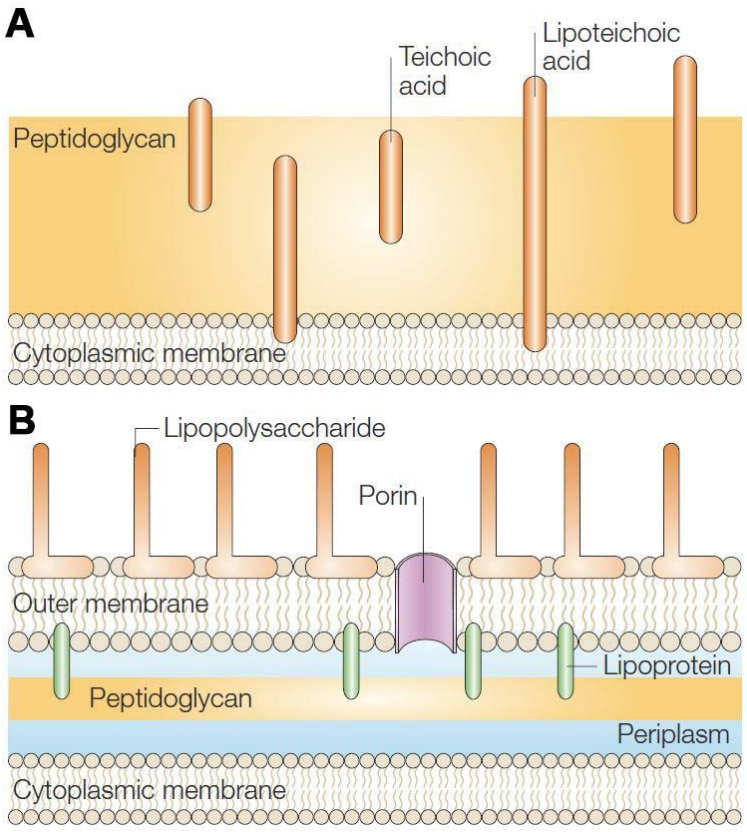

Figure 1.2 (A) Gram-positive and (B) Gram-negative cell walls.[24] Copyright 2005 Nature Publishing Group.

1.1.3 Antimicrobial agent-physical and chemical agents

Antimicrobial agents are classified into different categories in several ways. According to the bacterial species that affected, antibacterial materials are classified into broad, intermediate and narrow-spectrum antibacterial, with broad spectrum active for both Gram-positive and Gram-negative bacteria and narrow spectrum only against particular species. Based on the effects of bacteria affected, materials are also classified into bactericidal (kill bacteria) or bacteriostatic (inhibit or delay bacteria growth) drugs. Based on the intrinsic properties of materials, antimicrobial agent are classified into physical agents, chemical agents and antimicrobial drugs as shown in Figure 1.3.[25]

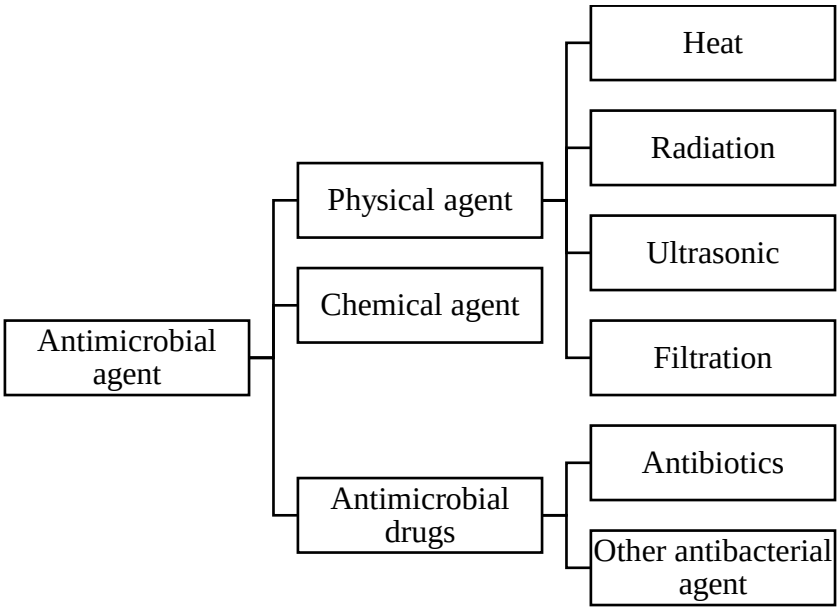

Figure 1.3 Classification of antimicrobial agent.[25]

Typically, sterilization utilizes physical agent such as heat, radiation, pressure and filtration to ensure the materials, including surfaces, medium, devices, etc., free of all living organisms.[26] Disinfection, on the other hand, uses chemical agents to reduce the level of organisms outside or on the surface of the human body to prevent the occurrence of infection.[27] Antimicrobial drugs use chemical agents for administration into human body to treat infections.

Among the physical agents, heating, as a simple, effective, cheap and rapid method, kills bacteria by elevating the temperature and are applicable to sterilize various objects such as flasks, oils and milk. Bacteria can be inactivated by dry heat or moisture heat.[27] Under dry condition, cells lose enzyme activities and result in cell death due to oxidation process. Under moisture condition, cell protein coagulate, DNA strands break and cell membrane integrity will be lost by heating. The killing efficiency depends on the heating temperature, time and bacteria types. On the other hand, radiation, in the range of ultraviolet (ultraviolet radiation) and cathode to X-ray (ionizing radiation), helps to sterilize closed environment, pharmaceuticals, and medical supplies by damage or destroy DNA.[28] Ultrasound disrupts cells based on its high frequency sound waves.[29] The waves induce the formation of microscopic bubbles in their applied fluid, which collapse and generate shock waves. These shock waves are strong enough to disintegrate bacteria. Moreover, filtration method separates microorganism from the filtrates by appropriate filter with specialized pore size. The method is typically used in dealing with vaccines, culture mediums, enzymes, etc.[30]

Compared to sterilization, disinfection destroy microbes based on active chemical agents.[31] They are extensively used in hospital, food, healthcare devices

and general consumer markets. Disinfectants are commonly active against wide spectrum of organism by damaging cell envelope and cytoplasmic membrane, crosslinking of macromolecules, interfering DNA, oxidizing cellular compounds, etc.[32] A short summary of representative antiseptics and disinfectants with their mechanisms are shown in Table 1.2.[27,33]

Table 1.2 Mechanisms of various antiseptics and disinfectants.

Chemical agent	**Target**
Glutaraldehyde	Cross-linking of proteins, RNA, DNA.
Chlorhexidine	Destroy membrane integrity; Intracellular coagulation.
Alcohol	Membrane damage; Protein denaturation.
Diamines	Amino acid leakage.
Anilides	Destroy semipermeable property of cytoplasmic membrane.
Halogen-releasing agent	Oxidize thiol groups; Inhibit DNA synthesis.
Peroxygens	Generate hydroxyl radicals and oxidize thiol groups; DNA strand breakage.
Phenols	Intracellular compounds leakage.

1.1.4 Antimicrobial agent-antibiotics

Disinfectants, which inhibit microbial growth by destroying multiple components of organisms at the same time, are too toxic to be applied for human uses. Chemotherapy, thus, is introduced to treat infections inside body by introducing antimicrobial drugs with lower toxicity. Antibiotics, low molecular weight substances produced by microorganisms that fight against another microorganism, constitute a major subcategory of chemotherapy agents.[34] More than 2000 years ago, Greece, China, Egypt and Serbia used moldy bread to dress infections, which nowadays were believed to generate raw antibiotics. In 1928, Fleming discovered the miracle antibiotic penicillin.[35] However, the antibiotic was not realized for application until 9 years later when Florey and Chain achieved large scale production of this first antibiotic. In 1942, the introduction of penicillin was largely produced by industry to save life. In 1945, Florey and Chain shared the Nobel Prize for Physiology and Medicine. The success in penicillin opens the door to the search of various other antibiotics. Figure 1.4 demonstrates the history of discovery and introduction of key antibiotics afterwards.[36,37]

The antibiotics act in different modes against bacteria: 1) by affecting their proteins through denaturizing or alternating their protein structure. This denaturation can be either permanent or temporary. Permanent denaturation leads to the mechanism called bactericidal while temporary refers to bacteriostatic, which means bacteria can restore their state and structure afterwards; 2) by affecting their cell membrane proteins or membrane lipids. Concerning proteins, the mode of action consists of denaturalisation whereas lipids are dissolved, for

instance by a surfactant, and their cell membrane turns out to be damaged; 3) by affecting the cell-wall formation through blocking its synthesis; 4) by preventing replication, transcription and translation of the nucleic acid structure; and 5) by disturbing the metabolism.[38,39]

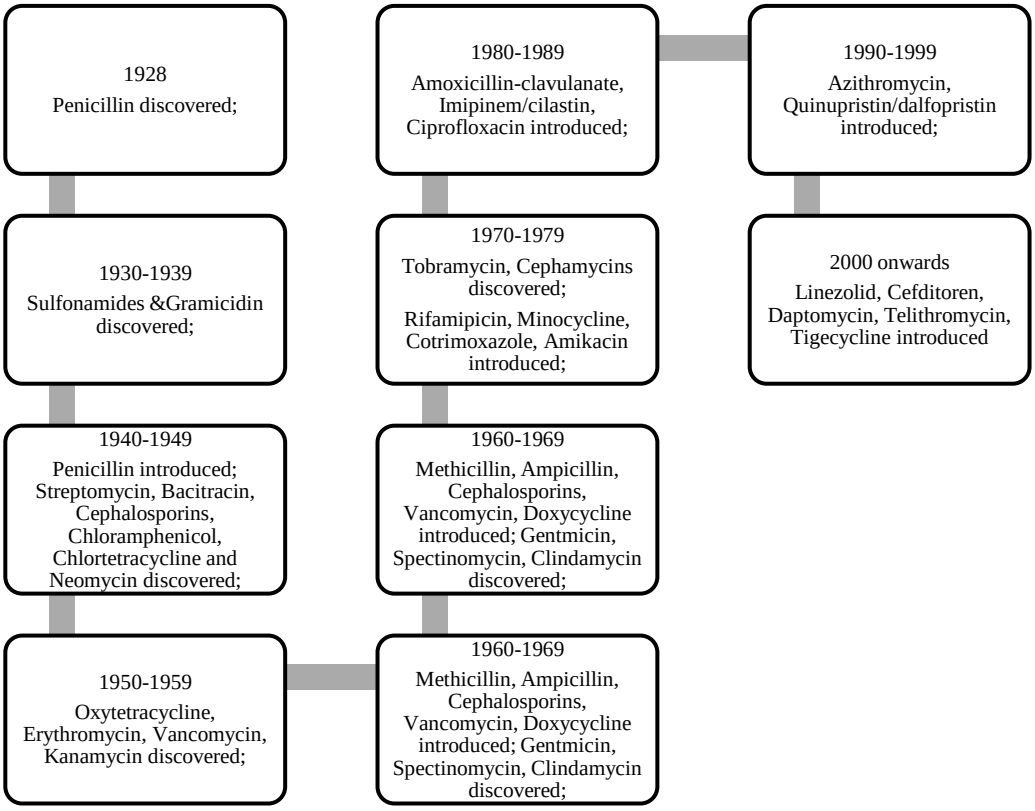

Figure 1.4 History of antibiotics.[36,37]

The application of antibiotics has been spectacularly successful in the twentieth century.[40] They help to extend human life expectancy tremendously, especially in developed countries. Upon introduction of sulphadiazine, more than half of the deaths from *Streptococcus pyrogenes* related childbed fever were reduced in England and Wales. In the USA, mortality arising from infectious disease decreased from 797 to 36 per 100,000 from 1900 to 1980 due to

development of antibiotics against various diseases such as tuberculosis, pneumonia, smallpox, etc.[41] The life span in USA in 1997 reached 76 years.[19] At that time, the society felt optimum in treating, controlling and preventing infectious diseases and thought it was time to stop the effort to deal with infectious disease. During 1980s, pharmaceutical companies even believed that it was time to reduce the development of new antibiotics as it was enough for application.[42,43] However, the story went away from expectation when a series of new, resurgent and multidrug resistant infections broke out, such as HIV, bovine spongiform encephalopathy and Ebola virus.[44] The emerging infections result from increase in host susceptibility, new disease and increase in disease transmission, which are the consequences of social and technological variations such as variations in demographics and behaviour, developments in technology and industry, breakdown of public health measures, microbial adaptation and mutation, international travel and commerce and environmental changes. For example, the fast-food hamburger brought about *E. coli O157:H7*, which causes bloody diarrhoea and haemolytic uremic syndrome.

Bacteria are intrinsically resistant to certain antibiotics and can mutant to acquire resistance.[45] Bacterial species are made up of less sensitive variants that are more resistant to antibiotics and more sensitive variants that are easily killed by the antibiotics.[46] The alive bacteria may further develop cellular modifications to enhance their viability. Hence, the probability of bacteria resistance generally increases with the usage of antibiotics. Some micrograms resist to only one drug, but more resist to several drugs, which are called “multidrug resistance”. There are various mechanisms that bacteria has developed to fight against antibiotics:

generation of inactivating enzymes so that antibiotics cannot have effect on the enzyme; receptor modification to prevent binding of antibiotics; changes in cell membrane by reorganizing structure channels or transport mechanisms; enhancement of efflux to pump antibiotics out of the cells; overexpression of the target molecules so that the reduction of the molecules would not be a problem; and alteration of the target metabolism so that cell function would not be affected.[47]

Besides studying the mechanisms for emerging infections, there are several aspects that scientists can contribute to control or prevent the outbreak of infections. Firstly, develop, modify or search new antimicrobial agents, which bacteria have not developed resistance against or are difficult to develop resistance against, to treat diseases. Secondly, develop vaccines or immunomodulators that can reduce host susceptibility. Thirdly, develop new technologies for surveillance to monitor and control pathogens. Last but not least, explore appropriate technologies for efficient and safe drug usage to reduce chances of resistance generation.

1.1.5 Evaluation methods of antibacterial effect

Standard evaluation methods have been developed so that quantitative data are able to screen antibacterial activities between different materials and laboratories. The experimental methods include in this thesis are MIC and plate count methods.

1.1.5.1 MIC test

The MIC test is used to quantify a specific antimicrobial agent by determining the minimum concentration needed to prevent the growth of bacteria. It is widely used in industry and lab to test MIC of various antibiotics and novel agents.

There are basically two ways to perform MIC: agar dilution and broth dilution.[48] For agar dilution, the material is initially mixed with dry agar power, which is subsequently wetted by water and poured onto agar plates. Different concentrations of material is added to the mixture. Bacterial colonies in medium are then spread onto the plates. After incubation overnight. The plate with no bacterial growth indicates the MIC of the material. For broth dilution, on the other hand, bacterial colonies is first mixed with different concentrations of material. The turbidity of the media before and after incubation is observed to determine whether bacterial grow since the growth of bacteria will increase the turbidity of the media. Broth dilution can be classified as micro dilution (media < 500 μL) or macro dilution (>2 ml). Typically, the test result is in mg/ml, mg/l, or μg/ml. However, the limitation of MIC test is that it does not distinguish between biocidal or biostatic materials. For example, the bacterial may regrowth after removal of the material.

1.1.5.2 Plate count method

Plate count method, also named as viable count method, determines the density of living cells in a sample. Typically, microbes are incubated in liquid and diluted to different portions (serial dilutions), which is spread onto agar plates for counting numbers.[49]

As shown in Figure 1.5, the serial dilution is performed by transfer known concentration of samples down a line of dilution blanks, for example, buffer. Typically, the dilution is at diluted by 1/10 or 1/100 per step. Each dilution is then spread onto agar plates to generate countable plate, which contains colonies between 30 and 300. Because if the number is below 30, it is statistically unreliable while if greater than 300, it is too crowed to be counted. Based on the colony forming units (CFU: the number of colonies on the plate), sample volume and dilution degree, the cell density can thus be calculated. [50] Plate count method is generally accurate and count only viable cells. It is accepted as the best available method to count living cells. However, sampling error generally occurs during the technique because of uneven distribution of sample on the plate surface, which is unavoidable due to hand technique.

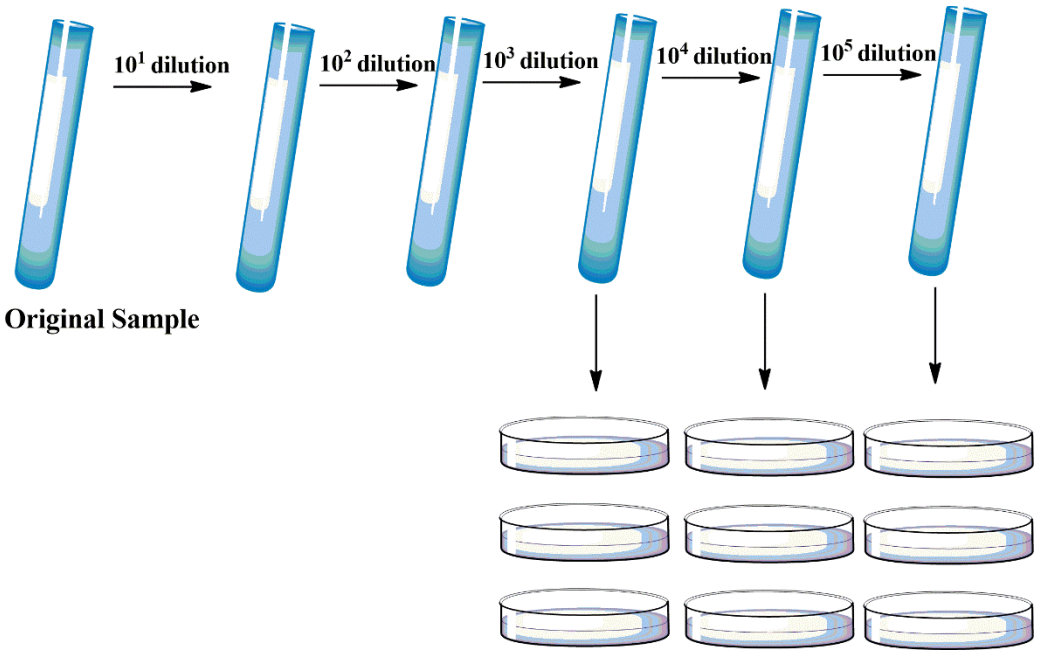

Figure 1.5 Scheme of serial dilution in plate count method.

1.2 Objectives

Hybrid materials combine unique properties of each component and potentially take advantages of each part for superior functionalities. The overall objective in this thesis is to develop polymer functionalized nanostructures for bacteria control.

For cationic polymers, charge density acts as a critical element that determines antibacterial efficiency. Considering graphene oxide, with high surface area and abundant functional groups, could be a good substrate and facile to localize polymers on its surface, the first objective is thus to construct and investigate the activity of quaternary polymers consisting of N-alkylated poly (4-vinylpyridine) on the surface of graphene oxide by atom transfer radical polymerization. The graphene oxide based materials are applicable for various surfaces by solidifying the material as paper format or coating while other nanostructures are difficult to apply. Since graphene oxide and cationic polymers are reported to possess antibacterial properties, we hypothesize that the synthesized composites display better solubility and higher antibacterial activity.

Biodegradable materials offer unique advantages over other materials such as environmental friendly and fewer post application requirements.[51] Since quaternized poly(4-vinylpyridine) is not biodegradable, later we attempt to develop hybrid antimicrobial nanoparticles with cationic biodegradable polycarbonate polymers grafted on superparamagnetic $MnFe_2O_4$ nanoparticles with the high surface to volume ratio. Superparamagnetic nanoparticles have special magnetic heating effects that other nanoparticles lack. Investigation

should be made towards the synergistic effect of membrane destruction by the cationic polymer shell and hyperthermia heating by the nanoparticles. Here, we hypothesize that grafting polymers onto nanoparticles enhance materials' antibacterial activity and nanoparticles may be utilized for magnetic hyperthermia effect by localized heating.

Besides developing new antimicrobial agents, improved antibiotic delivery systems not only enhance properties of current drugs but also those that will be developed in future. Thus, we attempt to develop vesicles made from biodegradable polymeric nanoparticles to achieve on demand inhibition of bacteria growth. The vesicles, composed with superparamagnetic nanoparticles with high magnetic separation efficiency, should be explored to improve therapeutic efficiency of antibiotics. We hypothesize that the vesicle system acts as good carrier for antibiotics to achieve selective delivery of drugs. Additionally, the system, with special magnetic potentials, can be used to enrich the system to achieve higher antibacterial activity.

Chapter 2. Literature Review

2.1 Nanomaterials

Nanomaterials refer to tiny materials with at least one dimension in the range of 1-100 nm.[52] Among the new antimicrobial agent, novel nanosized materials in an emerging technological field have been developed for microbial control applications.[53,54] Materials of nanosize differ from bulk materials in specific physicochemical and biological properties.[55] With high surface area to volume ratio, they are typically more reactive and facile to modify with more polymers on their surfaces.[56,57] Small sized materials are also well tolerated by human beings, promoting it for real applications.[58] Nanoparticles depend on different antibacterial mechanisms from that of antibiotics, potentially avoiding the problem of antibiotic resistance development.[59] The limitations of such inorganic antimicrobial materials lie on the fact that the accumulation of metals that damage the environment.[60] Besides, they may form insoluble minerals and become ineffective. The representative nanomaterials that have been synthesized for antibacterial research include but not limited to silver nanoparticles, zinc oxide nanoparticles, magnetic nanoparticles, graphene related materials.

2.1.1 Silver nanoparticles

Silver nanoparticles, typically at the size smaller than 100 nm with around 10000 to 15000 atoms in each particle, display unique advantages as antibacterial agents.[61,62] They are highly effective against wide spectrum of microbes at full inhibition doses as low as a few mg/ml.[63] At the effective doses, they possess

minimal toxicity to human cells. Additionally, their crude material is abundant and relatively cheap.[64]

The action modes of silver nanoparticles have not been fully understood. Various mechanisms have been proposed to explain the result (Figure 2.1).[65] Since silver nanoparticles have been observed to accumulate and form aggregates at the bacteria membrane, some authors believe the mechanism relied on destroying membrane integrity.[66] Meanwhile, a high level of reactive oxygen species (ROS) has been detected in cells after treatment with Ag NPs.[67] Some researchers treat ROS as the main mode of action, which induces a high oxidative stress and thus cell death. The ROS are believed to be naturally produced by oxygenic respiration. The more dominate opinion depends on the release of Ag^+ from silver nanoparticles either by oxidative dissolution of Ag nanoparticles or from chemisorbed Ag^+ ions on Ag NP surfaces. Silver ions are proved to interact with thiol groups, phosphates and amines in DNA, proteins and enzymes, disrupting cell biological functions.[68] They also bridge the linkages between thiols to form irreversible aggregations inside cell. Instead of targeting at only one group like antibiotics, the ions will absorb whichever part they have the affinity. It is proposed that the combined effects lead to cell death, which may be the reason for silver nanoparticles against wide spectrum of micro-organisms.

The bactericidal activity of silver nanoparticles varies with the particle size, shape and concentration. Smaller sizes nanoparticles have higher surface area to volume ratio, contributing to a higher degree of interaction than particles of larger size. It was reported that the silver nanoparticles with a size of 25 nm demonstrated best antibacterial activity.[69] Besides size, bactericidal properties is

also shape ratio dependent.[66] By comparing silver nanoparticles in the shape of spherical, rod and triangular against *E. coli*, nanoparticles with triangular shape showed highest activity.[70] Similar to other materials, the concentration or dosage of silver nanoparticles is the critical parameter for application. Higher concentration favors the higher activity.[66]

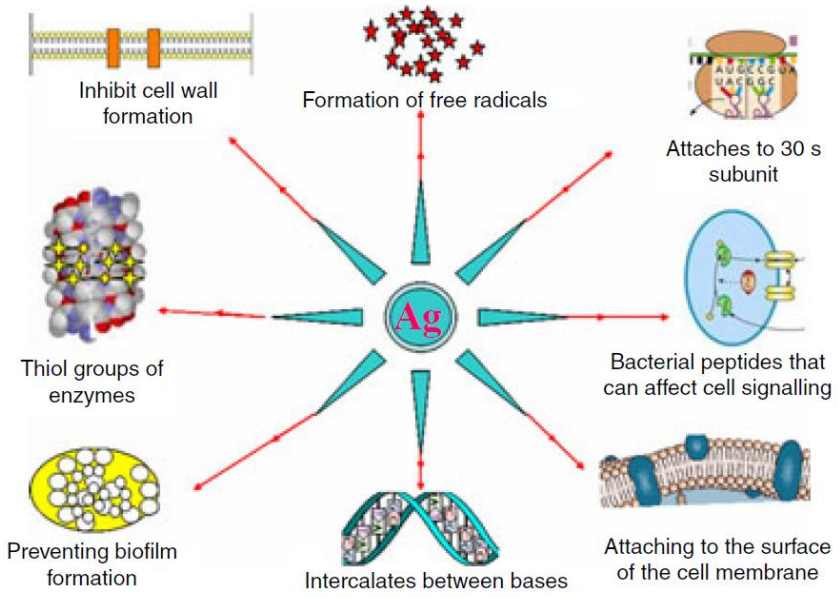

Figure 2.1 Mode of action of silver nanoparticles.[71] Copyright 2012 John Wiley & Sons, Inc.

Besides Gram-negative bacteria, such as *Escherichia, Pseudomonas and Vibrio*, and Gram-positive bacteria, such as *Staphylococcus, Clostridium and Enterococcus*, silver nanoparticles also significantly inhibit the growth of antibiotic resistant bacteria such as methicillin- and vancomycin-resistant *Staphylococcus aureus (*MRSA and VRSA*)* and *Enterococcus faecium.*[72] The effective concentration for 100 nm silver nanoparticles against both MRSA and *S. aureus* was evaluated. Similar result was obtained for the minimum inhibitory

concentration for both MRSA and *S. aureus* and 1.35 mg/ml was enough to inhibit both cells.[73]

Silver, in the form of pure silver nanoparticles or soluble silver salts, have been introduced into inorganic substrates such as glasses, titania particles, silica particles, ceramics, inorganic fibres and medical alloys to make them commercially available. However, the application of silver nanoparticles has an ecological impact as they can be released upon washing, which may interfere with other organisms in the environment.

2.1.2 Zinc oxide nanoparticles

ZnO nanoparticles, with high catalytic and photochemical activities, are facile for diverse applications such as energy harvesting, sensors and electronic devices.[74] Besides, they display better biocompatibility compared to other metal oxides, high solubility in alkaline condition and polar surface properties terminated by Zn-O, suitable to be used in biomedical and antiviral areas.[75]

ZnO nanoparticles are active in UV light absorption and generate photocatalytic responses.[76,77] Exposed to UV, the conductivity of nanoparticles elevates, which significantly promotes the interaction of nanoparticles with bacteria and enhances antibacterial activity than in the case without UV exposure.[78] The nanoparticles in suspension produce ROS including superoxide ions (O^{2-}) and hydrogen peroxide (H_2O_2) under UV light, inducing phototoxic effect.[79] These active species are able to kill or inhibit bacteria after penetrating through cell membrane. The generation of ROS is based on intrinsic semiconductor properties of ZnO, which includes the conduction band (CB) and

valence band (VB).[80-82] As long as the incident photos have energy higher than 3.3 eV, the electrons in the CB are promoted to VB, leaving a positive hole in the VB. The positive hole acts as an oxidant to generate hydroxyl radicals, inducing other free radicals generation as shown in the following equations.[83]

$$ZnO + hv \rightarrow e^- + h^+ \qquad \text{Equation 2.1}$$

$$h^+ + H_2O \rightarrow {}^{\cdot}OH + H^+ \qquad \text{Equation 2.2}$$

$$e^- + O_2 \rightarrow {}^{\cdot}O_2^- \qquad \text{Equation 2.3}$$

$$^{\cdot}O_2^- + H^+ \rightarrow HO_2^{\cdot} \qquad \text{Equation 2.4}$$

$$HO_2^{\cdot} + H^+ + e^- \rightarrow H_2O_2 \qquad \text{Equation 2.5}$$

Among diverse antibacterial mechanisms proposed, numerous believed that the ability to generate ROS by ZnO nanoparticles is the main cause for nanotoxicity against bacteria as ROS leads to autoxidation of NADH dehydrogenase II of cells' respiratory system.[84] Similar to silver nanoparticles, others believe that ZnO nanoparticles also release Zn^{2+}, which inhibit active transport process in cells, affect amino acid metabolism and disrupt enzyme system.[85-89] Further suggestions proposed that ZnO nanoparticles are internalized into the cell and alter membrane permeability, resulting in release of intracellular contents.[90]

2.1.3 Magnetic nanoparticles

Magnetic nanoparticles, such as Fe_3O_4 and related spinels with Co, Ni or Mn, offer distinct possibilities in microbial control.[91] Firstly, they are facile to be modified with distinct targeting agents to interact with different bacteria. Secondly, they respond to external magnetic fields following Coulomb's law. The permeability of magnetic fields offer the possibility to act at a distance. The nanoparticles can thus transport drugs to targeted areas within the body. Thirdly, if exposed to alternating magnetic field, the nanoparticles are able to generate energy and heat up as hyperthermia agents.[92]

The applications of nanoparticles depend on the principle of magnetism, which depends on atomic structure and temperature of materials. If a material is exposed to a magnetic field with strength H, the magnetization M is related to H by introducing the volumetric magnetic susceptibility χ:

$$M = \chi H \qquad \text{Equation 2.6}[93]$$

Where χ is dimensionless and M and H are in the units of A/m. For majority of materials, minimum magnetism is present with the application of a magnetic field. Among them, paramagnets are classified for $\chi = 10^{-6}$ to 10^{-1} while diamagnets are for $\chi = -10^{-6}$ to -10^{-3}.[94] On the other hand, some materials have ordered magnetic states with large χ values such as ferromagnet, ferrimagnet and antiferromagnet. For these ordered materials, M does not have a linear shape with H but gives a M-H curve with sigmoidal shape and M reaches saturation value at large H. More specifically, ferromagnetic and ferrimagnet nanoparticles show hysteresis loop. Open hysteresis loop is the result of pinning of magnetic dolman

walls and intrinsic magnetic anisotropy of crystalline lattice. The shape of M-H curve is related to particle size. Larger particles at the size of micron, with multi-domain ground state, gives narrower loops while for smaller particles in single-domain ground state, it takes higher field energy to move domain walls and demonstrate broader loops. When particle size get closer to around tens of nanometres scale or even less, the magnetic moment can be treated as a whole one with each atomic moments maintain the same ordered state, resulting in the single sigmoidal M-H curve without loop as shown.

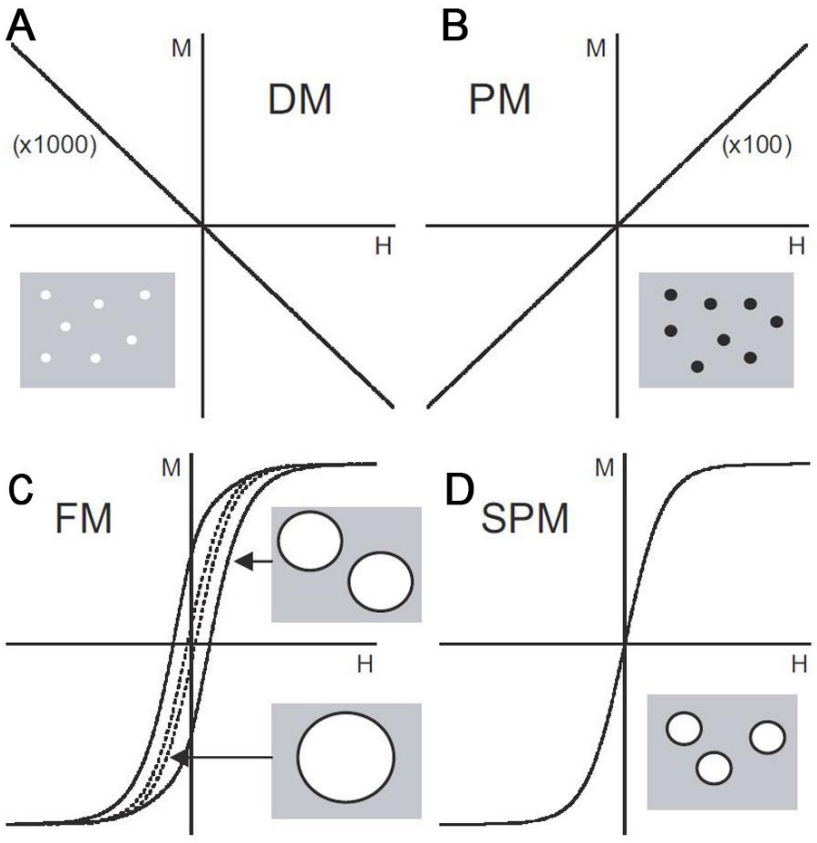

Figure 2.2 (A) M-H curves for diamagnetic material. (B) M-H curves for paramagnetic material. (C) M-H curves for ferromagnetic material. (D) M-H curves for superparamagnetic material.[93] Copyright 2003 IOP Publishing.

Magnetic nanoparticles are able to assist in separating of specific entities from the others by a two-step process: (1) the targeting agent coated nanoparticles recognise or label desired entities; (2) separating these entities by applying magnetic separation field in fluid. With high surface to volume ratio and easy ability to enter cells, these nanoparticles ensure high performance in separation. Vancomycin attached FePt nanoparticles were reported to effectively capture Gram-positive strains *S. aureus* of 8 CFU/ml, *S. epidermidis* of 10 CFU/ml, and a coagulase negative *staphylococci* of 4 CFU/ml via recognition of terminal peptide D-Ala-D-Ala on Gram-positive cell wall.[95]

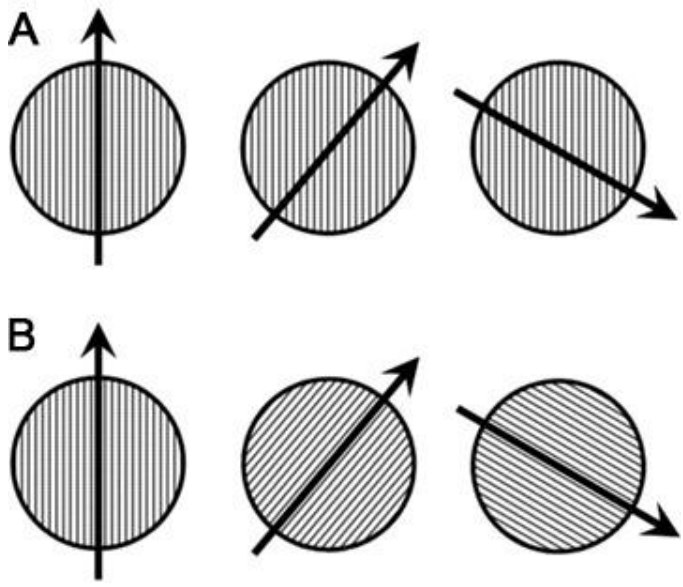

Figure 2.3 (A) Néel rotation: the particle remains fixed while magnetic moment rotates. (B) Brownian rotation: the particle rotates while the magnetic moment fixes with respect to the particle axes.[96] Copyright 2014 Elsevier B.V.

In addition, magnetic nanoparticles can be heated remotely under alternating magnetic field of high frequency.[97,98] The magnetic losses depends on frictional losses, hysteresis loss and Brown and Néel relaxation.[99,100] Frictional losses generate heat by viscous friction between particles and fluid. Hysteresis loss is produced by shifting in magnetic domain walls and can be calculated based by integrating the area of hysteresis loop. For Néel relaxation, it refers to the magnetic moment changes between parallel and antiparallel orientations assuming physical orientation is constant. Brown relaxation comes from reorientation of the whole particle. For superparamagnetic nanoparticles with single domain, Néel and Brownian relaxation contributes as a major part of energy source.

2.1.4 Graphene oxide

Graphene was first isolated in 2004 by scotch tape peeling. It is a two-dimensional hexagonal arranged carbon atoms in a single sheet form composed of sp^2 and sp^3 carbon atoms.[101,102] Graphene has been demonstrated to exhibit outstanding properties, such as high Young's modulus up to 1TPa, high thermal conductivity up to 5000 W/mK, high surface areas up to 2630 m^2/g and excellent chemical durability and electron mobility.[103] The precursor for graphene synthesis: Graphene oxide (GO), has attracted great attention for its chemical and thermal modification.[104] GO is a single layer of graphite oxide. After oxidizing graphite, it is dispersed and exfoliated in solvents to make it single layer.[105,106] As a result, various oxygen groups are present in the form of hydroxyl and epoxy groups on the basal plane and carboxylic groups on the edges. These polar groups improve water solubility of GO, making it available to form films by various

coating method. Besides, they are main targets for modification and functionalization of GO. The unique properties attract attention for biomedical applications such as biosensing, drug delivery, photothermal therapy and antibacterial materials.[107-110] GO has been demonstrated to possess excellent antibacterial properties with mild cytotoxicity.[108,111,112] Comparison of toxicity toward *Escherichia coli (E. coli*) between graphite, graphite oxide, GO and reduced Graphene oxide (rGO) indicates the highest antibacterial activity of GO. It was proposed that GO killed bacteria by a three step mechanism. Bacteria were firstly wrapped around by thin layers of GO nanosheets. These nanosheets were then able to induce both membrane stress by disrupting membrane and superoxide anion-independent oxidative stress by interfering with bacteria lipids, proteins and DNA.[113] Additionally, a new material was synthesized by absorbing tetradecyltriphenylphosphonium bromide (TTP) onto water-soluble brilliant blue-functionalized rGO by noncovalent π-π interactions. The material combined advantages of both rGO and TTP, exhibiting excellent bacterial toxicity. [114]

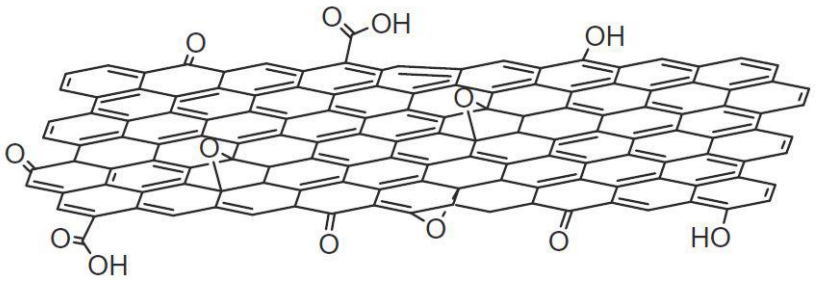

Figure 2.4 Structure of GO.[101]

2.2 Antimicrobial polymers with quaternary nitrogen atom

A Polymer is a substance composed of macromolecules, which represents large molecules of a high molecular weight with repeating units of low molecular weight. The repeating units derive from monomers through polymerization processes. Apart from antimicrobial polymers which contain groups themselves that can kill bacteria, others may be modified by attaching active antimicrobial groups or mimic protein to reduce toxicity. Polymers are also facile to form polymer-antibiotic composite or polymer-inorganic composites. This research field starts with the synthesis of 2-methacryloxytroponones related antimicrobial polymers in 1965, which exhibit wide spectrum activity.[115] Since then, broad polymers have been tested to potentially overcome the shortcomings of conventional antibiotics or strongly biocidal chemicals, simultaneously affording longer lifetime and less toxicity, combating antibiotic resistance, and incurring lower production costs.[116]

Antimicrobial polymers do possess superior properties than conventional antimicrobial agents.

1. Current agents with low molecular weight are easily leaching out from the surfaces and diffusing into the environment. As low molecular weight agent typically possesses higher toxicity, their diffusion may cause environmental problems. Polymeric materials act as matrix to trap these small weight agents, enhancing its long term activity and minimizing the environmental contamination.

2. Polymers are quite stable, non-volatile and do not permeate through skin. Hence the antibacterial material is stable for transporting and storage.

3. Polymers, with higher molecular weight, typically have lower toxicity.

4. Their nonleaching properties are more suitable for surface coating, reducing the leaching out of active substances, which is particularly suitable for textile field.[117]

5. Polymers, which act to penetrate and destroy membrane physically, aid the prevention of drug-resistance problems.

Hence, the polymeric materials potentially improve stability, reduce diffusion, reduce skin irritation, reduce toxicity, possess higher biocompatibility, corrodes less of metals and plastics and provide longer activity.[116]

Most antimicrobial polymers are designed to possess positive charges since bacteria cell walls are typically negatively charged as introduced in the background section. Among all the polymers, those with quaternary ammonium salts (QAS) are probably most extensively studied for antimicrobial applications.[118] The positively charged polymers attract negatively charged bacteria membrane through electrostatic interactions, followed by penetrating through the bacteria membrane, leading to cell lysis. Quaternized polymers interact with cells to a better extent compared to cationic low molecular weight monomers due to higher charge density for binding with bacteria membrane.[119]

2.2.1 Polymers with aromatic or heterocyclic groups

Cationic polymers with aromatic or heterocyclic structures and quaternary ammonium functional groups can lead to bacteria killing effect.[120,121] MIT/Northeastern group demonstrates antibacterial activity of N-alkylated poly (4-vinylpyridine) groups against both Gram-positive and Gram-negative bacteria, with N-alkyl chain of six carbon most effective.[122] Li *et al.* also synthesized insoluble pyridinium based copolymers with different ratios of 4-vinylpyridine and styrene and subsequently quaternized by benzyl bromide. The polymers achieved higher activity with increasing amount of pyridinium groups and killed both Gram-positive and Gram-negative bacteria. On the other hand, they display weak toxicity with median lethal dose of 2330 mg/kg.[123] Additionally, the influence of counterion in the polymers was investigated for activity differences. By anion exchange of counter anion (Cl^-) in poly(4-vinyl 2-hydroxyethyl pyridinium) chloride with Br^-, OH^-, SH^-, NO_3^-, BF_4^- and CF_3COO^-, strongest antibacterial ability was obtained with polymers having OH^- as the counterion, achieving lowest MIC values of 0.065 mg/ml against *Bacillus coagulans*.[124]

Another family in this category is imidazolium salts by alkylation of nitrogen atoms of imidazole.[125] Unlike imidazole that forms hydrogen bonds with drugs and proteins, the imidazolium salts mainly interact with biological systems such as bacteria via electrostatic forces.[126] For example, polysiloxanes were synthesized to possess pendent imidazolium side groups and quaternized by alkyl halide, with MIC against *E. coli* at 10 to 30 μg/ml.[127]

2.2.2 Biodegradable cationic polycarbonate

Recently, biodegradable polycarbonates polymers have been investigated against bacteria for multi-drug resistant microbes.[128,129] A peptide mimic structure of block copolymers have been synthesized by ring opening polymerization to form a cationic secondary structure to interact with microbial membranes by enhancing local hydrophobicity and charge density as shown in the Figure 2.5. On the contrary, the toxicity limit is well above its MIC values. Later, scientists start to optimize the quaternization by varying the quaternizing agents ranging from trimethylamine to pyridines and imidazoles and by varying the side chains. Higher hydrophobicity enhances the toxicity against bacteria since N-heterocycle quaternized polymers are more toxic to bacteria compared to trimethylamine quaternized ones.[130]

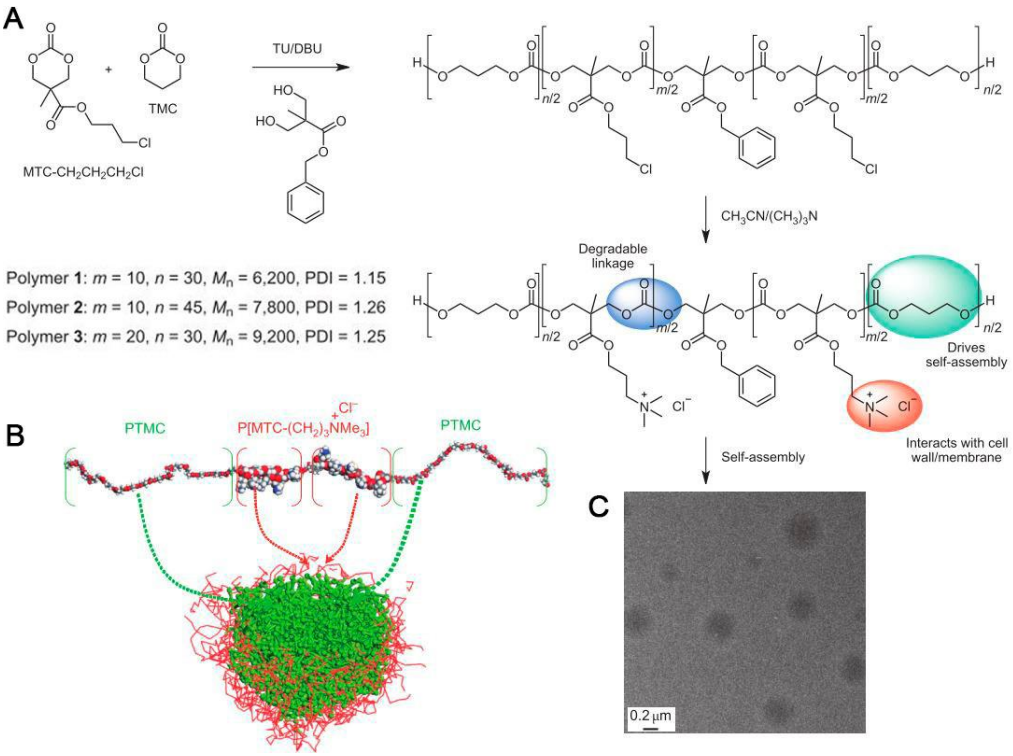

Figure 2.5 Synthesis of micelles formed by cationic amphiphilic polycarbonates. (A) Scheme for polycarbonates synthesis. (B) Simulation of micelle formation by molecular modelling using Materials Studio Software (red, O; white, H; grey, C; blue, N). (C) TEM image of polymer 3.[131] Copyright 2011 Macmillan Publishers Limited, part of Springer Nature.

2.2.3 Acrylic or methacrylic polymers

Polymers synthesized based on acrylic or (meth)acrylic monomers are also facile to obtain quaternary ammonium salts. These activity of polymers depends on the counterion, charge density and hydrophobicity.[117] Among these polymers, many are synthesized based on commercially available monomers such as 2-dimethylaminoethyl methacrylate (DMAEMA) and methyl methacrylate (MMA).[132,133] Additionally, polymers based on methacrylate monomers involving 1,4-diazabicyclo-[2.2.2]-octane with a butyl or a hexyl

group on one nitrogen atom and methacrylate groups on another nitrogen atom were synthesized. They moderately killed bacteria at MIC values of 250 μg/ml for polymers with butyl groups and 62.5 μg/ml for polymers with hexyl groups.[134]

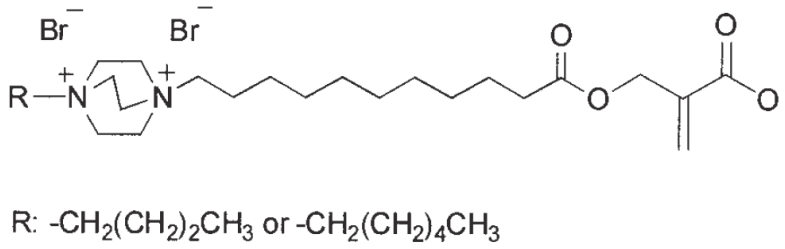

Figure 2.6 1,4-diazabicyclo-[2.2.2]-octane related methacrylate monomers.[134] Copyright 2004 John Wiley & Sons, Inc.

2.2.4 Polymers with quaternary nitrogen atoms in the main chain

Quaternary nitrogen atoms within the backbone are called ionene polymers, which are usually synthesized by step-growth polymerization or post cationic functionalization.[135-138]

Various ionene polymers has been synthesized for antimicrobial applications. For example, a series of cationic comb-like ionenes of different aliphatic side chains were synthesized with high charge density. The comb-like ionenes demonstrated higher activity against *E. coli* than linear ionenes.[139,140] Moreover, the ionene polymers, with low density polyethylenes, showed antimicrobial and antistatic properties.[124,125] Yudovin-Farber and coworkers synthesized octyl alkylated polyethyleneimine (PEI)-based nanoparticles, which is prepared by cross-linking of polyethyleneimine, alkylation by octyl halide and

quaternization by methyl iodide. After embedding the nanoparticles in dental composite resin at 1% w/w, the material demonstrated superior activity against *Streptococcus mutans.*[141,142]

While similar to other cationic polymers, ionenes are able to destroy cell membrane, they also form complexes with biological polymers such as DNA and herpin.[143] Ikeda *et al.* reported that polyionenes with rigid spacers are able to cause phase separation in bacteria mixed bilayer membranes and active in antimicrobial killing. When incorporating flexible spacers coexisting in the polymers with rigid spacers, the product reduces its ability to cause phase separation.[144]

Mattheis *et al.* investigated the effects of pendent alkyl chain lengths, counterions and backbone spacer lengths by comparing various alkyloxyethylammonium ionenes.[145] It was reported that antimicrobial activity is highest for pendent alkyl chains of short methyl or relatively long octyl groups. The backbone spacer also has an effect and polymers with the short ethyl spacer give the lowest activity. However, the counterions, such as hydroxide, bromide and phosphate, did not have a significant effect in biocidal effect by materials.

2.2.5 Hyperbranched and dendritic polymers

Branched polymers, with their three-dimensional structures, are compact, multi-functional, and highly soluble and active, suitable for novel antimicrobial material design.[145-147] They are typically in star-shape, dendritic or hyperbranched.

Chen *et al.* synthesized the hyperbranched polyester modified with hexadecyldimethylamine and applied them to silk fabric.[148] The treated fabrics demonstrated effective antibacterial acitivties against *E. coli* and *S. aureus* even after using 15 times. Worley *et al.* synthesized NO-releasing and quaternized ammonium modified poly(amidoamine) (PAMAM) dendrimers for synergetic antibacterial properties, with longer quaternized ammonium alkyl chains more effective than shorter chains. The addition of NO release properties in dendrimers markably enhance antibacterial activity due to synergetic bacteria killing effect, especially for polymers modified with shorter alkyl chains.[149]

2.3 Immobilization of antimicrobial polymers on nanomaterial surfaces

Immobilizing polymers onto surfaces of nanoparticles such as gold, silica, carbon nanotubes, etc, not only generates antimicrobial properties of polymers at nanoscale, but also provides the opportunity to incorporate different functional properties from the nanomaterials. The chemical linkage between polymer and nanomaterials prevents release of polymers into environment.[150]

Recently, Russell *et al.* has prepared the quaternized PDMAEMA coated magnetic nanoparticles by the surface initiated ATRP method. The hybrid responded to external magnetic field and can be easily separated from suspensions by magnetic fields after antibacterial applications. They maintained antibacterial efficiencies of 100% biocidal activity against *E.coli* after repeated eight recycles.[151]

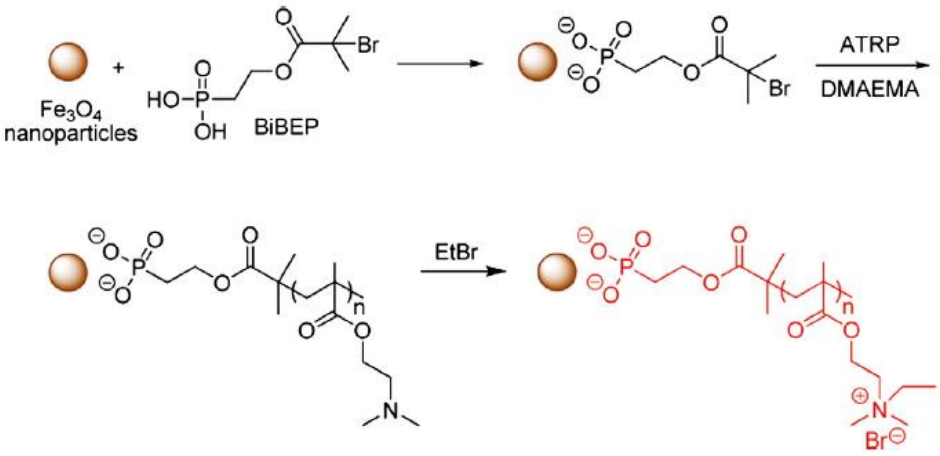

Figure 2.7 PDMAEMA coated magnetite nanoparticles.[151] Copyright 2011 American Chemical Society.

Kong *et al.* synthesized polymer poly[2-(*tert*-butylamino)ethyl methacrylate-co-ethylene glycol dimethacrylate] coated TiO_2 nanoparticles. The obtained structures displayed synergistic antibacterial effect under UV light irradiation due to biocidal ability of both the polymers and light activated TiO_2 core. Besides, the composite overcomes the shortcomings of many TiO_2 nanoparticles that do not have antibacterial activity in the dark and does exhibit biocidal activities without light.[152]

Various one-dimensional antimicrobial polymer nanostructures have also been developed. For example, Joo *et al.* prepared PDMAEMA functionalized carbon nanotubes by atom transfer radical reactions with good water and organic solubility. After quaternization, the material is active against both *E. coli* and *S. aureus*. It was demonstrated that higher polymer content in the structure contributes to higher material activity with highest antibacterial efficiency at 53.9

wt% of PDMAEMA. The author suggested the material could be used in application of EMI shielding or ESD area.[153]

2.4 Nanocarriers to deliver antibiotics on demand

Apart from materials to kill bacteria, appropriate delivery systems have been developed to improve therapeutic efficiency.[154] Polymeric nanoparticles display better stability and improved drug payload than traditional liposomes. They are synthesized by coating solid nanoparticles by a polymer matrix or a polymer shell. The active reagents can be entrapped inside structures or chemically linked to the polymers.[155]

Apart from natural polymers including gelatine, collagen and chitosan, which are quite expensive, synthetic polymers, such as poly(lactide), poly(esters) and poly(amino acids), are used to prepare polymeric nanoparticles to lower the cost and improve the product purity.[156] Besides, they are typically able to degrade into biologically safe molecules which can be metabolised and secreted out from human body. The polymeric nanoparticles are unique in self-assembly into devices for drug delivery by emulsion polymerization, film rehydration or nanoprecipitation methods.[157]

The drug delivery system, which responds to metabolic states or physiological conditions, achieves on-demand drug release purposes. For example, negatively charged liposomes stabilized by positively charged chitosan-modified gold nanoparticles encapsulate the antibiotic vancomycin and respond to bacteria secreted toxins. The toxins can penetrate through liposome membrane and leave holes, resulting in vancomycin leakage and *S. aureus* killing

in reverse.[158] Xiong *et al.* also have reported the development of polymeric triple-layered nanogel, which encapsulated hydrophilic vancomycin and prevented premature loss of cargo. The drug release was triggerd by bacteria lipases as a consequence of PCL degradation, enabling on-demand drug release. The nanodevice exhibited strong ability to inhibit bacteria growth by its released antibiotics when active bacteria lipases are secreted.[159] Apart from substances secreted by bacteria, pH is also an available factor for drug delivery. Poly(lactide-co-glycolide)-b-poly(l-histidine)-b-poly(ethylene glycol) based nanoparticles loaded with vancomycin were synthesized and demonstrated surface charge-switching properties upon pH changes. At acidic conditions, the positively charged nanoparticles rapidly bind to bacterial cell walls of both Gram-positive bacteria (*S. aureus*) and Gram-negative bacteria (*E. coli*). After encapsulating vancomycin in the structure, the drug reduced the loss of its activity in the acidic environment.[160]

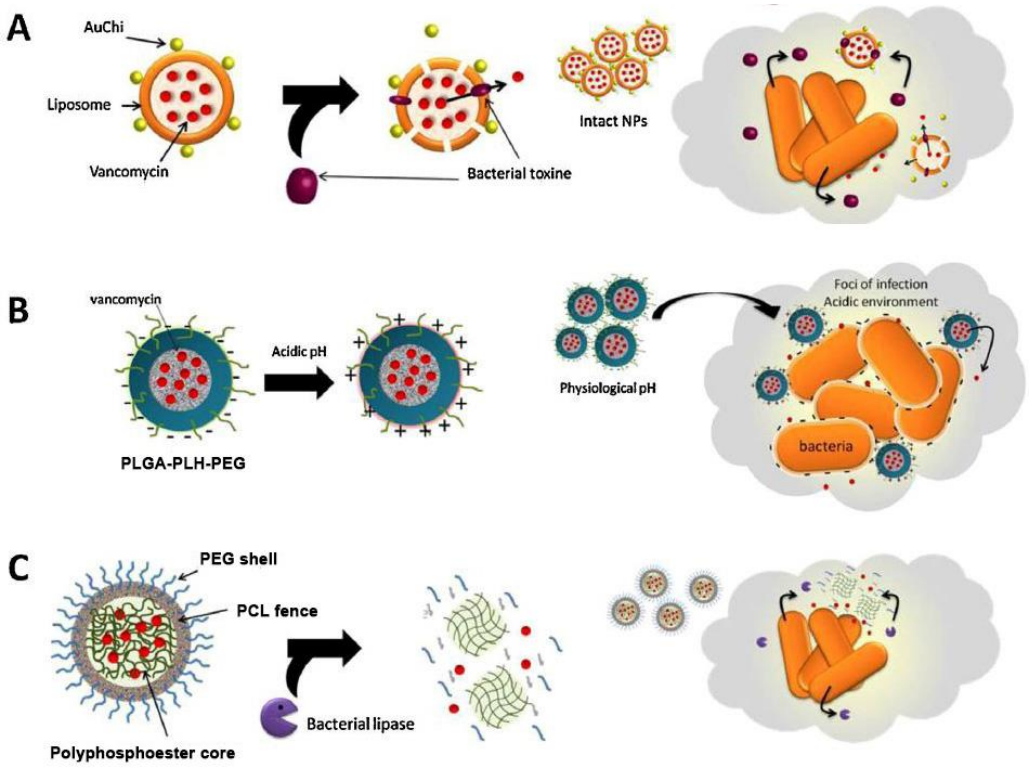

Figure 2.8 (A) Toxin triggered delivery of vancomycin from liposomes made of chitosan-modified gold nanoparticles (AuChi).[158] (B) pH responsive polymeric nanoparticles loaded with vancomycin.[160] (C) Bacteria lipase triggered delivery of drug by polymeric triple-layered nanogel.[159,161] Copyright 2014 Elsevier B.V. and the International Society of Chemotherapy.

Chapter 3. Tailor antibacterial property of graphene oxide by quaternized polymer brushes

3.1 Introduction

GO, with oxygen-containing functional groups such as hydroxyls, epoxides on the basal plane and carboxylic acids at the edges for facile surface modification, are able to form paper formats to decorate ordinary subjects.[101,102] GO was reported to possess antibacterial activity based on membrane destruction mechanism and superoxide anion-independent oxidative stress as discussed in the literature review section. On the other hand, cationic polymers with aromatic or heterocyclic structures also displayed high antibacterial effect based on membrane destruction mechanism. Based on the fact that charge density played an important role in cationic polymers for antibacterial applications, in the first project we developed GO grafted with polymer brushes consisting of N-alkylated poly (4-vinylpyridine) (Q-PVP) against both Gram-negative bacteria (*E. coli*) and Gram-positive bacteria (*S. aureus*) in both aqueous dispersion and paper form.[162] Well-defined polymers are covalently grafted onto GO by atom-transfer radical polymerization (ATRP), and subsequently quaternized by alkyl chains with carbon lengths of 2, 4, 6, and 8 respectively. ATRP is a straightforward method that achieves exceptional uniform molecular weight of polymers to control surface properties of GO-polymer composites, facilitating real biological applications.[163] The GO nanosheet not only killed bacteria itself, provided the platform to locate polymers and enhanced localized charge density of polymers, they also enabled surface applications in paper formats for distinct surface

applications. Free-standing paper-like materials are widely used in various areas such as filters, adhesive layers, molecular storage, electronic or optoelectronic components, and protective layers. GO related materials typically display excellent mechanical and electrical properties, high chemical resistance, superior sealability against temperature and impermeability against fluids.[105] The hybrid combined advantages of GO and polymers with tremendous enhancement of charge density of polymers and improvement in solubility of GO, displaying higher antibacterial activity than GO or polymers alone.

3.2 Experimental section

3.2.1 Materials and characterization

Phosphate-buffered saline (PBS) was purchased from BASE and diluted to the desired concentration before usage. Luria Bertani (LB) broth and Bacto Agar were purchased from Becton and Dickinson Company. *E. coli* (ATCC 8739) and *S. aureus* (ATCC 6538) were obtained from ATCC and used according to the protocols. The other chemicals were commercially available from Aldrich and utilized as received.

FTIR-Digilab FTS3100 FTIR spectrometer was use for FTIR test with potassium bromide (KBr) pellet. NMR Bruker Avance 300 spectrometer was used for NMR spectra. FESEM were taken by JEOL JSM-6700F. Thermogravimetric analysis (TGA) was performed by Perkin Elmer TGA/DTA equipment in nitrogen atmosphere between 40 to 600 °C at a temperature increase of 10 °C/min. The M_n and PDI of polymers were analyzed by Shimadzu liquid chromatography system together with a Shimadzu refractive index detector

(RID-10A) at room temperature with DMF (Dimethylformamide) as an eluent with 1.0 ml/min flow rate. Zeta potential and hydrodynamic diameter were recorded with BIC PALS ZetaSizer.

3.2.2 Synthesis of initator

Ditert-butyl dicarbonate (4.84 g, 22.17 mmol) in 80 ml dichloromethane was slowly added to the stirred solution of ethylenediammine (8 g, 133.1 mmol) in dichloromethane for 1 h at 0 °C. The solution was stirred at room temperature for 19 h. The precipitate was filtered off. Excess dicholorometnahe and ethylenediammine were removed under vacuum. The solution was dissolved in saturated aqueous sodium carbonate (60 ml) and extracted with dichloromethane (3×60 ml). Yield: 50.11 %. ^{1}H NMR ($CDCl_3$, 300MHz)): 1.46[(CH_3)$_3$C-], 2.80(-CH_2-NH_2), 3.15(-CH_2-NH-). (Figure 3.1A)

2-bromoisobutyryl bromide (3.86 g, 16.78 mmol) in 40 ml THF was added dropwise to the solution of N-Boc-ethylenediamine (1.78 g, 11.12 mmol) in 40 ml THF (tetrahydrofuran) in the presence of Et_3N (1.70 g, 16.78 mmol) at 0 °C. The reaction was stirred for 48 h at room temperature. The precipitate was filtered off. The solvent was evaporated to leave over a yellow solid, which was dissolved in methanol and precipitated in saturated aqueous Na_2CO_3 solution. The organic phase was dried with sodium sulfate and the solvent was evaporated under reduced pressure to form a yellow solid. The solid was washed with hexane 3 times and dried under reduced pressure to give a white solid (I). Yield: 47.84%.^{1}H NMR ($CDCl_3$, 300 MHz)): 1.45[(CH_3)$_3$C-], 1.96[(CH_3)$_2$C-], 3.35(-CH_2-NH-COO-), 3.38(-CH_2-NH-CO-).(Figure 3.1B)

Hydrogen chloride gas was produced by dropping concentrated H_2SO_4 into concentrated HCl. The HCl gas was introduced into a solution of (I) (1.64 g, 5.32 mmol) in 40 ml ethyl acetate until solution turned cloudy. The solvent was evaporated under reduced pressure to form a white solid. The solid was re-dissolved in water and the white precipitate was filtered off, freeze dried to afford a white solid (II). Yield: 74.29%. ^{1}H NMR (D_2O, 300 MHz)): 1.82[(CH_3)$_2$C-], 3.07 (-CH_2-NH_2), 3.45(-CH_2-NH-CO-). (Figure 3.1C)

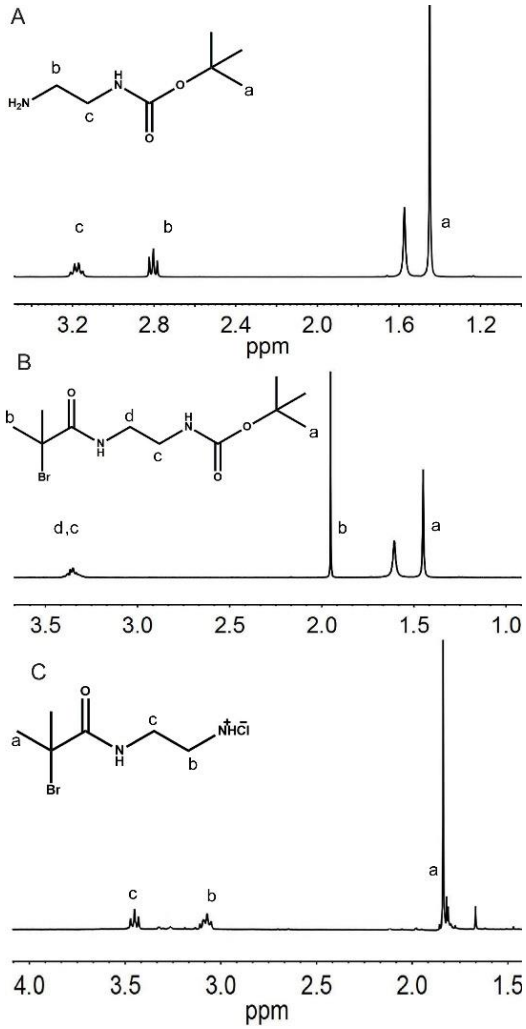

Figure 3.1^{1}H NMR spectra of synthesized intermediates and product for initiator.

3.2.3 Preparation of GO-Initiator

GO nanosheets were prepared by oxidizing graphite powder according to modified Hummer's Method.[164] GO was diluted to 3 mg/ml with ultrapure water and ultrasonicated for 40 min. 50 ml GO solution was mixed with 150 mg initiator and the pH value of the mixture was tuned to 9-10. After ultrasonication for another 40 min, the solution was deoxygenated by nitrogen purging for 15 min. During the process of reacting at 80 °C for 24 h under nitrogen atmosphere, the pH was continuously monitored and tuned to maintain the original pH range. The resulting solid was repeatedly washed with ethanol and water and re-dispersed in DMF. After centrifugation and ultrasonication, the supernatant was retained.

3.2.4 Preparation of GO-poly(4-vinylpyridine) (GO-PVP) by ATRP

5 ml GO-Initiator dispersed in DMF was added with a specific amount of 4-vinylpyridine and purged by nitrogen for 20 min. Then CuBr (12 mg) and PMDETA (45 mg) were added under nitrogen atmosphere. After reaction at 80 °C for 24 h, the obtained solid was repeatedly washed by methanol and redissolved in DMF. The free polymer PVP, arising from sacrificial initiator, was dried under vacuum and tested for molecular weight. (M_n = 59000, PDI= 2.26). (Figure A.1)

3.2.5 Preparation of poly(4-vinylpyridine) by ATRP

Similar ATRP process was performed to synthesize poly(4-vinylpyridine). Initiator instead of GO-Initiator launched ATRP process. The

molecular weight of the polymer synthesized was based on free polymers produced in GO-PVP above. (M_n = 59900, PDI= 1.7).

3.2.6 Quaternization of GO-poly(4-vinylpyridine)

The poly(4-vinylpyridine) functionalized GO was mixed with 1-bromoethane, 1-bromobutante, 1-bromohexne and 1-bromooctane and heated at 45 °C for 3 days to obtain GO-C_2PVP, GO-C_4PVP, GO-C_6PVP, and GO-C_8PVP respectively. The solid was recovered and washed 3 times by methanol and re-dissolved in water. The concentration of the products was obtained by calculating the dry weight after freeze drying. PVP was also mixed with 1-bromoethane to heat at 45 °C for 3 days to generate C_2PVP.

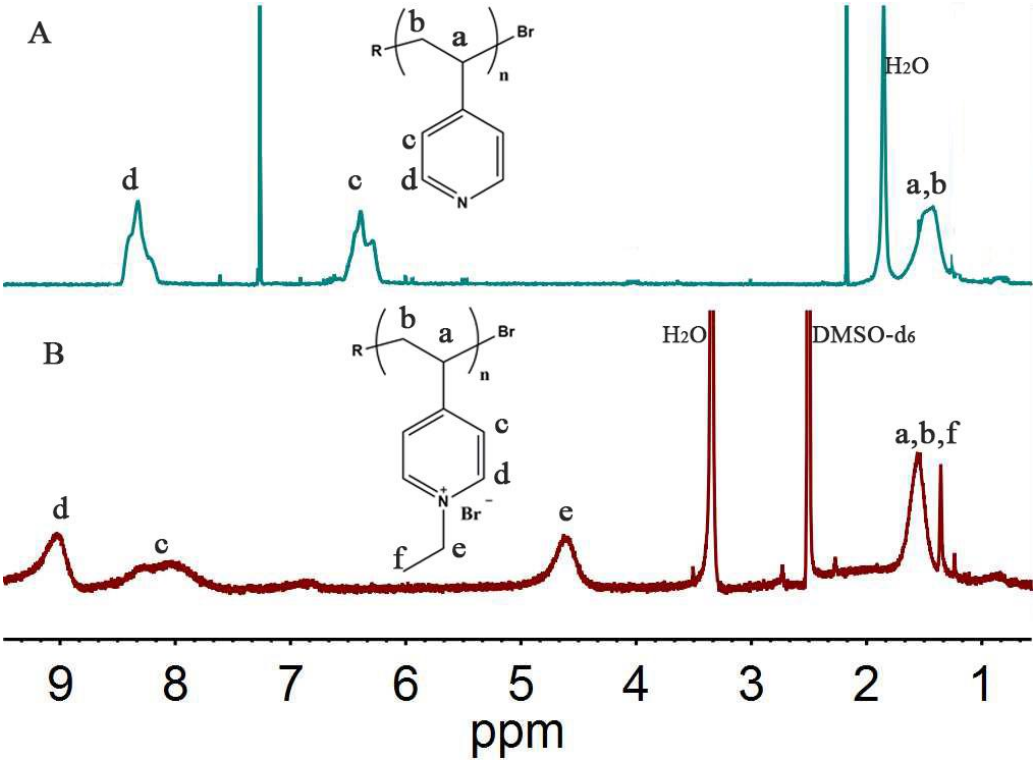

Figure 3.2 ^{1}H NMR spectrum for PVP in $CDCl_3$ (A) and C_2PVP in DMSO (B).

3.2.7 Paper Preparation

GO, GO-C_2PVP, GO-C_4PVP, GO-C_6PVP, and GO-C_8PVP of the same concentration were ultrasonicated for 30 min and poured onto Teflon plates and heated continuously at 40 °C. The papers were peeled off and cut to a 15mm×15mm dimension.

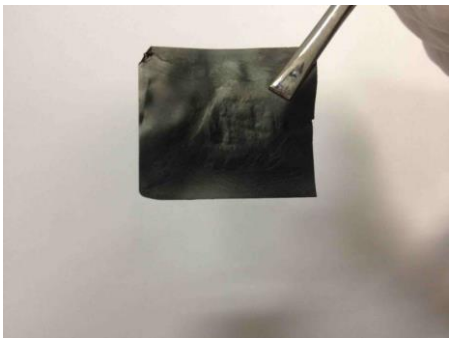

Figure 3.3 Photo of GO-C_2PVP paper.

3.2.8 Cell preparation

For both *E. coli* (ATCC 8739) and *S. aureus* (ATCC 6538), a single colony was inoculated in Luria-Bertani (LB) medium at 37 °C overnight in 15 ml tube. The tube was shaken overnight until the bacteria reaching midexponential growth phase. Cells were centrifuged at 7000 rpm for 5 min and washed with PBS for 3 times. The bacteria were then redispersed and diluted to the predesigned concentration. Cell concentration was calculated by plate count method.

3.2.9 Cell viability test for materials in solution

Cells at concentration of 10^6 to 10^7 CFU/ml was incubated with GO, GO-PVP, C_2PVP, GO-C_2PVP, GO-C_4PVP, GO-C_6PVP, and GO-C_8PVP dispersions at 10 μg/ml for *E. coli* and 10 μg/ml, 1 μg/ml for *S. aureus.* It is worth noting that GO dispersion in water was dialyzed to achieve neutral solution. After 1 h, the loss of viability of cells was evaluated by plate count method. Briefly, a series of 10-fold cell dilutions was spread onto agar plates and grown at 37 °C overnight. Colonies were counted and compared with control. Pure water without GO based materials was utilized as control. All experiments were performed in duplicate and repeated three times.

3.2.10 Cell viability test for materials in paper form

The papers were rinsed in sterilized PBS for 3 days and dried. 20 μl of each bacteria (10^8 CFU/ml) was spread onto GO, GO-C_2PVP, GO-C_4PVP, GO-C_6PVP, and GO-C_8PVP papers and incubated for 1 h at 37 °C, with a relative humidity of not less than 90%. 10 ml of PBS was added to wash paper and

recover any survivors. The loss of bacterial viability was evaluated by plate count method as previously mentioned. Glass slides were used as control.

3.2.11 Zone of inhibition test

GO and GO-C_2PVP paper was sterilized by ultraviolet lamp for 60 min. Bacteria were spread on the agar placed. The samples were carefully placed onto the plates. The plates were incubated at 37 °C for 24 h. The diameter of zone of inhibition was measured for free circles of the testing samples on the plate.

3.2.12 Cell morphology SEM images

Bacteria (10^6 to 10^7 CFU/ml) were mixed with C_2PVP solutions for 2 h. Subsequently, cells were fixed with 2% glutaraldehyde overnight, followed by dehydration with by 30, 50, 70, 80, 90, 100% ethanol for 30 min and then dried. The microbes were observed by FE-SEM (JEOL JSM-6700F) for morphology changes.

3.2.13 Live/Dead assay

Cells (10^8 CFU/ml) were incubated with C_2PVP dispersions for 2 h and then mixed with LIVE/DEAD BacLight Bacterial Viability kit for 30 min under dark at room temperature. After washing with PBS, the viability of bacteria was viewed by Olympus IX71 inverted microscope.

3.2.14 Hemolysis test

Fresh human blood (3.5 ml), donated by a healthy volunteer, was centrifuged at 700 rpm for 5 min and washed three times. The final concentrated

erythrocytes was diluted to 5% by PBS. The GO-C_4PVP at different concentrations (500 μl) was mixed with 500 μl erythrocytes stock. The mixture was shaken at 37 °C for 1 h at a speed of 150 rpm, and was then centrifuged. 500 μl of supernatant was added to 24-well microplate. The hemoglobin release was determined by measuring absorbance at 576 nm using a microplate reader. Pure water was used as a positive control and pure PBS served as a negative control. The hemolysis percentage was calculated using the equation below:

$$Hemolysis(\%) = \frac{A_p - A_b}{A_t - A_b} \times 100\% \qquad \text{Equation 3.1}$$

Where A_p, A_t and A_b is the absorbance value for the sample, positive control and negative control, respectively.

3.3 Results and Discussion

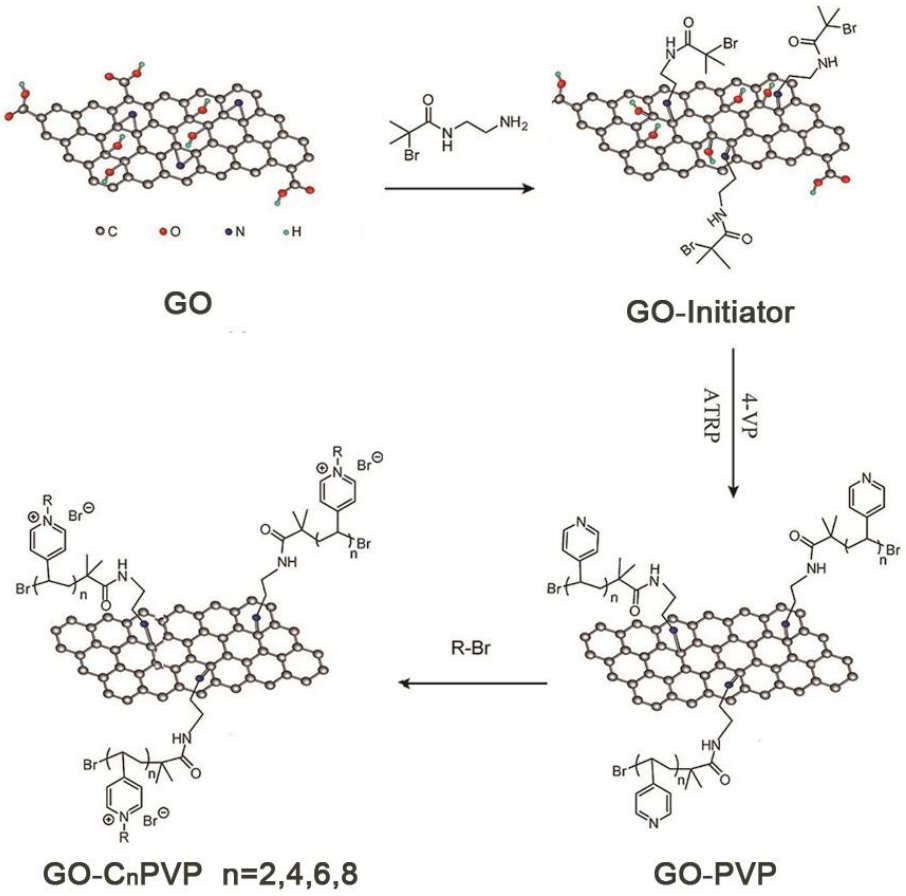

Figure 3.4 Stepwise synthesis route for GO-C_nPVP.

3.3.1 Synthesis of GO-C_nPVP in solution and in paper form

A typical stepwise synthesis route for GO-C_nPVP is displayed in Figure 3.3. After prepration of GO by modified Hummer's method, GO-C_nPVP were prepared taking advantages of oxygen functionalities of GO: (1) Grafting ATRP initiator onto GO by mixing in alkaline condition, (2) polymerization of 4-vinylpyridine on the surface of GO by ATRP with well-defined polymer chains grown in the initiating sites of bromine, and (3) quaternization of polymer brushes by reacting with 2,4, 6, 8 alkyl bromide to obtain bactericidal GO-C_nPVP.

There are several advantages in the design of our material. Firstly, polymer is covalently linked to GO surface, which is quite stable. Secondly, Polymerization is synthesized by "grafting from" method, which does not have a limit on the chain growth of the polymer and researchers can design the chain length individually.

The GO, GO-Initiator were characterized by infrared spectroscopy in Figure 3.5A while the data for GO-C_nPVP and their quaternized products were shown in Figure 3.5B. GO exhibit characteristic FTIR bands: C-O stretching at 1072 cm^{-1}, C-OH stretching at 1262 cm^{-1}, OH bending at 1430 cm^{-1}, C=C stretching at 1602 cm^{-1}, C=O stretching vibrations at 1720 cm^{-1} and O-H stretching at 3430 cm^{-1}.[165] After grafting inititator, a new peak at 1639 cm^{-1} appears for N-C=O vibration, confirming successful modification process.[166] The spectrum at 1599, 1597 and 1415 cm^{-1} in Figure 3.5B originated from pyridine vibrations of polymer brushes. In addition, the quaternization reaction resulted in the shifting of spectrum from 1599 cm^{-1} (a) to about 1630 cm^{-1} (b,c,d,e), due to quaternized ammonium group. The peaks confirmed sucessful polymerization of 4-vinylpyridine on the surface of GO and quaterniation process.

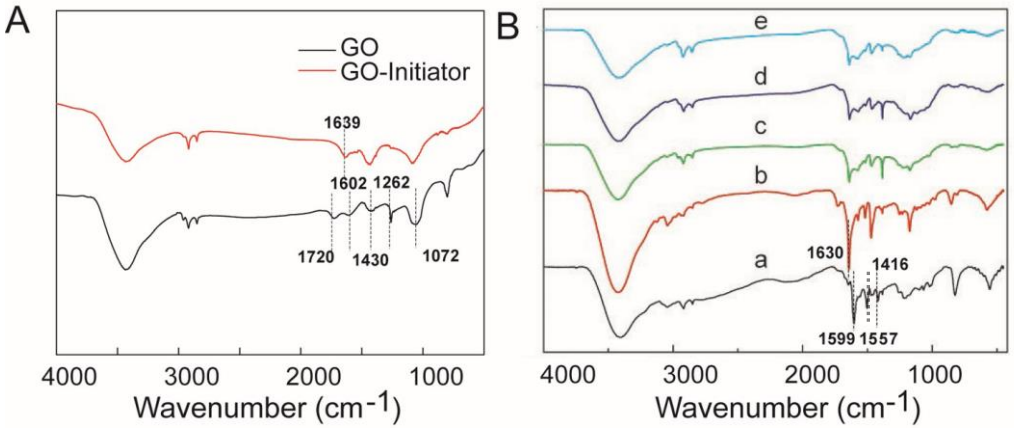

Figure 3.5 FT-IR characterization of (A) GO, GO-Initiator, and (B) GO-C_nPVP a-e: n=0,2,4,6,8.

Thermogravimetric analysis was also performed to analyze thermal stability of the samples as a function of temperature for GO, GO-Initiator and GO-C_nPVP (Figure 3.6). GO is thermally unstable and displayed the weight loss below 150 °C due to water loss, which is stored in the Π-stacked strucuture. Between 150 °C and 220 °C, GO experinces the loss of weight for CO, CO_2 and steam release from labile functional groups. Above 220 °C, more stable functional groups were degraded, with a final weight loss of 45%.[167,168] GO functionalized with initiator displays a totally different thermogram with improved thermal stability. Its weight loss below 220 °C was significantly less than that of GO, revealing the reduced amount of oxygen species and thus the amount of desorped CO_x. By burning out initiator and thermally labile oxgen groups, GO-Initiator has a weight loss of 40% until 600 °C.[169-171] After grafting polymer brushes, TGA curve exhibits a sharp decrease in mass between 300 °C and 390 °C for GO-PVP due to thermal decomposition of PVP, corresponding to a weight loss of 60%. GO-C_nPVP experiences a even greater extent of decomposition due to additional akly chains attached to polymer brushes. The weight losses are 72%, 79%, 77%, and 83% for GO-C_2PVP, GO-C_4PVP, GO-C_6PVP, and GO-C_8PVP respectively in the temperature range of 150 °C and 400 °C.

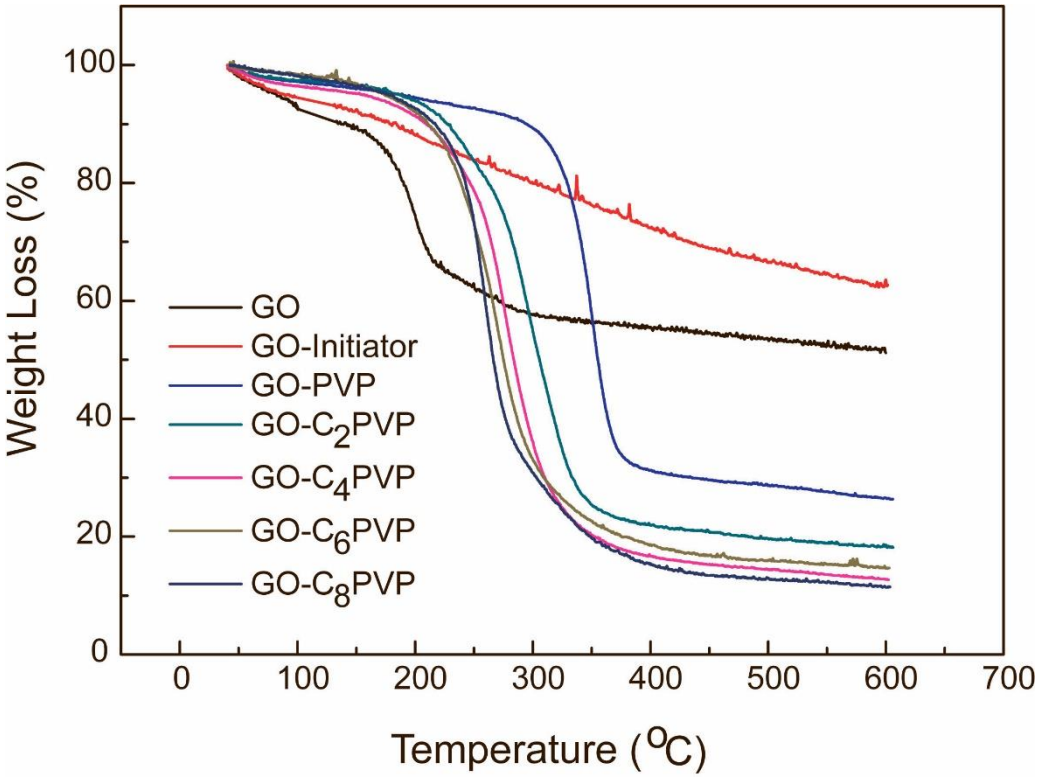

Figure 3.6 TGA characterization of GO, GO-Initiator, GO-PVP and GO-C_nPVP (n=2,4,6,8).

Zeta potential of various materials were listed in Table 3.1. GO and GO-PVP displayed negative values due to the presence of negatively charged functional groups on the surface of GO. The polymer C_2PVP alone and GO-C_nPVP possess positive charges, confirming successful quaternization processes.

Table 3.1 ζ potential of GO-related materials.

Material	GO	C_2PVP	GO-PVP	GO-C_2PVP	GO-C_4PVP	GO-C_6PVP	GO-C_8PVP
ζ Potential (mV)	-19.17 ± 2.81	12.26 ± 1.26	-2.99 ± 0.96	27.36 ± 1.19	31.55 ± 0.91	16.34 ± 1.64	15.84 ± 0.78

Both GO and GO-C_nPVP dispersions could be easily made into macroscopic, flexible and free standing papers, convenient and suitable for practical applications.[108] The formed papers of GO and GO-C_2PVP had a thickness of about 10 μm (Figure 3.7A,D). The cross-sectional view of both papers indicated layered structure. However, the lamination of GO-C_2PVP is more vague than that of GO because attached polymer brushes fill in gaps between layers as shown in Figure 3.7B,E, forming a continuous network in the composite. Since quaternized polymer brushes functionalized GO dispersed more homogeneously than GO solution, the papers obtained after solvent evaporation thus was more uniform. Hence, the cross section of GO-C_2PVP was extraordinarily packed and the surfaces were smoother.

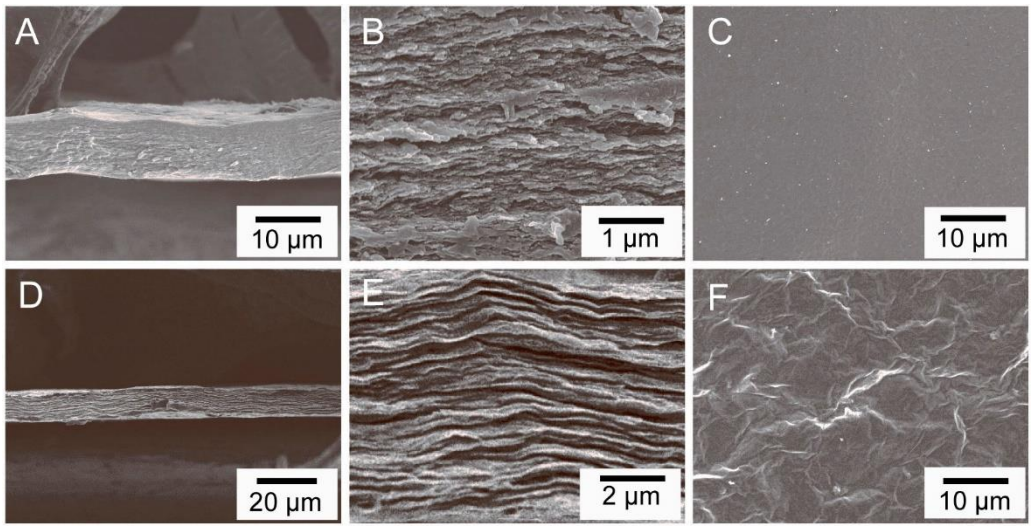

Figure 3.7 SEM images of the GO-C_2PVP paper and GO paper. A-C Cross-sectional and top view SEM images of GO-C_2PVP paper. D-F Cross-sectional and top view SEM images of GO paper.

3.3.2 Antibacterial activity of materials in solutions and in paper form

E. coli cells (10^6 to 10^7 CFU/ml) were incubated with GO, GO-PVP, C_2PVP and GO-C_nPVP (n=2, 4, 6, 8) at the same concentration (10 μg/ml). The loss of viability of bacterial cells was quantified by plate count method. Aqueous solution without materials was used as control. *S. aureus* cells were treated in the same manner, except that materials of two concentrations (10 μg/ml and 1 μg/ml) were assessed. As shown in Figure 3.8, for materials at 10 μg/ml, GO dispersions exhibit moderate cytotoxicity with cell death rate at 44.0 ± 1.5% and 55 ± 0.6% for *E. coli* and *S. aureus* respectively. GO-PVP displays a slightly higher antibacterial activity at 51.8 ± 3.6% and 63.8 ± 1.4% for *E. coli* and *S. aureus*. C_2PVP presented stronger toxicity, reaching 80% for both bacteria (82.2 ± 0.6% for *E. coli* and 81.2 ± 0.2% for *S. aureus*). GO-C_nPVP markedly reduced the number of viable cells, with most effective of GO-C_4PVP affording a 97 ± 0.4% and 99.8 ± 0.5% reduction of cells for *E. coli* and *S. aureus.* GO-C_2PVP underperformed GO-C_4PVP to a small extent, with 93.4 ± 0.2% for *E. coli* and 99.8 ± 0.5% for *S. aureus*. Beyond four carbon chain length, the antibacterial activity started to drop a little for GO-C_6PVP (*E. coli:* 90.5 ± 0.6% and *S. aureus*: 96.3 ± 1.2%), but dramatically for GO-C_8PVP (*E. coli:* 45 ± 1.7% and *S. aureus*: 76.8 ± 0.6%). The materials are more effective against *S. aureus* (Gram positive bacteria), than *E. coli*, (Gram negative bacteria). At 1 μg/ml, all GO-C_nPVP materials demonstrated similar trend of antibacterial effect toward *S. aureus*, but approached the toxicity of materials of 10 μg/ml against *E. coli.*

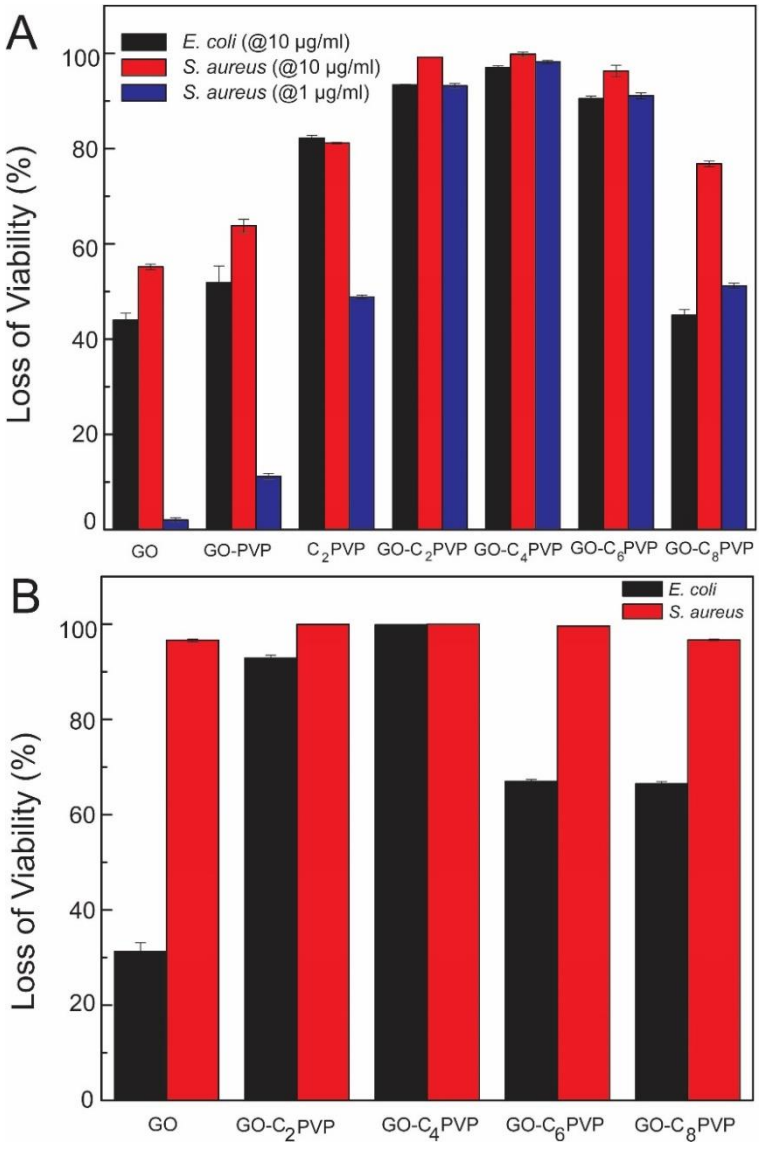

Figure 3.8 (A) Cell viability measurement after incubation with GO, GO-PVP, C_2PVP, GO-C_2PVP, GO-C_4PVP, GO-C_6PVP，GO-C_8PVP dispersions. Loss of cell viability rate was obtained by plate count method. (B) Cell viability measurement after incubation with papers made from GO, GO-C_2PVP, GO-C_4PVP, GO-C_6PVP, GO-C_8PVP dispersions. Loss of cell viability rates was obtained by plate count method.

Having tested the antibacterial activity of GO-C_nPVP in solutions, we explored their toxicity in paper form. GO alone exhibited low activity against *E.*

coli (31.3 ± 1.83%), All the GO-C_nPVP papers show outstanding activity, with 92.9 ± 0.6%, 99.9 ± 0.1%, 67.0 ± 0.4%, 66.0 ± 0.4% killing rate for GO-C_2PVP, GO-C_4PVP, GO-C_6PVP, GO-C_8PVP respectively. The trend is similar to solution test. However, GO-C_8PVP paper enhanced toxicity of GO to a greater extent compared to their solution form. In contrast, all the papers, including GO, possess high killing rate toward *S. aureus*, all reaching more than 95%, with 96.60 ± 0.26%, 99.92 ± 0.01%, 99.99 ± 0.03%, 99.64 ± 0.02%, 96.70 ± 0.15% killing rate for GO, GO-C_2PVP, GO-C_4PVP, GO-C_6PVP, GO-C_8PVP respectively.

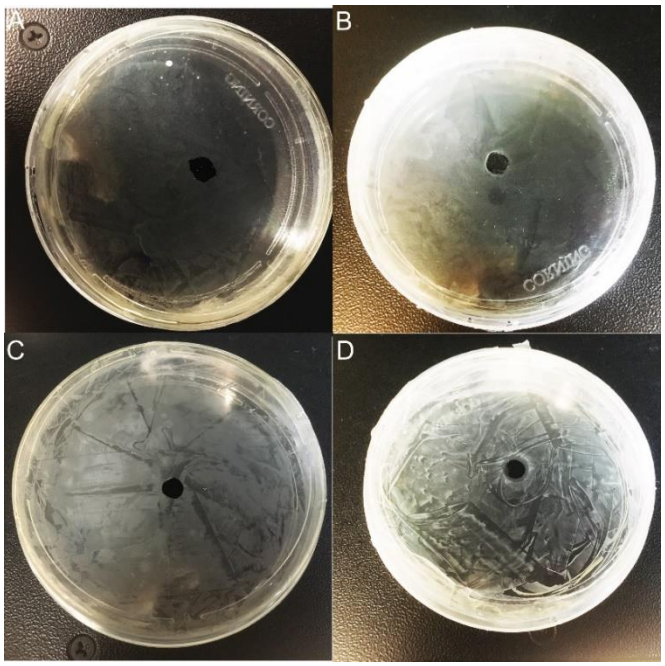

Figure 3.9 Zone of inhibition test of GO (A) and GO-C_2PVP (B) test against *E.coli*; Zone of inhibition test of GO (C) and GO-C_2PVP (D) test against *S.aureus*.

Similarly, zone of inhibition test was performed to validate the applicability of materials in paper form against bacteria. Figure 3.9A and C

demonstrates almost no zone against both *E.coli* and *S.aureus* by GO paper alone. While for GO-C2PVP, the zone of inhibition are 7.5 mm and 8.5 mm for *E.coli* and *S.aureus* respectively. The result is consistent with plate counting method. The material is applicable to kill bacteria in a paper form.

3.3.3 Membrane integrity observation and Live/Dead bacteria viability analysis

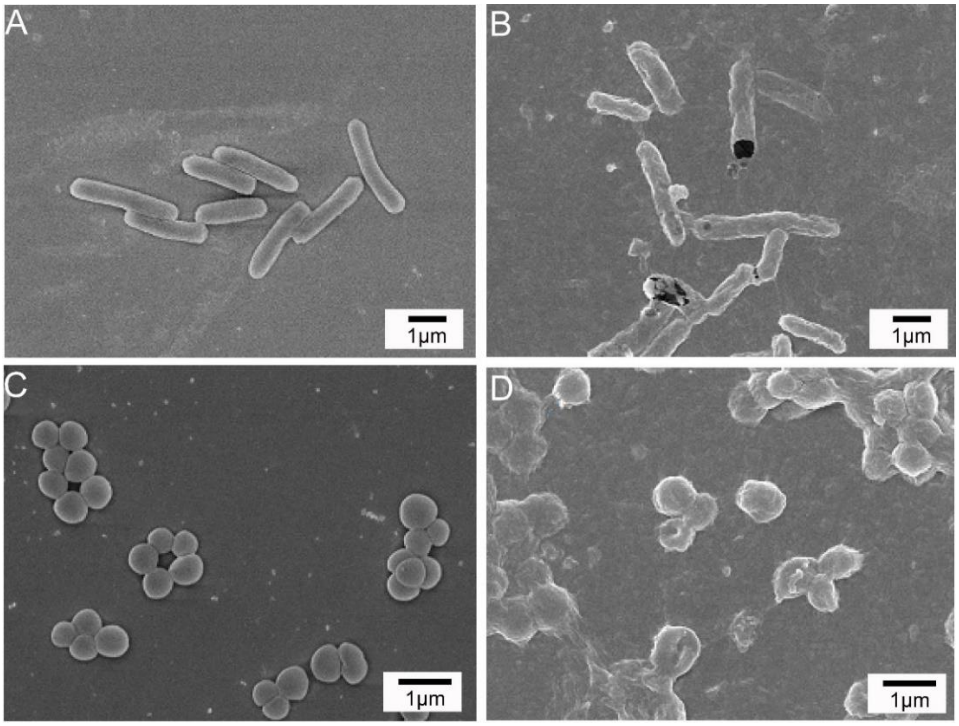

Figure 3.10 SEM images of (A,C) *E. coli* and *S. aureus* after incubation with PBS, (B,D) *E. coli* and *S. aureus* after incubation with GO-C_2PVP.

To investigate the mechanism of antibacterial effect of GO-C_nPVP, SEM images were taken to characterize membrane structures during the process. Figure 3.10B,D shows the images of normal *E. coli* and *S. aureus* treated with GO-C_2PVP. Figure 3.10A (*E. coli*) and Figure 3.10C (*S. aureus*) demonstrated smooth and integrated cell membrane of control samples. After treatment with

GO-C_2PVP, cells wrapped around the material and cell membrane was disrupted, clarifying irreversible damages.

Live/Dead analysis was also performed to qualitatively visualize the death of bacterial cells. Live/Dead *Bac*light kit utilizes mixtures of SYTO® 9 and propidium iodide to stain bacteria. Cells with damaged membranes were stained with fluorescent red and live cells with fluorescence green. Figure 3.11 shows both *E. coli* and *S. aureus* are alive in control but mostly dead after incubation with GO-C_2PVP, conforming the destruction of cell membrane. The number of dead cells are significantly improved after incubation with GO-C_2PVP compared to that with GO or C_2PVP alone.

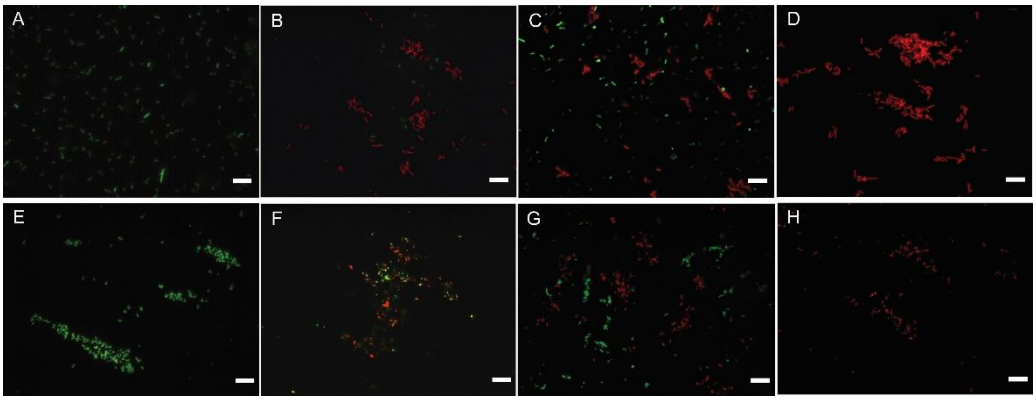

Figure 3.11 Fluorescence images of (A, E) *E. coli* and *S. aureus* after incubation with PBS, (B, F) *E. coli* and *S. aureus* after incubation with GO, (C, G) *E. coli* and *S. aureus* after incubation with GO, and (D, H) *E. coli* and *S. aureus* after incubation with GO-C_2PVP. Scale bar = 10 μm.

The hemolysis test was performed to access the material's toxicity against red blood cells as shown in Figure 3.12. The material demonstrates 9.8% hemolysis at 25 μg/ml and 30% hemolysis at 100 μg/ml. It is well above the level of

concentration against bacterial (10 μg/ml), facilitating application potentials of such materials.

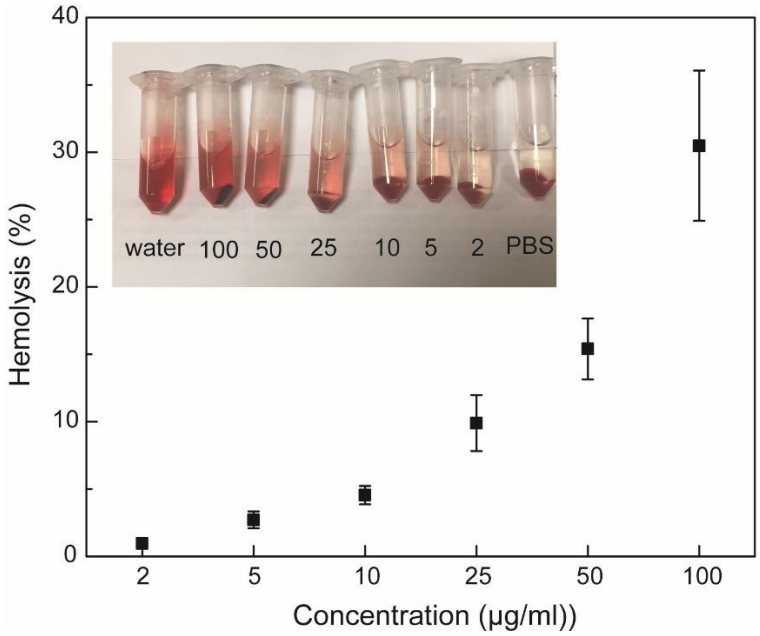

Figure 3.12 Hemolysis test of GO-C_4PVP

Both GO sheets and polymer brushes are proposed to synergistically deactivate and destroy cells. GO sheets interacted with cells by covering cell surfaces. Since monolayer GO sheets are impermeable membranes for many molecules. GO-C_nPVP is able to isolate cells from outside surface, inhibiting cell proliferation. C_2PVP alone, on the other hand, is able to kill bacterial by attracting to cell surface, discharge divalent ions away from negatively charged membrane and penetration through outer membrane and inner membrane for *E. coli* and directly penetrating cytoplasmic membrane for *S. aureus*, leading to cell death. Functionalized GO sheets take advantages of both GO and polymer brushes. They are positively charged and attracted to bacterial cells by electrostatic interaction, followed by wrapping around cells. Surface cationic polymer brushes on GO surfaces may simultaneously penetrate cell membrane and destruct

membrane integrity, resulting in cell lysis. GO-PVP is more effective than GO alone due to the additional hydrophobic interactions between polymer brushes and cell membrane, accelerating disruption of cells. Functionalized GO-C_nPVP differ in toxicity because of distinct charge densities and solubility. As shown in Table 3.1, GO-C_4PVP has the highest charge density of 31.55 ± 0.91 mV, followed by GO-C_2PVP (27.36 ± 1.19 mV), which is higher than that of C_2PVP (12.26 ± 1.26 mV). The antibacterial activity follow the same trend as zeta potential since the adsorption of materials onto negatively charged bacteria surface takes place to a higher degree at higher charge density. Nevertheless, GO-C_6PVP and GO-C_8PVP exhibits lower antibacterial activity but higher zeta potential compared to C_2PVP. This behavior correlates well with visual appearance of GO-C_nPVP solutions. The solubility of GO-C_nPVP decreases with increasing length of alkyl chains. While GO-C_2PVP and GO-C_4PVP maintain good solubility after free standing for 30 days, GO-C_6PVP and GO-C_8PVP tend to aggregate in the solution, which reduces the ability of material to interact with bacterial cells and toxicity. Last but not least, materials tested own higher antibacterial activity against *S. aureus*. *S. aureus* does not have an outer cell membrane, but consists of a thick hydrophobic peptidoglycan layer. In contract, *E. coli* has an outer membrane with lipopolysaccharides and phospholipids located outside thinner peptidoglycan layer, protecting cell from foreign attack. The existence of an extra barrier of *E. coli* results in differences in interaction with materials and their toxicity.

3.4 Conclusion

We have successfully functionalized GO with well-defined poly (4-vinylpyridine) brushes by ATRP and quaternized it with different alkyl chains. The composites in solution display excellent antibacterial activity at low concentrations of 10 μg/ml. Their paper forms demonstrate similar effect and are suitable for real applications. The paper made from polymer brushes quaternized with butyl chains demonstrates the highest toxicity up to 99.9% for both *E. coli* and *S. aureus* due to highly concentrated charge density and desirable solubility. The method is applicable to functionalize other polymers on the surface of GO and possibly loading of antibiotics or other nanoparticles for antibacterial applications.

Chapter 4. Cationic polycarbonate-grafted superparamagnetic nanoparticles with synergistic dual-modality antimicrobial activity

4.1 Introduction

In this chapter, a new class of hybrid antimicrobial nanoparticles with cationic polycarbonate brushes grafted on superparamagnetic $MnFe_2O_4$ nanoparticles were explored for antibacterial applications.

Facilitating by shortage of degradable ability of quaternized poly(4-vinylpyridine) in the first project, we thought of using polycarbonates, which emerged as highly valuable biomaterials due to their facile functionalities, biocompability and biodegradability by enzyme or hydrolysis.[172] Biodegradable materials are ideal for the local treatment of infection because they enable the degradation into oligomers within a controlled time frame to prevent undesired long-term toxicity and a second surgical intervention to remove the carrier is avoided.[172,173] On the other hand, if biodegradable materials are utilized in our daily life such as packaging materials, they demonstrate superior advantages for environmental concerns.[174]

Hedrick and Yang *et al.* has reported the first antimicrobial cationic polycarbonate.[128,129,131] In this study, oganocatalytic ring opening polymerization (ROP) of functional cyclic carbonate initiated by phosphonate molecules led to end-functionalized cationic polycarbonates that can be easily grafted onto magnetic oxide nanoparticle via a ligand exchange reaction.[175] A key finding is that anchoring the cationic polycarbonates on the nanoparticles reduced effective

antimicrobial concentrations by 3 orders of magnitude in comparison with that of free polymers, because forming polymer brushes afforded greatly increased local charge density.

On the other hand, recent developments in colloidal synthesis have continuously expanded the family of bactericidal inorganic nanostructures, which are traditionally represented by Ag nanoparticles.[67,176-178] Photoactive nanoparticles that exhibit photothermal conversion or photocatalytic properties have received increasing attention as emerging antimicrobial materials.[179-182] However, their applications are significantly limited when light penetration becomes an issue.[183] In this aspect, magnetic nanoparticles that can be remotely controlled by external magnetic fields show unparalleled advantages.[184] The use of magnetic nanoparicles in magnetic resonance imaging and biosenors is at the frontier of translation research.[93] Of particular interest for therapeutic applications is that heat is generated when magnetic nanoparticles are placed in alternating current magnetic fields as discussed in the literature review section.[185] The dependence of heat induction efficiency on the structure and composition of superparamagnetic oxide nanoparticles has been systematically studied for efficient magnetic hyperthermia of cancer cells.[97,186]

In our design of hybrid antimicrobial nanoparticles, superparamagentic $MnFe_2O_4$ nanoparticles not only can serve as scaffolds for the cationic polycarbonate grafts, their structural integration with the "soft" polymer shell also leads to a synergistic effect of two physical killing mechasisms, namely, membrane damage by the cationic shell and magnetic hyperthermia by the nanoparticle core, giving rise to improved bactericidal activities against both

Gram-positive and Gram-negative bacteria than either of individual modalities. As illustrated in Figure 4.1, the hybrids are absorbed onto bacteria surface through electrostatic interaction, which facilitates membrane destruction process and promote localized heating in alternating magnetic filed. Furthermore, the well-established biocompatibility and biodegradability of both building blocks of the hybrid nanoparticles offer unique opportunities for future translation of this nanoscale platform for practical applications.[187]

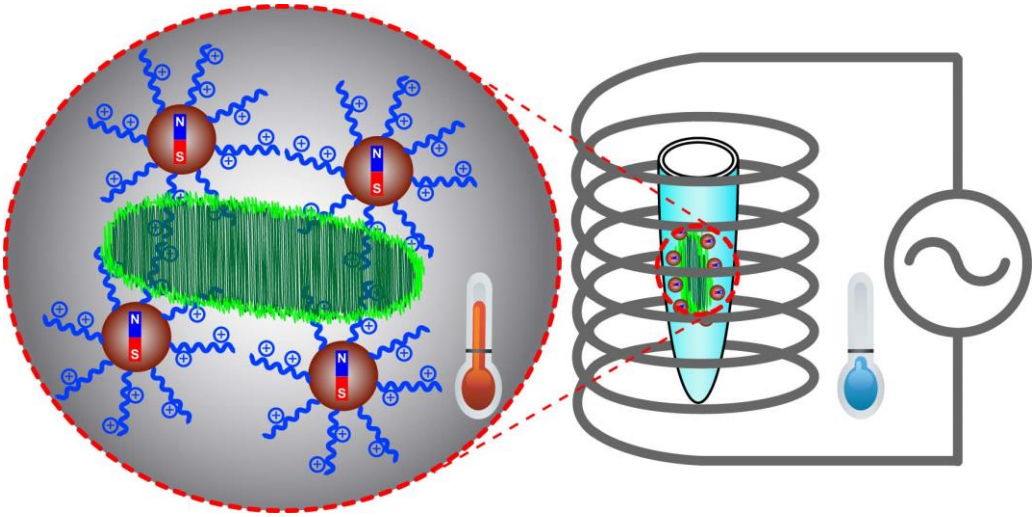

Figure 4.1 Schematic illustration of application of core–shell cationic polycarbonate grafted $MnFe_2O_4$ nanoparticles to kill bacteria.

4.2 Experimental Section

4.2.1 Materials

Dimethyl 2-hydroxyethyl phosphonate were purchased from Tokyo Chemical Industry Co., Ltd. N-(3,5-trifluoromethyl)phenyl-N'-cyclohexylthiourea (TU) was synthesized according to the previous reference.[188]

1,8-diazabicyclo[5.4.0]undec-7-ene (DBU) was dried with CaH_2, distilled, then stored over molecular sieves. Phosphate-buffered saline (PBS) was purchased from BASE and diluted to the desired concentration before usage. Luria Bertani (LB) broth and Bacto Agar were purchased from Becton and Dickinson Company. *E. coli* (ATCC 25922) and *S. aureus* (ATCC 6538) were obtained from ATCC and used according to the protocols. All other chemicals were commercially available from Aldrich and used as received.

4.2.2 Characterization

Nuclear magnetic resonance (NMR) spectra were recorded on a Bruker Avance 300 NMR spectrometer. Zeta potential and hydrodynamic diameter were obtained with BIC PALS ZetaSizer. Fourier-transform infrared (FTIR) spectra were performed on a FTIR-Digilab FTS3100 FTIR spectrometer. Transmission electron microscopy (TEM) images were obtained with JEM 3010 TEM and Field Emission Scanning Electron Microscopy images (FESEM) were taken by JEOL JSM-6700F. Magnetic heating was conducted by Magnetic AC hyperthermia (MACH) system (10 kW Ambrell Easyheat L1). The crystal structural characterization of the samples were characterized using a Shimadzu thin film X-ray diffractometer (XRD) with Cu Kα radiation (λ =0.15406nm). Static magnetic properties were measured on a vibrating sample magnetometer (VSM, ADE Magnetics EV-9). Thermogravimetric analysis (TGA) was carried out by Perkin Elmer TGA/DTA instrument under nitrogen in the temperature range of 100 to 550 °C at a heating speed of 20 °C/min. The number-average molecular weight (M_n) and polydispersity (PDI) of polymers were characterized

by Agilent Infinity-1260 GPC at room temperature with polystyrene as standards and THF as an eluent at a flow rate of 1.0 ml/min, using RID detector.

4.2.3 Synthesis of $MnFe_2O_4$ nanoparticles[189]

The nanoparticle was synthesized according to a method reported by Sun and coworkers. Generally, $Fe(acac)_3$ (0.2 mmol), $Mn(OAc)_2$ (0.1 mmol), oleic acid (2 ml) and benzyl ether (10 ml) were mixed with oleyamine (6.0 mmol) in a 3-neck bottom flask. The reaction temperature was then raised to 120 °C and low boiling point compounds were removed under reduced pressure at this temperature. Next, the temperature was elevated to 290 °C in 20 min under nitrogen flow. Dark-brown colored product (10 nm) were separated by an external magnet after the addition of ethanol.

4.2.4 Synthesis of MTC-$OCH_2CH_2CH_2Br$ (3-bromopropyl 5-methyl-2-oxo-1,3-dioxane-5-carboxylate)

2, 2-Bis(hydroxymethyl)propionic acid (bis-MPA) (9.00 g) and KOH (4.45 g) were dissolved in DMF (50 ml) under 100 °C (1 h) until a homogeneous solution was formed and benzyl bromide (13.80 g) was then added. DMF was then evaporated under vacuum when the solution was cooled to room temperature after 16 h stirring at 100 °C. The residues were dissolved in ethyl acetate/hexane, washed with water twice, dried over $MgSO_4$, filtered and dried under vacuum. The resulting solid was recrystallized from toluene (1.2 ml/g crude) to give a pure benzyl-2,2-bis(methylol)propionate white solid. Yield: 9.59 g (64%). ^{1}H NMR (300 MHz, $CDCl_3$): δ 1.09 (s, -C*H*$_3$), 3.73 (d, -C*H*$_2$OH), 3.92 (d, -C*H*$_2$OH), 5.19 (s, -C*H*$_2$Ar), 7.36 (m, *Ar*H) (Figure 4.2A).

Triethylamine (26.85 g, 266.00 mmol) was added dropwise to a mixture of benzyl-2,2-bis(methylol)propionate (9.59 g, 42.77 mmol), ethyl chloroformate (27.33 g, 251.56 mmol) and tetrahydrofuran (670 ml) at 0 °C in 30 min and the solution was stirred at room temperature for additional 2 h. Then, triethylamine hydrochlorides were filtered off and the resulting filtrates were concentrated under reduced pressure. White crystals **(1)** were obtained after recrystallizing from ethyl acetate. Yield: 4.50 g (42%). ^{1}H NMR (300 MHz, $CDCl_3$): δ 1.34 (s, -C*H*$_3$), 4.22 (d, -C*H*$_a$H$_b$-), 4.70 (d, -CH$_a$*H*$_b$-), 5.22 (s, -C*H*$_2$Ar), 7.35 (m, *Ar*H) (Figure 4.2B).

Monomer **(1)** (4.50 g), ethyl acetate (45 ml) and P_d/C (296 mg) were stirred under H_2 for 24 h. THF (250 ml) was added after the evacuation of the H_2 and the mixtures were filtered through THF-wetted Celite. MTC-OH was obtained as a white solid after the evaporation of filtrates. Yield: 2.20 g (79%). ^{1}H NMR (300 MHz, D_2O): δ 1.18 (s, -C*H*$_3$), 4.61 (d, -C*H*$_a$H$_b$-), 4.70 (d, -CH$_a$*H*$_b$-) (Figure 4.2C).

MTC-OH (2.20 g, 13.75 mmol) was dissolved in a THF (50 ml) with 3 drops of DMF and a solution of oxalyl chloride (3.25 g, 25.00 mmol) in THF (20 ml) was added dropwise to the mixture at 0 °C in 30 min. The reaction was then kept at 50 °C under nitrogen for another 4 h. Then, the volatiles were removed under reduced pressure and the residues were re-dissolved in THF (25 ml). An additional 3-bromopropanol (1.34 g, 9.63 mmol), pyridine (1.2 g, 15.2 mmol) and THF (50 ml) were added at 0 °C in 30 min. The reaction mixture was stirred at 0 °C for another 30 min before it was warmed to room temperature and stirred for 16 h. The precipitate that formed was filtered and volatiles were removed

under reduced pressure. The crude product was then re-dissolved with CH_2Cl_2 (160 ml) and washed with water (3 × 120 ml). The combined organic extracts were dried over $MgSO_4$, filtered and evaporated to give a yellow solid. The crude product was further purified by column chromatography silica (1:1 = ethyl acetate/hexanes). ^{1}H NMR (300 MHz, $CDCl_3$): δ 1.34 (s, -CCH_3), 2.15 (quin, -$CH_2CH_2CH_2$-), 3.62 (t, -CH_2Br), 4.23 (d, -CH_aH$_b$-), 4.38 (t, -OCH_2CH$_2$-), 4.70 (d, -CH$_a$$H_b$-) (Figure 4.2 D).

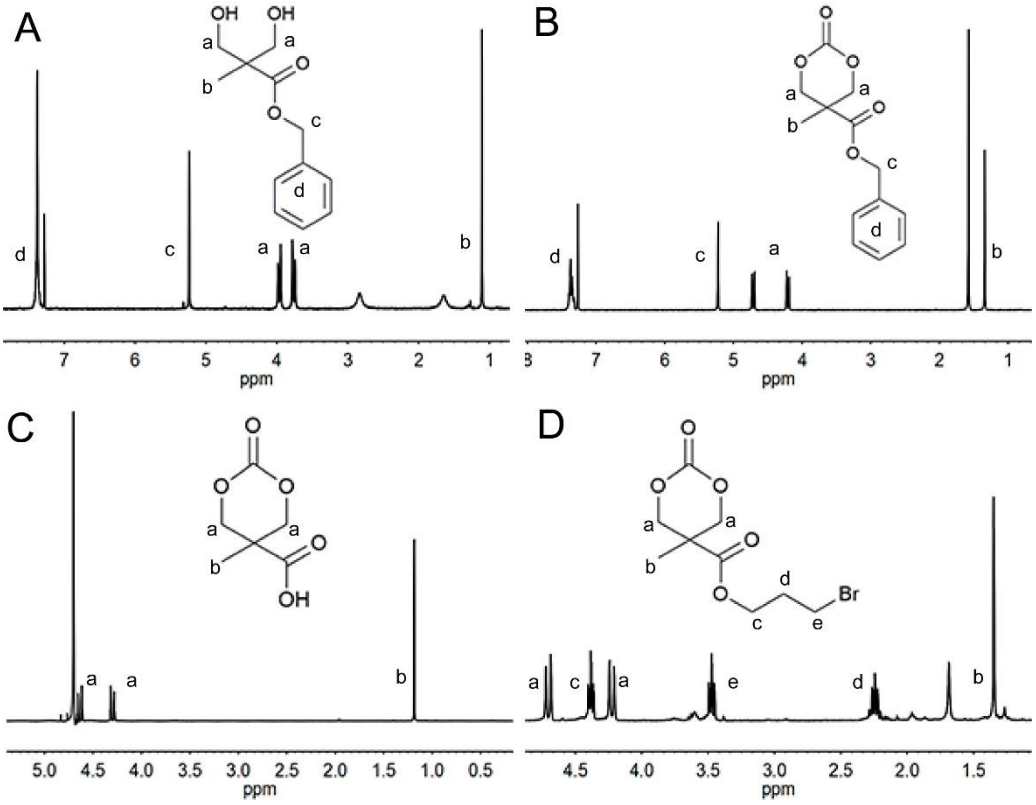

Figure 4.2 ^{1}H NMR spectra of synthesized intermediates and product for MTC-$OCH_2CH_2CH_2Br$.

4.2.5 Synthesis of poly(MTC-$OCH_2CH_2CH_2Br$)[190]

MTC-$OCH_2CH_2CH_2Br$, dimethyl 2-hydroxyethylphosphonate and N-(3,5-trifluoromethyl)phenyl-N'-cyclohexylthiourea (TU) were charged to a vial

with anhydrous methylene chloride (1 ml) at predetermined concentrations. 1,8-diazabicyclo[5,4,0]undec-7-ene (DBU) was then added under nitrogen to start the polymerization and benzoic acid was introduced to quench the reaction after 24 h. The polymer was obtained by precipitation in isopropanol and dried under vacuum. Polymers with two molecular weight were prepared (M_n = 4000, PDI= 1.47; M_n = 6600, PDI = 2.20). ^{1}H NMR (300 MHz, $CDCl_3$): δ 4.51-4.12 (m, -OCH_2- and -CH_2OCOO-), 3.50-3.38 (m, -CH_2Br), 2.26-2.12 (m, -CH_2CH_2Br), 1.31-1.23 (s, -CH_3). ^{31}P NMR (300 MHz, $CDCl_3$): δ 28.68 (-PCH_2-) (Figure 4.3, 4.4A).

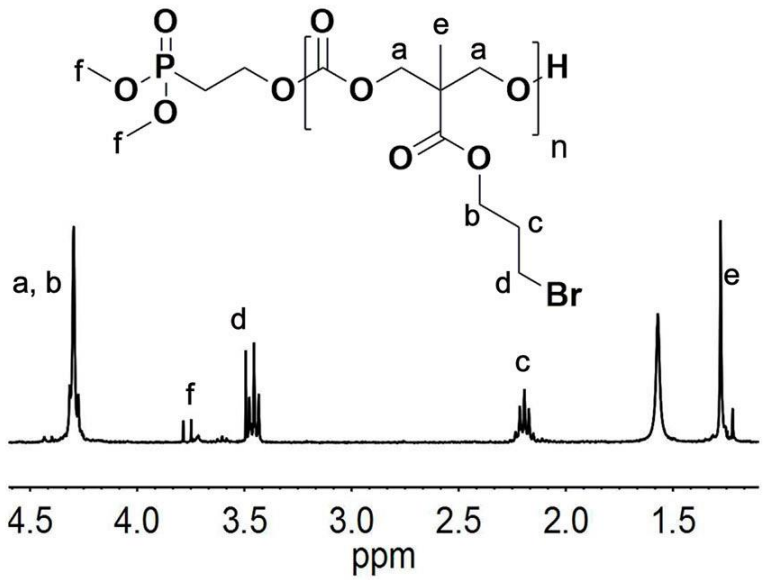

Figure 4.3 ^{1}H NMR spectra of poly(MTC-O$CH_2CH_2CH_2$Br).

4.2.6 Deprotection of poly(MTC-O$CH_2CH_2CH_2$Br)

Trimethylsilylbromide (0.5 g, 3.2 mmol) was added dropwise to a solution of the polymer (0.45 g) in 20 ml anhydrous dichloromethane under nitrogen. The volatiles were then evaporated under reduced pressure after 24 h and methanol (1 ml) was added to the residues after dissolving the polymer with

DMSO (20 ml). The solution was further stirred for 12 h. Deprotected polymer was obtained by precipitating in water twice and then dried under vacuum. ^{31}P NMR (300 MHz, $CDCl_3$): δ 23.40 (-*P*CH_2-) (Figure 4.4B).

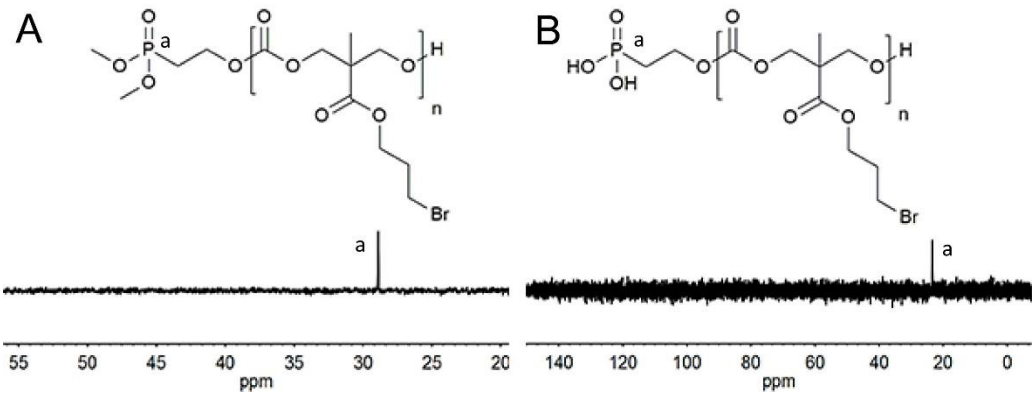

Figure 4.4 ^{31}P NMR spectra for poly(MTC-$OCH_2CH_2CH_2Br$)-methylphosphonate (A) and poly(MTC-$OCH_2CH_2CH_2Br$)-phosphonic acid (B) in $CDCl_3$.

4.2.7 Synthesis of quaternized poly(MTC-$OCH_2CH_2CH_2Br$) (PrBrT)

N, N, N', N'-tetramethylethylenediamine (TMEDA, 0.8 ml, 5.4 mmol) was charged into the vial with the polymer solution (0.4 g polymer, 10 ml DMSO) under nitrogen. After stirring for 24 h at room temperature, the cationic polymer PrBrT was precipitated into THF twice and dried under vacuum. ^{1}H NMR (300 MHz, D_2O): 4.04-4.33 (m, -C*H*$_2$OCOO- and -OC*H*$_2$-), 3.48 (s, br, -C*H*$_2$$N^+$-), 3.09 (s, br, -$N^+$C*H*$_3$), 2.61 (s, br, -NC*H*$_2$-), 2.15 (s, br, -NC*H*$_3$), 2.02 (s, br, -C*H*$_2$$CH_2$ N^+-), 1.17 (s, -C*H*$_3$) (Figure 4.5).

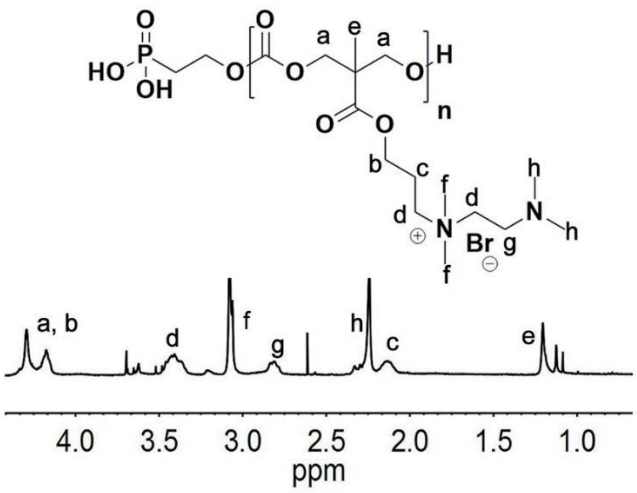

Figure 4.5 ^{1}H NMR spectra of PrBrT.

4.2.8 Synthesis of PrBrT-coated $MnFe_2O_4$ nanoparticles

PrBrT (200 mg in 1 ml DMSO) was added dropwise to the solution of oleic acid-stabilized $MnFe_2O_4$ nanoparticles (10 mg in 10 ml chloroform). The mixture was stirred for 32 h at room temperature and sonicated for 10 min in every hour of the first 8 h. For the polymer of M_n = 6600, a second sample was prepared by stirring for 6 h only ($MnFe_2O_4$@PrBrT-2) to obtain nanoparticles with lower grafting density. Finally, a permanent magnet was applied to collect the nanoparticles and the samples were precipitated by a THF/hexane mixture, and the dispersion/precipitation cycle was repeated 3 times. The obtained nanoparticles were dried under vacuum for further analysis.

4.2.9 Synthesis of $MnFe_2O_4$@PEG

4-Dimethylaminopyridine (DMAP) (3.66 mg) was added to the mixture of CH_3O-PEG-carboxylic acid (MPEG-COOH, M_n = 5000, 300 mg), dimethyl 2-hydroxyethyl phosphonate (150 mg, 1 mmol), N,N’-dicyclohexylcarbodiimide

(61.9 mg) and dichloromethane (20 ml). The mixture was filtered and evaporated after stirring for two days. The product was precipitated with a co-solvent of diethyl ether/acetone for three times and dried to give a white solid mPEG-phosphonate. ^{1}H NMR (300 MHz, $CDCl_3$): δ 3.40 (s, -OCH_3), 3.58 (m, -OCH_2CH_2-), 3.78 (d, -POCH_3) (Figure 4.6A).

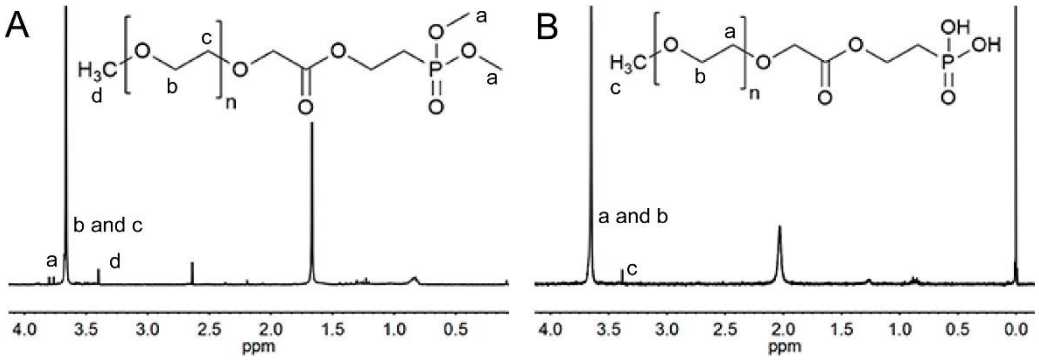

Figure 4.6 ^{1}H NMR spectra for mPEG-methylphosphonate (A) and mPEG-phosphonic acid (B) in $CDCl_3$.

The product obtained (0.25 g) was dissolved in anhydrous dichloromethane (20 ml). Trimethylsilyl bromide (0.5 g, 3.2 mmol) was added dropwise to the mixture under nitrogen. The solvent was evaporated after the reaction was maintained at room temperature for 24 h. The residues were re-dissolved in 5 ml methanol and further stirred for 12 h. A yellow oil mPEG-phosphonic acid was obtained after the evaporation of the volatiles. ^{1}H NMR (300 MHz, D_2O): δ 3.38 (s, -OCH_3), 3.58 (m, -OCH_2CH_2-) (Figure 4.6B).

$MnFe_2O_4$@PEG was synthesized in a similar way as that was used to prepare $MnFe_2O_4$@PrBrT by a ligand exchange reaction as shown in Figure 4.7. A permanent magnet was utilized to collect the magnetite nanoparticles and the obtained nanoparticles were dried under vacuum for further analysis.

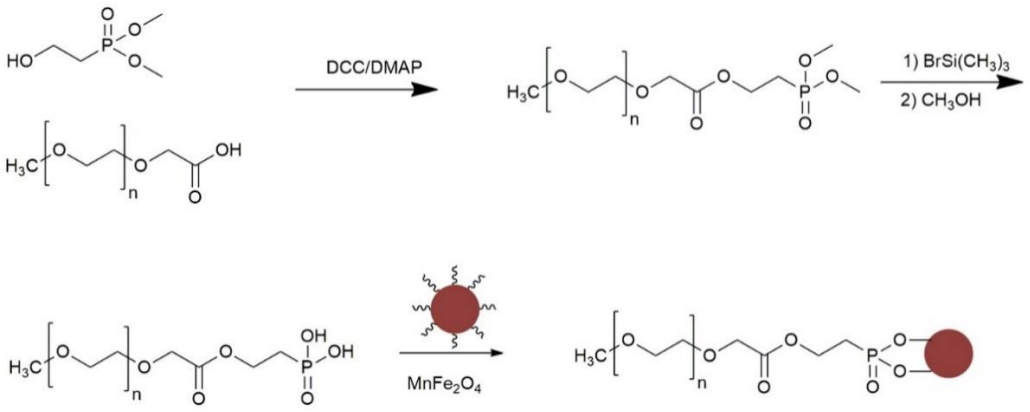

Figure 4.7 Schematic representation of $MnFe_2O_4$@PEG synthesis.

4.2.10 Cell preparation

A single colony of both *Escherichia coli* and *Staphylococcus aureus* were inoculated in Luria-Bertani (LB) medium (T = 37 °C) overnight (shaking at 200 rpm) and harvested in the mid-exponential growth phase. After centrifugation at 6000 rpm for 10 min, cells were washed with PBS solution 3 times and the final cell pellets were dispersed and diluted to the desired concentration. Cell concentration was verified by plating dilutions of inoculum onto agar plates.

4.2.11 Cell viability test

200 µl of bacteria (10^5-10^6 CFU/ml) in sterilized PBS were placed into 2 ml tubes. In each tube, 200 µl saline solution of the test materials at different concentrations was added and PBS buffer was used as a control. Votex (30 min at 300 rpm) was applied to cells before samples underwent serial dilutions. For cells to undergo magnetic hyperthermia treatment, after vortex (10 min), the treatment was conducted for 20 min using an alternating current of 380 A for *E. coli* and 410 A for *S. aureus,* respectively. Finally, 100 µl aliquots from each dilution were spread onto agar plates and grown overnight at 37 °C for counting

survivors. To measure the localized temperature exerted on bacteria, a mixture of 120 μg/ml $MnFe_2O_4$@PrBrT and bacteria suspension (10^5 to 10^6 CFU/ml) were shaken for 10 min and centrifuged to remove supernatant. The sample temperature profiles of the mixture in solution form and the sediment under magnetic heating were recorded by an infrared thermographic camera (FLIR T420) after the treatment.

4.2.12 Minimum inhibitory concentrations (MICs)

A series of dilution of 100 μl material in LB broth was made on a 96-well microplate, followed by addition of 100 μl bacteria suspensions (~10^5 CFU/ml). The microplate was kept at 37 °C for 48 h. The solution absorbance at 600 nm was read by a microplate spectrophotometer. The solution without materials was used as control. Each sample was repeated in triplicate.

4.2.13 Live/Dead assay

Cells (10^8 CFU/ml) were prepared in a similar way as stated above. The samples were then stained with LIVE/DEAD BacLight Bacterial Viability kit for 15 min at room temperature and the bacterial viability was assessed by an Olympus IX71 inverted microscope.

4.2.14 Samples for cell morphology observation

Cells at a concentration of 10^8 CFU/ml in sterilized PBS were placed into 2 ml tubes and cells suspended in PBS buffer were used as a control. Cells were homogeneously suspended by vortex (300 rpm, 30 min). In case of cells exposed to hyperthermia treatment (20 min), vortex (10 min at 300 rpm) was done before

the treatment. Subsequently, cells were fixed with 2% glutaraldehyde for overnight. The solution was spread onto glasses and dried. The samples were dehydrated with sequential treatments by 30, 50, 70, 80, 90, 100% ethanol for 20 min and then dried again.

4.2.15 Hemolysis assay

Fresh human blood (3.5 ml), donated by a healthy volunteer, was centrifuged at 700 rpm for 5 min and washed three times. The final concentrated erythrocytes was diluted to 5% by PBS. The $MnFe_2O_4$@PrBrT at different concentrations (100 μl) was mixed with 100 μl erythrocytes stock. The mixture was shaken at 37 °C for 1 h at a speed of 150 rpm, and was then centrifuged. 100 μl of supernatant was added to 96-well microplate and diluted with 100 μl PBS. The hemoglobin release was determined by measuring absorbance at 576 nm using a microplate reader. 0.1% Triton X-100 was used as a positive control and pure PBS served as a negative control. The hemolysis percentage was calculated using the equation below:

$$Hemolysis(\%) = \frac{A_p - A_b}{A_t - A_b} \times 100\% \qquad \text{Equation 4.1}$$

Where A_p, A_t and A_b is the absorbance value for the sample, positive control and negative control, respectively.

4.3 Results and discussion

4.3.1 Synthesis of cationic polycarbonate

The biodegradable polycarbonates were synthesized by ring opening polymerization (ROP) of MTC-$OCH_2CH_2CH_2Br$ monomer at room temperature with DBU/TU as the catalyst and dimethyl 2-hydroxyethyl phosphonate as the initiator (Figure 4.8). We prepared poly(MTC-$OCH_2CH_2CH_2Br$) with M_n of 4000 (PDI= 1.47) and 6600 (PDI = 2.20) g/mol (Figure 4.9A), which correspond to a repeating unit of 14 and 23, respectively.

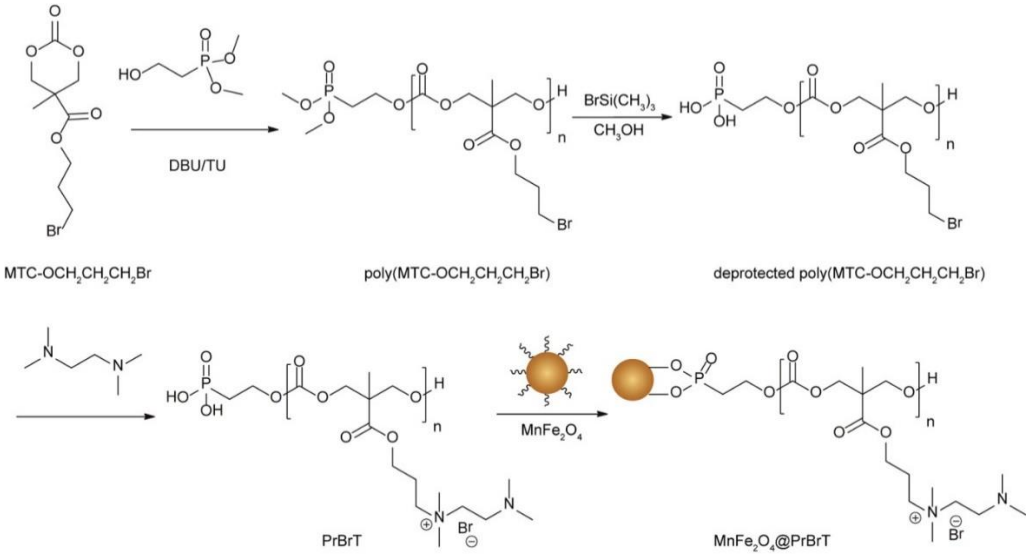

Figure 4.8 Synthesis of cationic polycarbonate PrBrT and $MnFe_2O_4$@PrBrT core–shell nanoparticles.

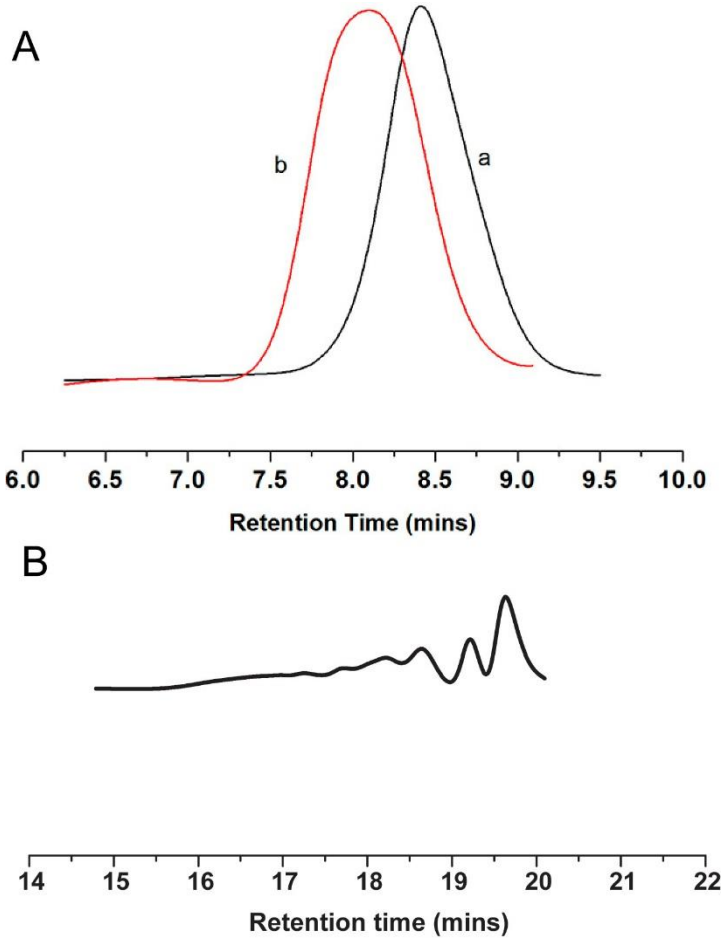

Figure 4.9 GPC curves of poly(MTCOCH$_2$CH$_2$CH$_2$Br): (a) M_n= 4000 Da, PDI = 1.47; (b) M_n = 6600 Da, PDI = 2.20 (A) and the polymer stored for two years at room temperature (B).

Subsequently, the methyl protective groups of the phosphonate initiator were removed to obtain the polycarbonate with a phosphoric acid chain end. Quarternization of poly(MTC-OCH$_2$CH$_2$CH$_2$Br) was conducted using excess amount of TMEDA, leading to cationic PrBrT$_m$ with m representing the number of repeating units. ^{1}H NMR (Figure 4.5) confirmed that 100% of bromide was converted into quaternized amine after the reaction.

To test the degradability of the materials, after the material has been stored for two years at room temperature, the molecular weight was tested as

shown in Figure 4.9B. The molecular weight of the polymer degraded to about five different peaks with molecular weight distribution of 2924, 972, 668, 444 and 271 g/mol, confirming the biodegradability of the polymer.

4.3.2 Antimicrobial assessment of cationic polycarbonate

We next tested the antimicrobial activity of the PrBrT polymer. As shown in Figure 4.10, $PrBrT_{14}$ does not kill *E. coli* until the concentration reaching 12.5 mg/ml, and kills 100% of live *E. coli* at a concentration of 100 mg/ml. The effective killing of PrBrT against *S. aureus* is similar to *E. coli*, starting to suppress *S. aureus* at 25 mg/ml.

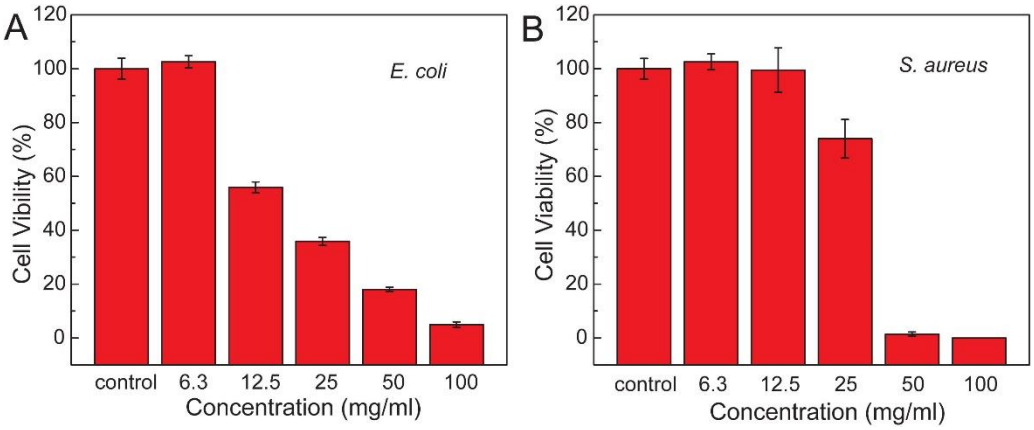

Figure 4.10 Dependence of bacteria cell viability on $PrBrT_{14}$ concentrations on: *E. coli* (A) and *S. aureus* (B).

4.3.3 Synthesis of colloidal $MnFe_2O_4$ nanoparticles

High temperature colloidal synthesis of $MnFe_2O_4$ nanoparticles using $Fe(acac)_3$ and $Mn(OAc)_2$ as precursors led to 10 nm nanoparticles capped by oleic acids (Figure 4.11A).[189,191] XRD of the synthesized nanoparticles (Figure 4.11B) exhibit eight characteristic peaks, which are consistent with (220), (311),

(222), (400), (422), (511), (440) and (531) crystal planes of $MnFe_2O_4$ (JCPDS No. 75-0034). Magnetic hysteresis loop (Figure 4.11C) of the nanoparticle at room temperature shows the absence of coercivity and remanence with saturation magnetization (M_s) of 53 emu/g, confirming its superparamagnetic nature.

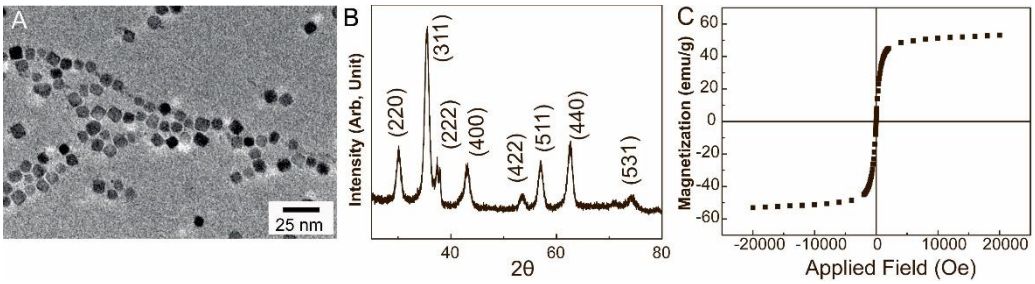

Figure 4.11 (A) TEM image of $MnFe_2O_4$ nanoparticles capped with oleic acid. (B) XRD pattern of $MnFe_2O_4$ nanoparticles. (C) Hysteresis loop of $MnFe_2O_4$ nanoparticles at room temperature.

4.3.4 Synthesis of $MnFe_2O_4$@PrBrT and $MnFe_2O_4$@PEG

The phosphoric acid end group of cationic PrBrT polymers has a greater affinity with metal ions on the nanoparticle surface than that of carboxylic groups of oleic acid capping ligands, allowing for grafting the polymers on the nanoparticles by means of ligand exchange.[175,192] After the reaction with $PrBrT_{14}$, the 10 nm nanoparticles, which originally were only dispersible in non-polar solvents such as hexane and chloroform, showed excellent colloidal stability in aqueous media, indicative of a successful ligand exchange. Zeta potential of $MnFe_2O_4$@$PrBrT_{14}$ in deionized water is 49.0 ± 2.9 mV, indicating a high graft density of the cationic PrBrT polymer. TEM observation (Figure 4.12A) reveals individual nanoparticles without large clusters. In line with this observation, DLS measurement showed that the $MnFe_2O_4$@$PrBrT_{14}$ core-shell nanoparticles have

a hydrodynamic diameter of 17 nm. The nanoparticles coated with poly(ethylene glycol) (PEG) ($MnFe_2O_4$@PEG), which would be used as a control in antimicrobial tests, were prepared in a similar way using phosphoric acid-ended PEG and showed a zeta potential of −1.3 ± 1.2 mV.

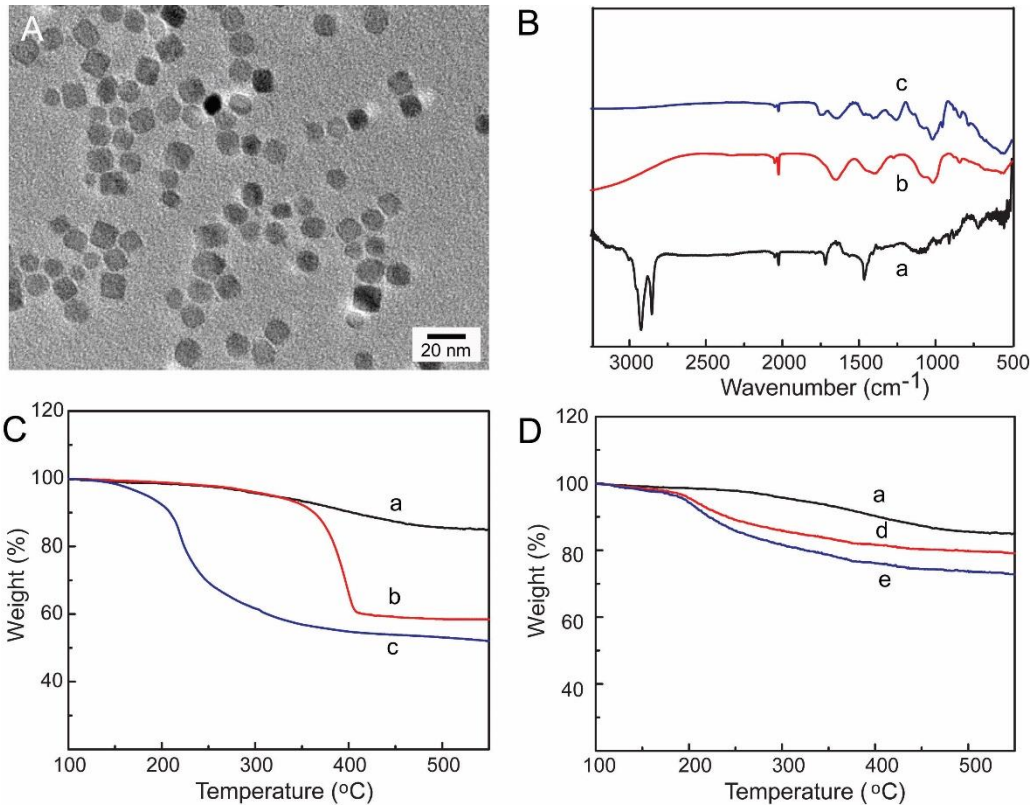

Figure 4.12 (A) TEM images of $MnFe_2O_4$@$PrBrT_{14}$ nanoparticles. (B) FTIR spectra and (C) TGA results of oleic acid capped $MnFe_2O_4$ (a), $MnFe_2O_4$@PEG (b), and $MnFe_2O_4$@$PrBrT_{14}$ (c) nanoparticles. (D) TGA curves of oleic acid capped $MnFe_2O_4$ (a), $MnFe_2O_4$@$PrBrT_{23}$-2 (d), and $MnFe_2O_4$@$PrBrT_{23}$-1 (e) nanoparticles.

The presence of polymers on the surface of the $MnFe_2O_4$@$PrBrT_{14}$ nanoparticles was verified through FT-IR spectroscopy (Figure 4.12B) and the amount of grafted polymer was quantified by TGA (Figure 4.12C). In the FT-IR spectrum of the original nanoparticles (Figure 4.12B curve a), two sharp bands

at 2920 and 2840 cm^{-1} are attributed to the asymmetric and symmetric CH_2 stretch vibration of oleic acid. The peak at 1750 cm^{-1} arising from the C=O stretch vibration only appears in the spectrum of $MnFe_2O_4$@PrBrT, suggesting the successful functionalization of PrBrT onto $MnFe_2O_4$ nanoparticles.[39] Similarly, the presence of C-O-C stretch vibration at 1030 cm^{-1} for the PEGylated nanoparticles indicates the successful ligand exchange with phosphoric acid-ended PEG. More quantitative results were obtained from TGA. Between 120 and 400 °C, the weight loss of oleic acid capped $MnFe_2O_4$ nanoparticles is 15%, while the weight loss increases to 40% for $MnFe_2O_4$@PEG and 42% for $MnFe_2O_4$@PrBrT grafting of the polymers.

The number of chains of polymers grafted onto nanoparticle surfaces can be calculated by the following method. Taking $MnFe_2O_4$@ $PrBrT_{14}$ for example, firstly, the weight of polymer was divided by the molecular weight of the polymer and multiplied by Avogadro's number to calculate the number of polymer molecules lost. Then, the weight of total nanoparticles was divided by weight of one nanoparticle to obtain the number of $MnFe_2O_4$ nanoparticles. The weight of one nanoparticle can be calculated from the volume and density (5.368 g/cm^3). As one nanoparticle diameter is around 10 nm. The calculated nanoparticle (NP) weight is around 2.809×10^{-18} g/NP. The average number of polymer grafts can be calculated by Equation 4.2, where weight fraction of the polymer is 42% and the rest is nanoparticle core weight fraction. It is thus estimated that on average 213 $PrBrT_{14}$ chains were grafted on the nanoparticle at a graft density 0.68 chain/nm^2.

$$N_{\text{grafts per nanoparticle}} = \frac{W_{\text{polymer}} / M_{\text{polymer}}}{W_{\text{MnFe2O4 nanoparticle}} / M_{\text{MnFe2O4 nanoparticle}}}$$

Equation 4.2

Notably, ligand exchange with $PrBrT_{23}$ gave rise to $MnFe_2O_4$@$PrBrT_{23}$-1 nanoparticles with a polymer weight fraction of 29% (Figure 4.12D curve e) and a graft density of 0.36 chain/nm^2. The lower graft density should result from a combination effect of the lower content of functional ends and more significant steric hindrance in "grafting to" reactions of the longer polymer chains. To examine the impact of polymer graft density on the antimicrobial activity of the nanoparticles, $MnFe_2O_4$@$PrBrT_{23}$-2 nanoparticles with a graft density of 0.25 chain/nm^2 (Figure 4.12D curve d) were prepared by terminating the ligand exchange reaction at 6 h. Moreover, measurements show that $MnFe_2O_4$@$PrBrT_{23}$-1 had a zeta potential of 36.1 ± 0.9 mV, which further decreased to 20.8 ± 1.0 mV in $MnFe_2O_4$@$PrBrT_{23}$-2.

4.3.5 Antimicrobial assessment of the hybrid material with or without hyperthermia effect

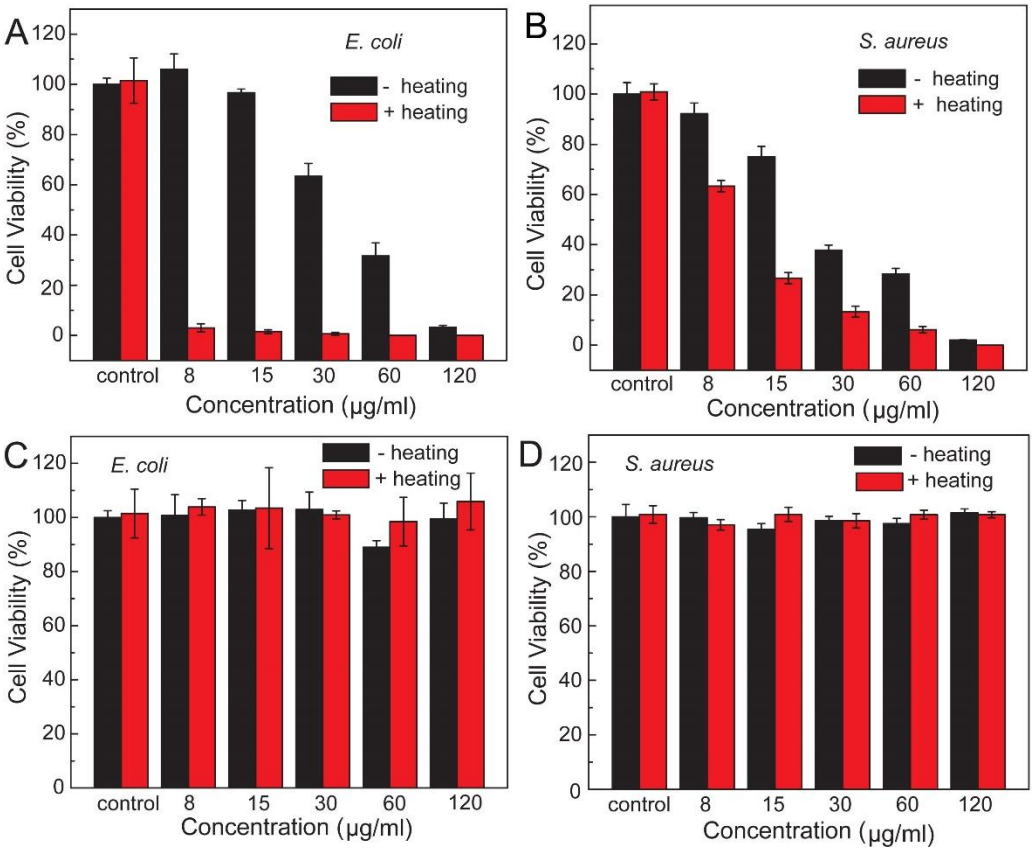

Figure 4.13 Dependence of bacteria cell viability on $MnFe_2O_4$@$PrBrT_{14}$ concentrations and magnetic hyperthermia treatment: *E. coli* (A) and *S. aureus* (B) exposed (red) or not exposed (black) to magnetic heating. Dependence of bacteria cell viability on $MnFe_2O_4$@PEG concentrations and magnetic hyperthermia treatment: *E. coli* (C) and *S. aureus* (D) exposed (red) or not exposed (black) to magnetic heating.

We evaluated the antibacterial effect of $MnFe_2O_4$@$PrBrT_{14}$ core-shell nanoparticles on both Gram-negative bacteria *E. coli* and Gram-positive bacteria *S. aureus*. Figure 4.13 shows that bacteria cell killing efficiency of the hybrid nanoparticles is dependent on their concentrations. For *E. coli* bacteria,

$MnFe_2O_4$@$PrBrT_{14}$ doesn't kill any cells at a concentration of 8 μg/ml. However, increasing the concentration from 15 to 120 μg/ml, the killing efficiency increases from 3 to 97%. Similarly, the *S. aureus* killing efficiency (from 7 to 98%) also rises with the increasing concentrations of the nanoparticles (from 8 to 120 μg/ml). Notably, the effective concentration of the $MnFe_2O_4$@$PrBrT_{14}$ decreased by 3 orders of magnitude in comparison with that of PrBrT polymer alone. As summarized in Table 4.1, minimum inhibitory concentrations (MICs) of the free polymers and the $MnFe_2O_4$@$PrBrT_{14}$ nanoparticles also showed 3 orders of differences.

Table 4.1 Antimicrobial activities of $PrBrT_{14}$ and $MnFe_2O_4$@$PrBrT_{14}$.

Material	MIC (μg/ml)	
	S. aureus	*E. coli*
PrBrT	100,000	>100,000
$MnFe_2O_4$@PrBrT	240	480

Positively charged polymers kill bacteria by means of electrostatic interaction with net negatively charged bacteria, which leads to cell membrane disruption, leakage of intracellular components and finally cell death. Therefore, the charge density of the polymers is a critical element that determines antibacterial efficiency. Grafting a large number of PrBrT on the same nanoparticles concentrates the cationic quaternary amine and affords a greater charge density, which results in a considerably improved antimicrobial activity. This analysis was further supported by the decreasing bacteria killing efficiency of $MnFe_2O_4$@$PrBrT_{23}$-1 and $MnFe_2O_4$@$PrBrT_{23}$-2. For example, at 120 μg/ml,

$MnFe_2O_4$@PrBrT_{23}-1 led to a killing efficiency of 57% for *E. coli* and 80% for *S. aureus*, which dropped to 40% and 72% for $MnFe_2O_4$@PrBrT_{23}-2 (Figure 4.14). Importantly, $MnFe_2O_4$@PrBrT nanoparticles also caused minimal hemolysis (<3%) at concentrations up to 1mg/ml (Figure 4.15), indicative of their excellent biocompatibility and great potential for translation studies.

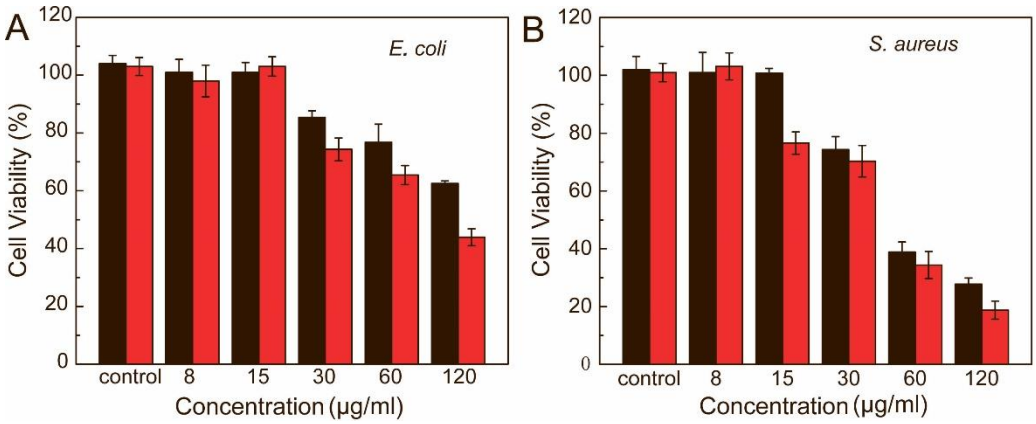

Figure 4.14 Dependence of bacteria cell viability on the concentration of $MnFe_2O_4$@PrBrT_{23}-1 (red) and $MnFe_2O_4$@PrBrT_{23}-2 (black) concentrations for *E. coli* (A) and *S. aureus* (B).

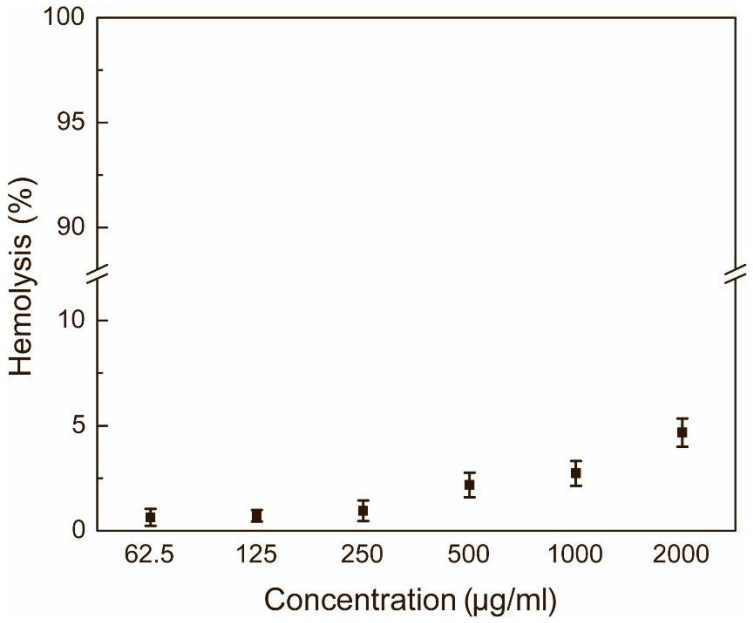

Figure 4.15 Hemolysis of $MnFe_2O_4$@$PrBrT_{14}$ nanoparticles at different concentrations.

We next investigated the magnetic hyperthermia effect of $MnFe_2O_4$@$PrBrT_{14}$ nanoparticles on bacteria killing in Figure 4.13. In an alternating current magnetic field, superparamagnetic nanoparticles generate heat via Néel and Brownian relaxation. Here, for *E. coli*, the killing efficiency experienced a sharp increase from nearly zero to 97% at a concentration of 8 μg/ml, which further reached 100% at 60 μg/ml. The killing efficiency of *S. aureus* showed a similar trend in response to magnetic hyperthermia, reaching 94% and 100% at 60 and 120 μg/ml, although the killing efficiency of *S. aureus* at lower concentrations is not as significant as that of *E. coli*.

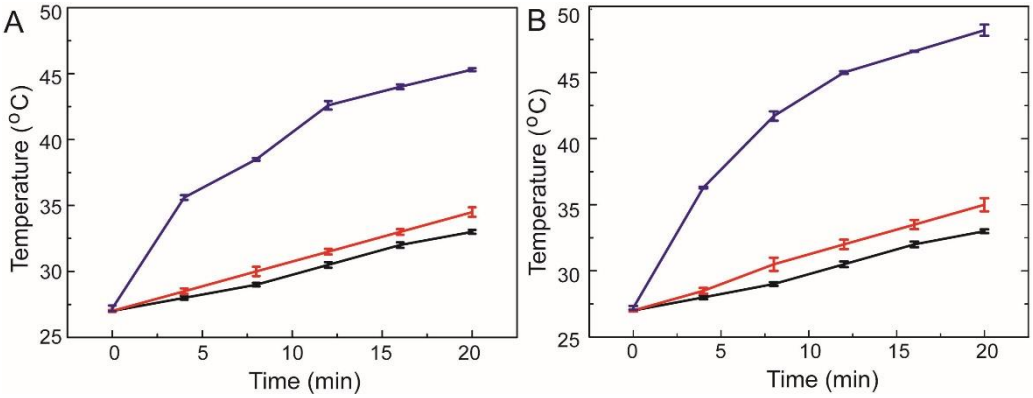

Figure 4.16 Temperature profiles of pure PBS (black), $MnFe_2O_4$@PrBrT (120 μg/ml) dispersion (red), $MnFe_2O_4$@ $PrBrT_{14}$-bound bacteria (blue) by heating at 380 A for *E. coli* (A) and at 410 A for *S. aureus* (B), respectively.

The dramatic enhancement in bacteria cell killing efficiency of the hybrid nanoparticles under magnetic heating should result from the localized heating effect of $MnFe_2O_4$ attached on bacteria cell surface, which kills the bacteria in synergy with cationic polymers.[193] Measurements (Figure 4.16) by an infrared thermographic camera showed that the temperature of the nanoparticle dispersion at the concentration of 120 μg/ml had an increase of 8 °C and reached 35 °C after a treatment at 380 A for 20 min, which is only 2 °C higher than that of PBS control solution. In contrast, the nanoparticle-bound *E. coli* separated by centrifugation had a temperature 45 °C after the treatment and *S. aureus* treated at 410 A reached 48 °C which are strong evidence of localized heating. The collective antimicrobial effect of two physical killing mechanisms imparted by the $MnFe_2O_4$@PrBrT holds great promise in addressing multidrug resistance of superbugs because these mechanisms are believed to have less susceptibility of developing resistance. It is also interesting to see that neutrally charged $MnFe_2O_4$@PEG nanoparticles did not cause any bacterial death even under magnetic heating. PEGylation is known to afford non-fouling surfaces.

Apparently, since these nanoparticle are not able to attach on bacterial surfaces, the heating is mostly in the medium rather than localized on the bacterial surface. Thus, when the heat is dissipated, temperature change experienced by the bacterial is not enough to cause cell death. The results further highlighted the importance of the synergetic action of cationic charge polymer coating and the superparamagnetic nanoparticle core.

4.3.6 Live/Dead bacteria viability analysis

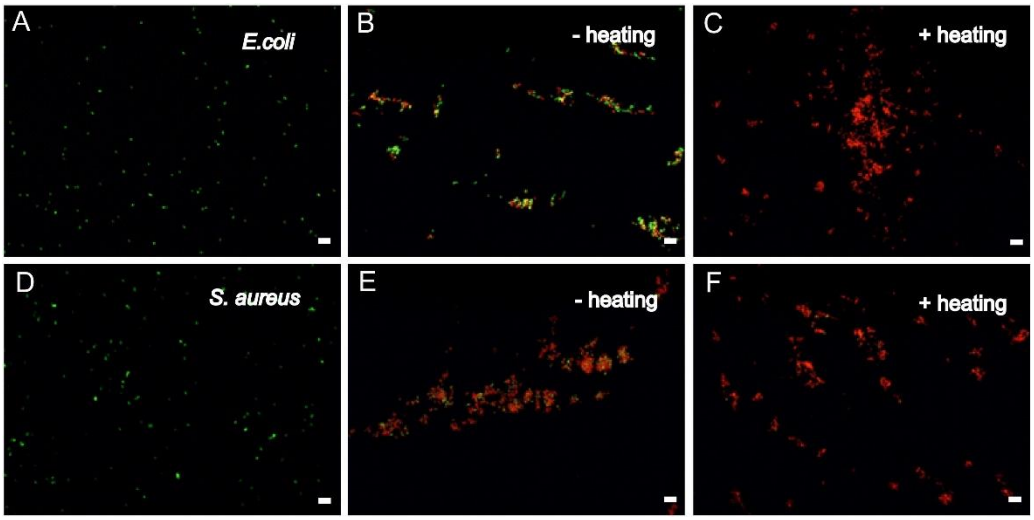

Figure 4.17 Fluorescence images of bacteria: (A, D) control *E. coli* and *S. aureus*, (B, E) *E. coli* and *S. aureus* without exposing to magnetic heating after incubation with $MnFe_2O_4$@$PrBrT_{14}$, and (C, F) *E. coli* and *S. aureus* exposing to magnetic heating for 20 min after incubation with $MnFe_2O_4$@$PrBrT_{14}$ for10 min. scale bar =10 μm.

Live/Dead analysis was performed to visualize the death of bacterial cells by staining bacteria with Baclight kit utilizing a mixture of SYTO® 9 and propidium iodide (PI). Stained dead cells and live cells show red and green fluorescence, respectively. Figure 4.17A,D shows that both *E. coli* and *S. aureus*

are alive in untreated control samples. A mixture fluorescence of red and green in Figure 4.17B,E confirms that there are membrane damage generated after the treatment because the cell-impermeant PI dye stained the cells, indicating that bacteria cells are partially killed after incubation with $MnFe_2O_4$@$PrBrT_{14}$. However, almost all bacteria cells are dead in Figure 4.17C,F after an extra magnetic heating, which is in line with the antimicrobial results discussed above, supporting the effectiveness of bacteria killing by the synergistic effect of $MnFe_2O_4$@PrBrT nanoparticles.

4.3.7 Bacteria morphology analysis

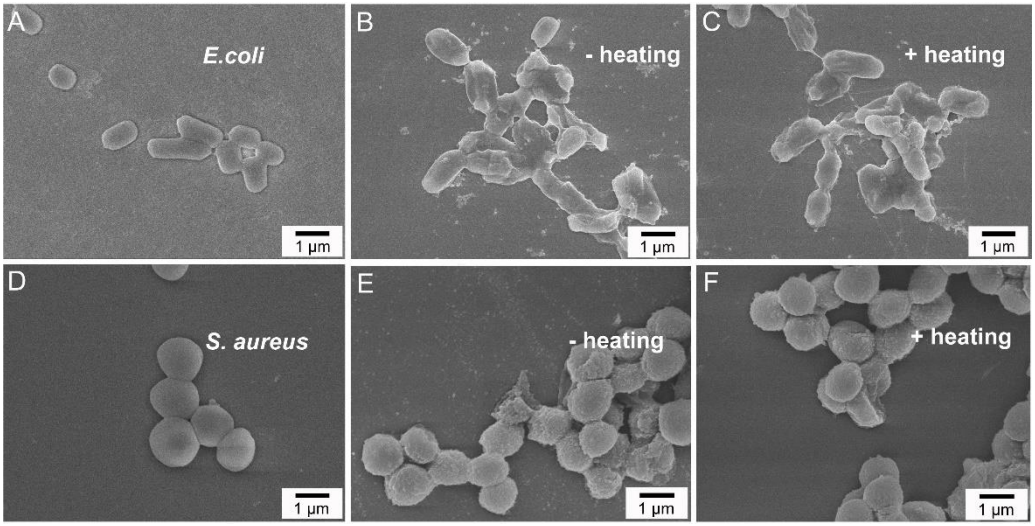

Figure 4.18 SEM images of bacteria: untreated *E. coli* (A) and *S. aureus* (D) cells, *E. coli* (B) and *S. aureus* (E) without exposing to magnetic heating after incubation with $MnFe_2O_4$@$PrBrT_{14}$, and *E. coli* (C) and *S. aureus* (F) exposed to magnetic heating for 20 min after incubation with $MnFe_2O_4$@PrBrT for 10 min.

We finally examined the morphological changes of bacteria cell after the antimicrobial treatment. Figure 4.18A,D shows the SEM images of the control

sample, while Figure 4.18B,E and C,F show *E. coli* and *S. aureus* bacteria treated by $MnFe_2O_4$@$PrBrT_{14}$ without and with magnetic heating. In contrast to the smooth surface of the control bacteria, the bacteria treated by $MnFe_2O_4$@$PrBrT_{14}$ display collapsed cell envelopes, indicative of the physical damage of the cell membrane and release of intracellular components. No obvious difference was observed for bacterial undergoing magnetic heating, which is not surprising because magnetic heating also is expected to cause membrane damage.

The result is consistent with our hypothesis in the objective section. Localizing cationic polymers onto nanoparticle surfaces achieves a high positive zeta potential, which facilitates killing of bacteria, with the higher charges the higher efficiency because higher charges improve the attachment of materials onto bacteria surface, which is the first step in the killing mechanism of the cationic materials. As cationic nanoparticles kill bacteria after they attach to bacteria surface, they also act as heating pots under the magnetic field to generate local heating and synergistically kill bacteria. The combined effect improves killing efficiency to a higher level. Besides, here the bacteria destroy cell membrane based on both mechanical destruction and heating effect. Multi-mechanism killing further reduces the chance of resistance generation.

4.4 Conclusion

In summary, we have successfully synthesized biodegradable cationic polycarbonates grafted superparamagnetic nanoparticles. Our results have demonstrated that structural integration of the "soft" polycarbonate shell and the "hard" superparamagnetic core in the hybrid nanoparticles core offers the

possibility of exerting synergistic dual-modality physical killing resulting from membrane disruption by cationic polymeric shell and magnetic heating by the nanoparticle core. The hybrid nanoparticles could effectively kill both *E. coli* and *S. aureus* at a much lower concentration and the killing efficiency could increase to a much higher level. We envision that the development of the new synergetic antibacterial hybrid nanoparticles could find broad applications in therapy and medical devices.

4.5 Declaration

This work presented in this chapter has been published in Biomaterials Science. Reproduced by permission of The Royal Society of Chemistry.

Pu, L.; Xu, J.; Sun, Y.; Fang, Z.; Chan-Park, M. B.; Duan, H. *Biomaterials Science* **2016**, *4*, 817.

Chapter 5. Lipase-sensitive vesicle for on demand antibiotic delivery

5.1 Introduction

Besides looking for alternative antimicrobial materials as in previous two projects, which may not keep effectiveness for a long time since bacteria might carry on developing resistance, novel drug delivery systems are also explored to address the challenges related with conventional antibiotics such as over dosage, limited solubility and stability in physiological conditions and non-specific targeting towards bacteria.[194-197] Despite the application of antibiotics as primary weapon for bacteria control, their overconsumption and inappropriate usage create increasing emergency towards bacteria resistance.[20,36,38] Bacterial pathogens find ways to survive in mammalian cells to escape from host defences and antimicrobial therapy where antibiotics are difficult to penetrate because of their hydrophilicity or achieve high enough effective concentration due to the limitation of pH or enzymatic inactivation, resulting in low killing effectiveness and high drug dose requirement.[198-200] The new delivery systems are suitable to improve therapeutic efficiency for both existing drugs and those that will be developed in future.[161]

Various kinds of nanocarriers such as liposomes, polymeric nanoparticles, dendrimers and solid lipid nanoparticles have been developed for efficient delivery of antibiotics to infection site and accurate control of amount and frequency, reducing over usage of drugs and related toxicities.[160,201-205] In particular, the use of polymers in the delivery system opens the door for triggered

drug release by specific physiological conditions or metabolic states such as pH, toxins and lipases as discussed in the literature review section.[155,158,160]

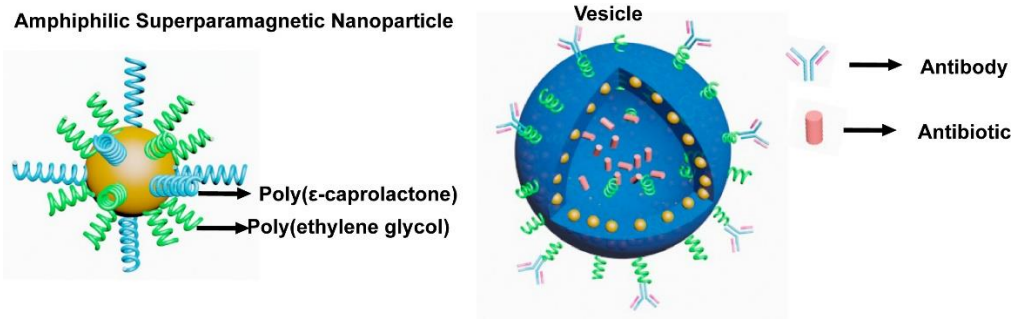

Figure 5.1 Schematic illustration of superparamagnetic nanoparticles coated with both PEG and PCL grafts and the antibiotic-loaded vesicle tagged with anti-*S. aureus* antibody.

Here we prepared one antibiotic loaded lipase-sensitive vesicles assembled from manganese iron oxide nanoparticles grafted with hydrophilic polyethylene glycol and hydrophobic poly(ε-caprolactone) ($MnFe_2O_4$@PEG/PCL) and investigated both the selective bacterial growth inhibition performance by the antibiotic deliver vesicles and their magnetic enrichment effect on bacteria. $MnFe_2O_4$ superparamagnetic nanoparticles coated with mixed brushes of end functional PEG and PCL were first synthesized by ligand exchange. Then, the functional vesicles with hydrophobic brushes and nanoparticles embedded in vesicle shell and the hydrophilic PEG extending into aqueous solution were prepared by film rehydration method, as illustrated in Figure 5.1. Active targeting vesicles to bacteria (*S. aureus*) was achieved by vesicle surface antibody conjugation.[206]

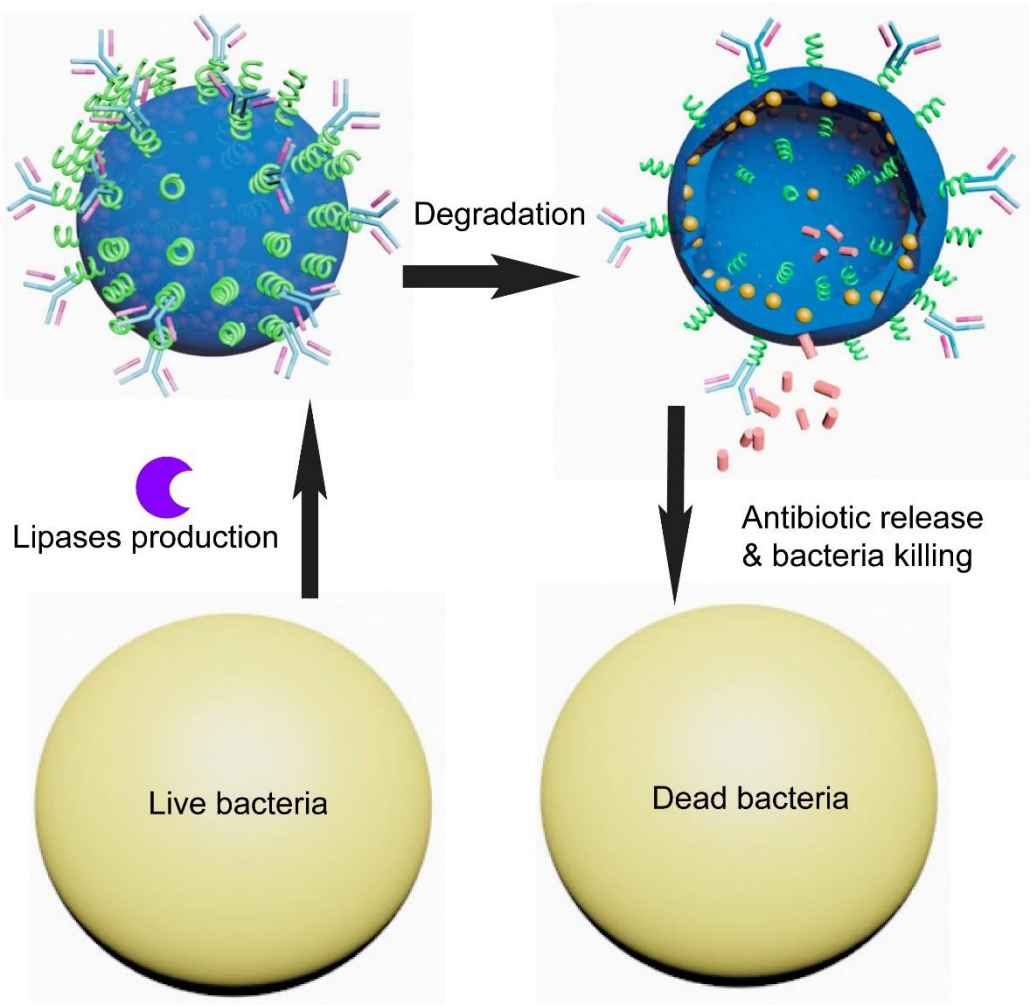

Figure 5.2 Schematic illustration of the antibiotic release stimulated by lipase secreting bacteria for antibacterial application using antibiotic-loaded vesicles.

On one hand, the assemblies with a hollow cavity act as antibiotics carriers to prevent premature antibiotic leakage and achieve antibiotic release for specific bacteria with PCL degradation induced structure dissociation (Figure 5.2). In this way, the vesicles demonstrated the on-demand antibiotic release and selective bacteria growth inhibition since bacteria lipases are produced by specific bacteria species such as *S. aureus* while absent in other types, such as *E. faecalis*.[207,208] On the other hand, superparamangentic nanoparticles exhibit unique benefits, such as response to external magnetic force and high surface to

volume ratio.[151] In our design, $MnFe_2O_4$ nanoparticles not only provide platform for polymer grafts, but also enable easy separation of vesicles. The antibody-conjugated vesicles show smart *S. aureus* recognition and enrich themselves together with the captured bacteria after magnetic separation, elevating the bacteria killing efficiency up to sixteen times, as presented in Figure 5.3.

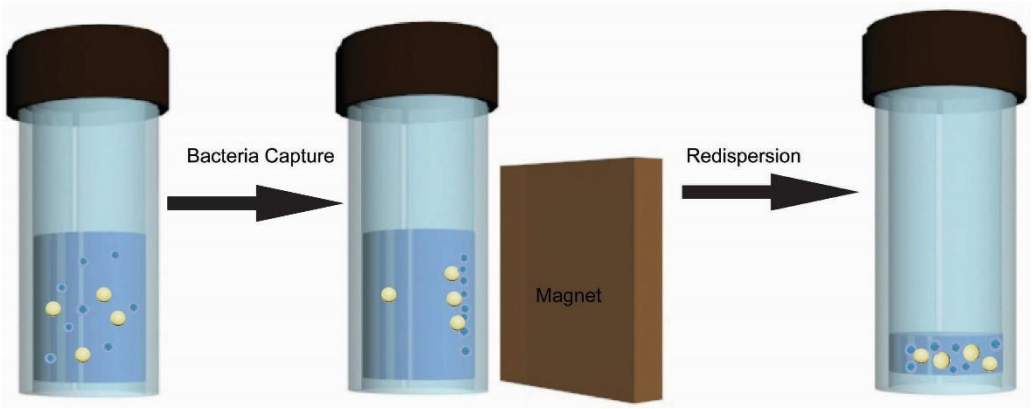

Figure 5.3 Schematic illustration of enrichment process of antibody conjugated and antibiotic loaded vesicles to enhance bacteria killing efficiency.

5.2 Experimental section

5.2.1 Materials

Dimethyl 2-hydroxyethyl phosphonate were purchased from Tokyo Chemical Industry Co., Ltd. Phosphate-buffered saline (PBS) was purchased from BASE and diluted to the desired concentration before usage. Luria Bertani (LB) broth and Bacto Agar were purchased from Becton and Dickinson Company. *E.faecails* (ATCC29212) and *S. aureus* (ATCC 6538) were obtained from ATCC and used according to the protocols. All other chemicals were commercially available from Aldrich and utilized as received.

5.2.2 Characterization

NMR Bruker Avance 300 spectrometer was used for NMR spectra. Zeta potential were obtained with BIC PALS ZetaSizer (T = 25 °C, pH = 6.6). FTIR-Digilab FTS3100 spectrometer was used for FTIR test with potassium bromide (KBr) pellet. TEM images were obtained with JEM 3010 TEM and FESEM were taken by JEOL JSM-6700F. Probe sonication was performed by SONICS VIBRA CELL VCX130. Thermogravimetric analysis (TGA) was performed by Perkin Elmer TGA/DTA equipment in nitrogen atmosphere from 100 to 700 °C at a temperature increase of 20 °C/min. The M_n and PDI of polymers were tested by GPC Agilent Infinity-1260 at 25 °C using THF as an eluent at 1ml/min flow rate and polystyrene as standards. The high performance liquid chromatography (HPLC) system includes quaternary pump, an Agilent 1100 series degasser, auto sampler, a variable-wavelength detector and Agilent Poreshell 120 column (50 x 4.6 mm i.d.) packed with EC-C18, average particle size 2.7 μm. UV absorbance was set at wavelength 278 nm at 25°C. The sample flow rate was 0.5 ml/min and the injection volume is 100 μL. The mobile phase consisted of 700 ml of water, 1.9 ml of orthophosphoric acid 85%, 1.4 g of tetrabutylammoniumiodide and 300 ml of methanol. The samples was filtered through membrane filter with 0.2 μm pore size before use.

5.2.3 Synthesis of poly(*ε*-caprolactone)-methylphosphonate (PCL-methylphosphonate)

PCL-methylphosphonate was synthesized by ring-opening polymerization of *ε*-caprolactone (*ε*-CL) with dimethyl (2-hydroxyethyl) phosphonate as the initiator and $Sn(Oct)_2$ as the catalyst. Typically, *ε*-CL (2.2 g,

19.2 mmol), dimethyl (2-hydroxyethyl) phosphonate (15.41 mg, 0.1 mmol) and anhydrous toluene (3 ml) were added to a flamed schlenk tube equipped with a magnetic stir bar in the nitrogen atmosphere. The tube was heated in an oil bath at 120 °C and $Sn(Oct)_2$ was added under nitrogen to begin the polymerization. The polymerization was then quenched by benzoic acid after 24 h. The product was washed in the large excess of cold diethyl ether three times and vacuum dried overnight. M_n =19000, PDI =1.36. Yield: 80%. ^{1}H-NMR (in $CDCl_3$, ppm): 4.03 (t, 2H, -OC*H*$_2$CH$_2$CH$_2$CH$_2$CH$_2$C(O)-), 3.75 (d, 6H, C*H*$_3$O-), 3.65 (t, 2H, -C*H*$_2$OH), 2.28 (t, 2H, -OCH$_2$CH$_2$CH$_2$CH$_2$C*H*$_2$C(O)-), 1.63 (m, 4H, -OCH$_2$C*H*$_2$CH$_2$C*H*$_2$CH$_2$C(O)-), 1.35 (m, 2H, -OCH$_2$CH$_2$C*H*$_2$CH$_2$CH$_2$C(O)-). (6.5A)

5.2.4 Preparation of poly(*ε*-caprolactone)-phosphonic acid

PCL-methylphosphonate (1.9 g, 0.1 mmol) and anhydrous methylene chloride (6 ml) were put into the round bottom flask. 0.1 ml (0.76 mmol) of bromotrimethylsilane was slowly added into the flask and the mixture was stirred at room temperature for 12 h. Most of the volatile residues and solvent were blown away by nitrogen and vacuum was used to further dry the polymer. After that, anhydrous methylene chloride (6 ml) was used to dissolve the resultant polymer and the solution was stirred overnight after adding 3 ml methanol. Poly(*ε*-caprolactone)-phosphonic acid was recovered by precipitation into diethyl ether and dried under vacuum. Yield: 90%. ^{1}H-NMR (in $CDCl_3$, ppm): 4.03 (t, 2H, -OC*H*$_2$CH$_2$CH$_2$CH$_2$CH$_2$C(O)-), 3.65 (t, 2H, -C*H*$_2$OH), 2.28 (t, 2H, -OCH$_2$CH$_2$CH$_2$CH$_2$C*H*$_2$C(O)-), 1.63 (m, 4H, -OCH$_2$C*H*$_2$CH$_2$C*H*$_2$CH$_2$C(O)-), 1.35 (m, 2H, -OCH$_2$CH$_2$C*H*$_2$CH$_2$CH$_2$C(O)-) (Figure 5.4B).

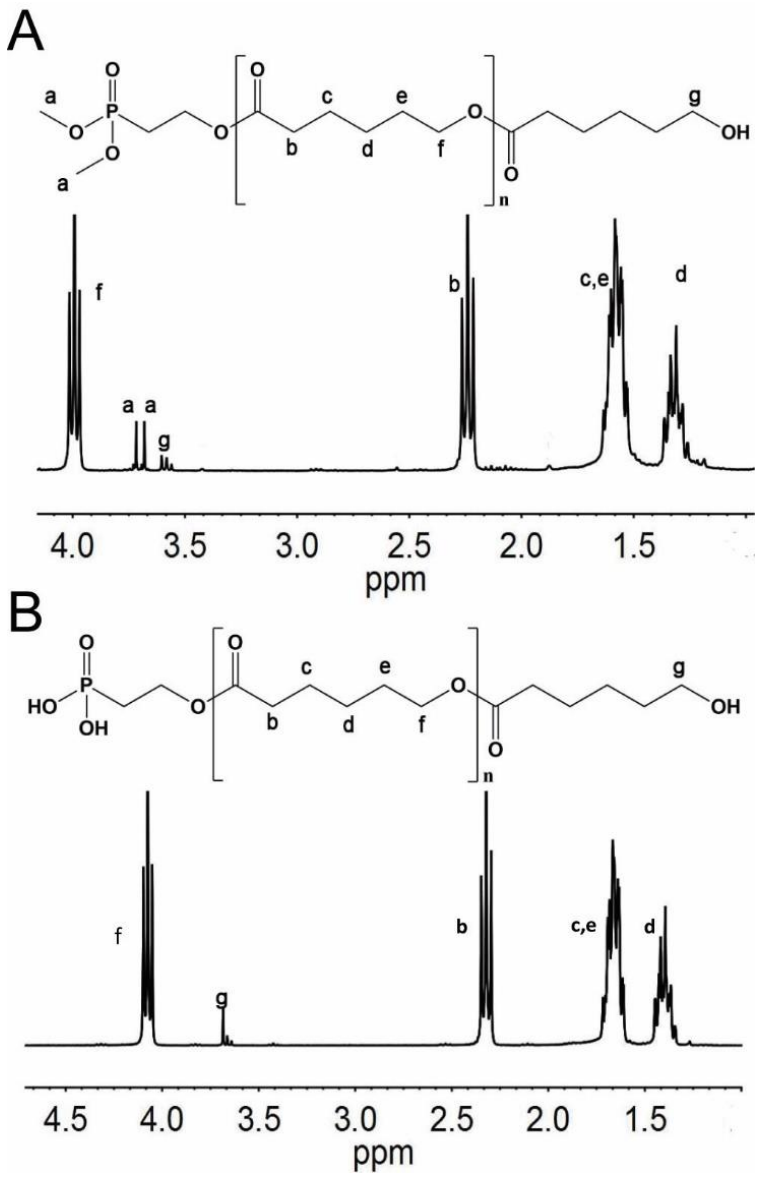

Figure 5.4 ^{1}H NMR spectra of PCL-phosphonate (A) and PCL-phosphonic acid (B).

5.2.5 Synthesis of Boc-poly(ethylene glycol)-methyl phosphonate

Boc-NH-PEG-C_3H_6-COOH (0.34g, 0.1 mmol) and dimethyl (2-hydroxyethyl) phosphonate (0.046g, 0.3 mmol) were dissolved in dichloromethane (6 ml). DCC (0.041 g, 0.2 mmol) was added to it slowly. After the solution continued at room temperature for 30 min in the dark, DAMP (0.003

g, 0.025 mmol) in 0.2 ml dichloromethane was added. The insoluble part was filtered after the solution was stirred overnight for 24 h in the dark. Then the polymer was precipitated in diethyl ether, washed with a mixture of diethyl ether and acetone (v/v = 6:1) and dried under vacuum. Yield: 80%. ^{1}H-NMR (in $CDCl_3$, ppm): 3.78 (d, 6H, C*H*$_3$O-), 3.65 (m, 4H, -C*H*$_2$C*H*$_2$O-), 1.44 (s, 9H, -Boc-) (Figure 5.5A).

5.2.6 Synthesis of NH_2-PEG-phosphonic acid

To the solution of Boc-poly(ethylene glycol)-methyl phosphonate (0.36 g, 0.1 mmol) in dry dichloromethane (4 ml) at 0 °C, trimethyl bromosilane (0.1 ml, 0.76 mmol) was added dropwise. Most of the volatile residues and solvent were blown away by nitrogen after 24 h room temperature stirring and vacuum was used to further dry the polymer. The polymer was re-dissolved in 2 ml dichloromethane. Additional 2 ml methanol was added to the residue and reacted overnight.[209] The NH_2-PEG-phosphonic acid was obtained after precipitating in diethyl ether and dried. Yield: 83%. ^{1}H-NMR (in $CDCl_3$, ppm): 3.65 (m, 4H, -C*H*$_2$C*H*$_2$O-) (Figure 5.5B).

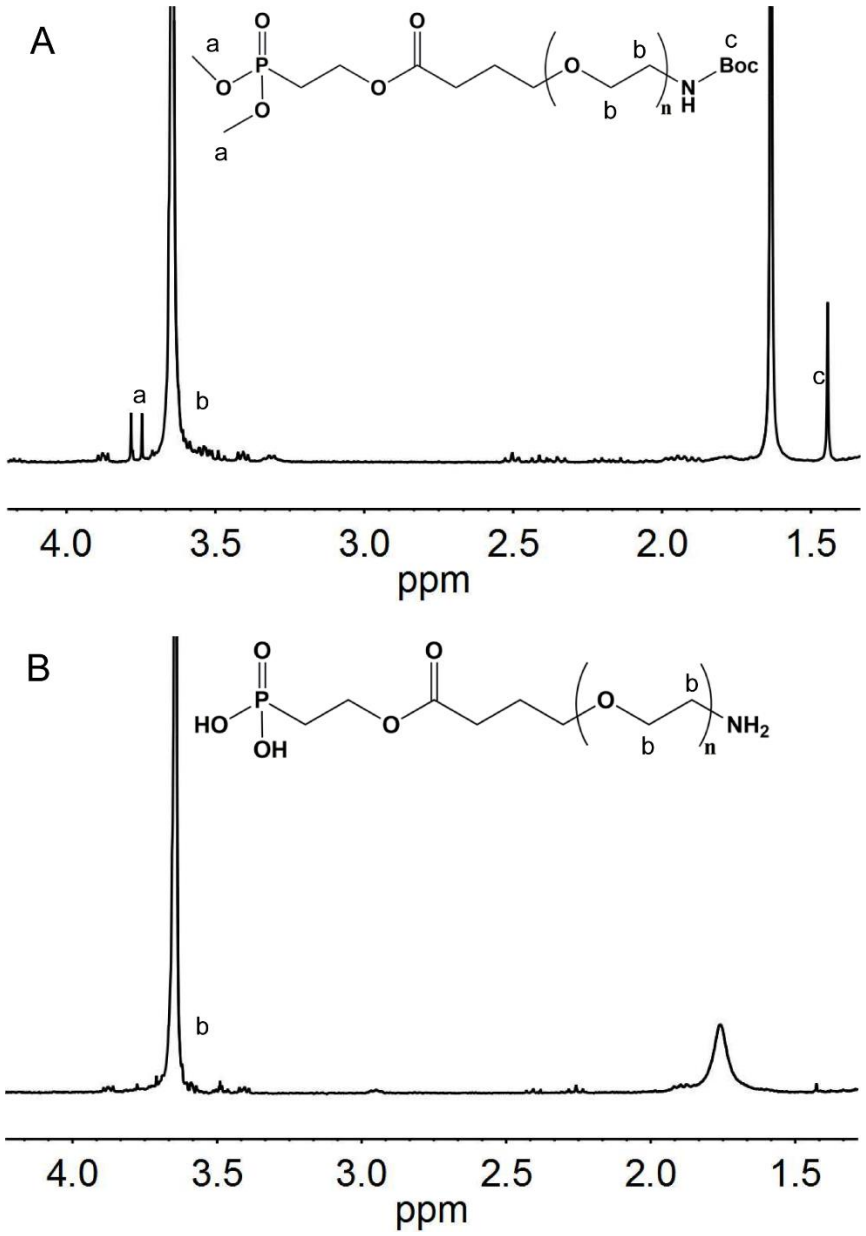

Figure 5.5. ^{1}H NMR spectra of PEG-phosphonate (A) and PEG-phosphonic acid (B).

5.2.7 Synthesis of $MnFe_2O_4$ nanoparticles coated with PCL and PEG

The $MnFe_2O_4$ nanoparticle was synthesized as described in the previous chapter. The amphiphilic $MnFe_2O_4$ nanoparticles with polymer brushes of PCL and PEG were prepared through "grafting to" reaction. 1 ml solution of PEG (5 mg, 1.47 mmol) and PCL (8 mg, 0.42 mmol) in chloroform was added dropwise

to $MnFe_2O_4$ dispersions and the solution was stirred for 12 h. The nanoparticles were collected via magnetic force after addition of hexane and the purifying procedure was repeated three times.

5.2.8 Synthesis of antibody conjugated $MnFe_2O_4$@PCL/PEG vesicles loaded with antibiotic

To fabricate norfloxacin-loaded vesicles, 100 μg norfloxacin was dispersed in chloroform. Subsequently, the clear and homogenous solution of $MnFe_2O_4$@PCL/PEG (250 μg) and norfloxacin were dried on a glass vial to form a flat film under moderate nitrogen flow. Then 2 ml water was added to rehydrate the film by bath sonication and probe sonication. The vesicles were centrifuged for three times to remove free antibiotics and then redispersed in borate buffer (pH=7.4) for later usage. The concentration of norfloxacin was determined by HPLC (Figure 5.6). The antibiotic loading was calculated based on the difference between unloaded amount of antibiotic and the total amount of norfloxacin used for antibiotic loading. The blank vesicle was prepared in similar condition without antibiotic. To conjugate anti-*S. aureus* antibody onto the vesicle, antibody (100 μg) and EDAC (0.15 mg) were mixed with the vesicle dispersion for 12 h at 4 °C in borate buffer (pH=7.4). The nanoparticles were collected by magnetic force to remove free antibody and the vesicles were stored at 4 °C in borate buffer for further usage.

5.2.9 Degradation study of vesicles

To analyse the vesicle degradation process by lipase, antibiotic loaded vesicle dispersion (250 μg/ml) were incubated with lipase from Pseudomonas

cepacia with a final concentration at 1 mg/ml at 37 °C in PBS. At predetermined time intervals, the vesicles were separated by magnetic force for SEM images. Control experiment was performed without enzyme addition at 48 h.

5.2.10 Cell preparation

A single colony of both *E. faecalis* and *S. aureus* were taken and inoculated in BHI (brain heart infusion) and Luria-Bertani (LB) medium respectively at T = 37 °C overnight in 15 ml tube. The tube was shaken overnight until the bacteria reaching midexponential growth phase. Cells were centrifuged at 7000 rpm for 5 min and washed with PBS for 3 times. The bacteria were then redispersed and diluted to the predesigned concentration. Cell concentration was calculated by plate count method.

5.2.11 Antibiotic release

The norfloxacin release from vesicles with lipase was investigated at 37 °C in PBS solution. Vesicles at a concentration of 10 μg/ml antibiotic in the solution in the presence or in the absence of lipase from *Pseudomonas cepacia* was centrifuged and the supernatant was filtered through 0.2 μm syringe filters at predetermined time intervals. The concentration in the medium was determined by HPLC analysis.

The release profiles of norfloxacin from the vesicle in the presence of bacteria was investigated at 37 °C in a bacteria cultivation tube. Vesicles in the medium with bacteria ($OD_{600\ nm}$ = 1) was centrifuged and the supernatant was filtered through 0.2 μm syringe filters at predetermined intervals. The norfloxacin in the medium was further extracted by chloroform solution. The extracted

antibiotic was dried and redissolved in water for HPLC analyses. Lipase-secreting bacteria *Staphylococcus* and low-lipase-secreting bacteria *Enterococcus faecalis* were investigated in the study.

5.2.12 Inhibitory effect of vesicle on bacteria

Norfloxacin, norfloxacin-loaded vesicles and bare vesicles at predetermined concentration (100 μl) were added into 96 well plates and 100 μl bacteria suspension at concentration of 10^5 CFU/ml were added. After 24 h, the vesicles were separated by magnetic force and the supernatant was used for recording OD_{600} by the microplate reader. For *E. faecalis*, norfloxacin-loaded vesicles without lipase and with lipase at 1mg/ml were investigated for bacteria inhibition test.

5.2.13 Bacteria capture by antibody conjugated blank vesicles

The blank vesicles were used to test capture efficiency. Vesicles at predetermined concentration (100 μl) were added to bacteria suspension at concentration of 10^5 CFU/ml (100 μl) in PBS for 0.5 h. PBS without vesicles was used as control. Vesicles, with their captured bacteria, were separated by magnetic force. Cell concentration in the supernatant was determined by plate count method. The capture efficiency is calculated based on the difference between the number of bacterial in control solution and supernatant.

5.2.14 Magnetic enhancement test

Vesicles at predetermined concentration (0.5 ml) were added to bacteria suspension at concentration of 10^5 CFU/ml (0.5 ml) for 0.5 h. Vesicles, with their

captured bacteria, were separated by magnetic force and re-dissolved in 50 μl growth medium. After 24 h, the vesicles were separated by magnetic force and the supernatant was remained to test OD_{600} by the microplate reader.

5.3 Results and discussion

5.3.1 Synthesis of amphiphilic $MnFe_2O_4$@PCL/PEG

The lipase-sensitive PCL was synthesized by ring opening polymerization (ROP) with $Sn(Oct)_2$ as the catalyst and dimethyl 2-hydroxyethyl phosphonate as the initiator at 120 °C (Figure 5.4A). The ROP polymerization offers flexible control over the molecular weight and the polycarbonate has M_n of 19000 and PDI of 1.36. Boc-NH-PEG-$(CH_2)_3$-COOH was modified to possess the phosphonate end group by dimethyl 2-hydroxyethyl phosphonate by DCC/DMAP catalysed reaction (Figure 5.5A). Then, the protective methyl groups in both PCL (Figure 5.4B) and PEG (Figure 5.5B) were removed to provide both polymers with functional phosphonic acid end groups. The disappearance of peaks at 3.78 ppm indicates the successfully dimethyl removing. Meanwhile, The Boc protective group in PEG was also removed during the deprotection process with the disappearance of single peak at 1.44 ppm. 10 nm $MnFe_2O_4$ nanoparticles stabilized by oleic acids through carboxyl groups were synthesized at high temperature. The phosphonic acid end group of PCL and PEG displays higher affinity with the surfaces of 10 nm $MnFe_2O_4$ nanoparticles than carboxyl groups of original ligand oleic acid. Thus, we proceeded the ligand exchange reaction by grafting the polymers PCL/PEG onto the $MnFe_2O_4$ nanoparticles in chloroform and the diminished solubility of the nanoparticles

suggested a successful ligand exchange as the original nanoparticles could dissolve well in hexane.

The presence of polymers on the nanoparticle surface was further verified by FT-IR spectroscopy and quantified by TGA. Figure 5.6A shows the FTIR of $MnFe_2O_4$ nanoparticles with oleic acid, PCL and $MnFe_2O_4$@PCL/PEG. The signal of the band at 1735 cm^{-1} of PCL was attributed to the ester O-C=O moiety, which also appears in the spectrum of $MnFe_2O_4$@PCL/PEG and does not exist in the spectrum of $MnFe_2O_4$ nanoparticles with oleic acid, confirming functionalization of PCL onto nanoparticles. In addition, the relatively strong signal of the C-H stretching at 2900 cm^{-1} and C-O-C stretch bond vibration at 1030 cm^{-1} in $MnFe_2O_4$@PCL/PEG spectrum indicate successful ligand exchange of PEG onto nanoparticles. More quantitative result was obtained from TGA. Between 100 and 700 °C, the weight loss of $MnFe_2O_4$ nanoparticles coated with oleic acids is 15% and it reaches 70% for $MnFe_2O_4$@PCL/PEG, further confirming the successful functionalization of PCL/PEG onto nanoparticles.

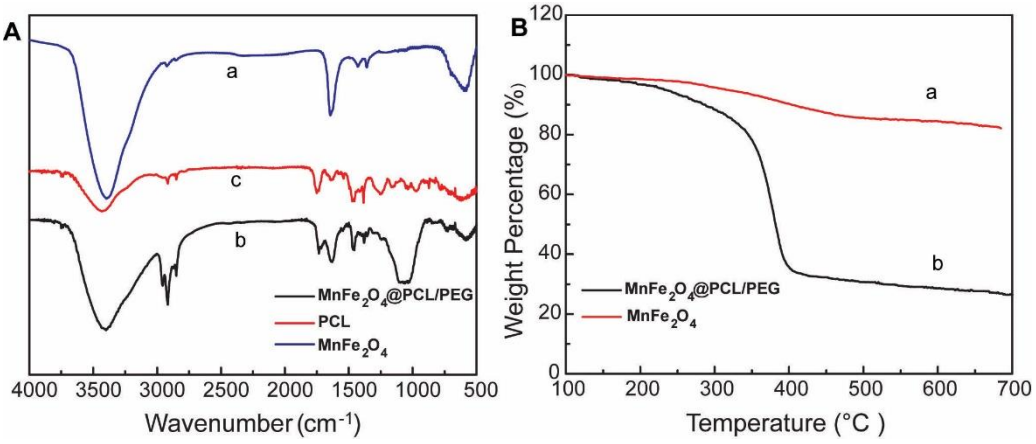

Figure 5.6 FTIR curves (A) of $MnFe_2O_4$ (a), $MnFe_2O_4$@PCL/PEG (b), and PCL (c). TGA curves (B) of $MnFe_2O_4$ (a), $MnFe_2O_4$@PCL/PEG (b).

5.3.2 Synthesis of $MnFe_2O_4$@PCL/PEG vesicle

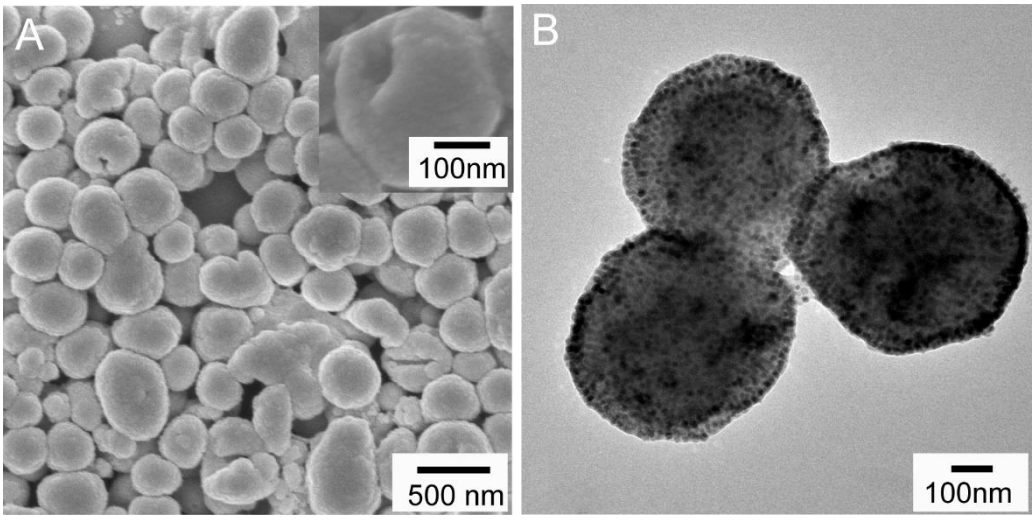

Figure 5.7 (A) SEM images of vesicles assembled from superparamagnetic nanoparticles grafted with PEG and lipase-sensitive PCL brushes. Inset: SEM image at higher magnification. (B) TEM image of vesicle.

The amphiphilic $MnFe_2O_4$@PCL/PEG nanoparticles were assembled into vesicles by film rehydration method as our group previously reported.[210] Briefly, the nanoparticles, with or without antibiotic, firstly formed clear dispersions in chloroform. After evaporation of solvent by a dry nitrogen, the nanoparticles form a film layer on a vial, with the uniformly distributed polymer brushes on the nanoparticle surfaces. Then water is added to hydrate the films, and the films roll up and rearrange to close the nanoparticle membrane with the help of additional ultrasonication to minimize interfacial energy. The TEM observation of the vesicles in Figure 5.7B indicate a difference between the inside and periphery, confirming that the vesicles have hollow structures and large cavity. The vesicle, with about 10 nm shell thickness and about 300 nm diameter,

has a monolayer of nanoparticles on the shell, which is consistent with the hypothesis that the hydrophobic PCL brushes collapse with nanoparticles to form the shell while hydrophilic PEG brushes spread among the interior and exterior of the shell. The SEM images, shown in Figure 5.7A further demonstrate the vesicular structure with a hollow cavity, which could be observed occasionally from the small holes in the intact vesicle structure.

During the vesicle synthesis, different amplitudes of probe sonication at 25%, 50% and 75% was applied for 30 s to make vesicles more uniform and unilamilar (Figure 5.8). At 25% amplitude, monolayer structure around 300 nm is readily formed. At 50% amplitude, the vesicles are more uniform since higher energy is available to break up multilayer structures into more uniform unilamilar vesicles. Further increase the amplitude to 75%, however, break up the vesicle structure with the membrane destroyed.

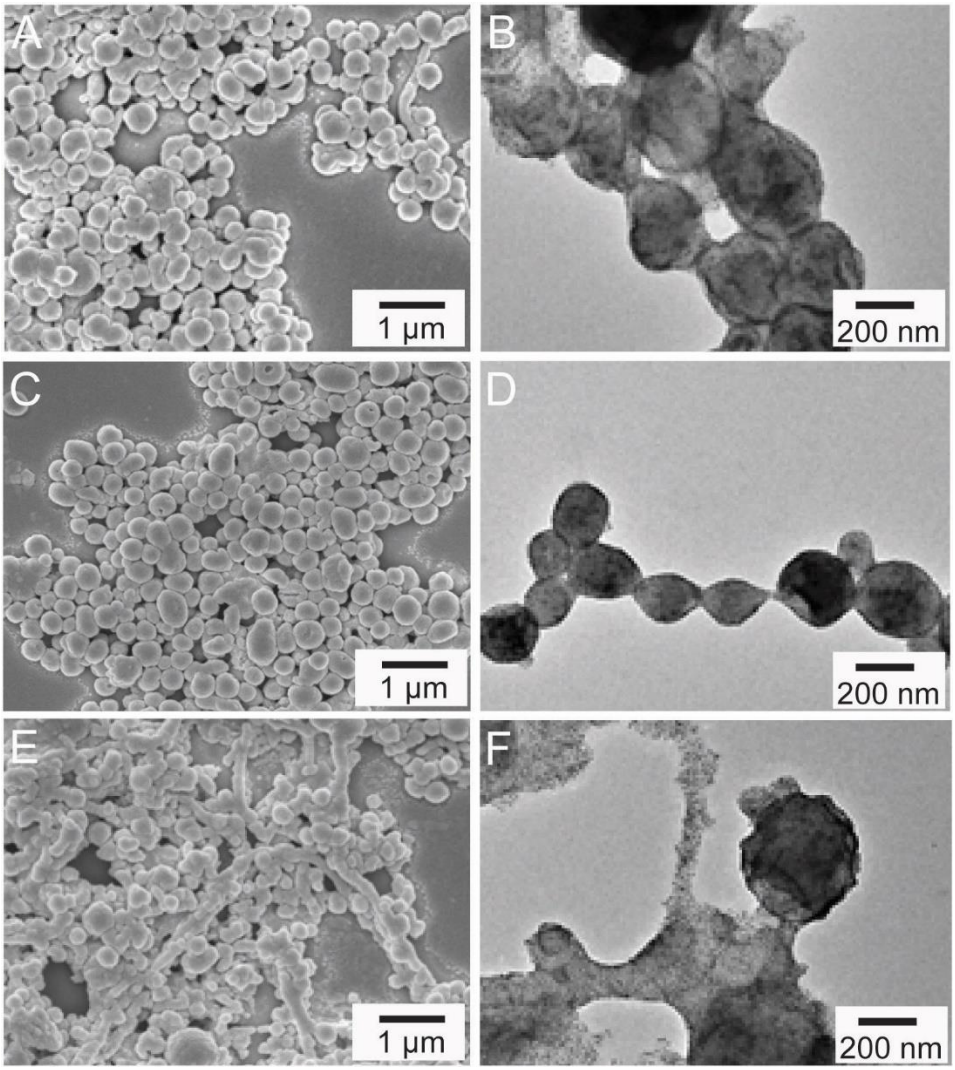

Figure 5.8 SEM images (A,C,E) and TEM images (B,D,F) of vesicle structures at different probe amplitudes for 30 s: (A,B) 25%, (C,D): 50%, (E,F): 75%.

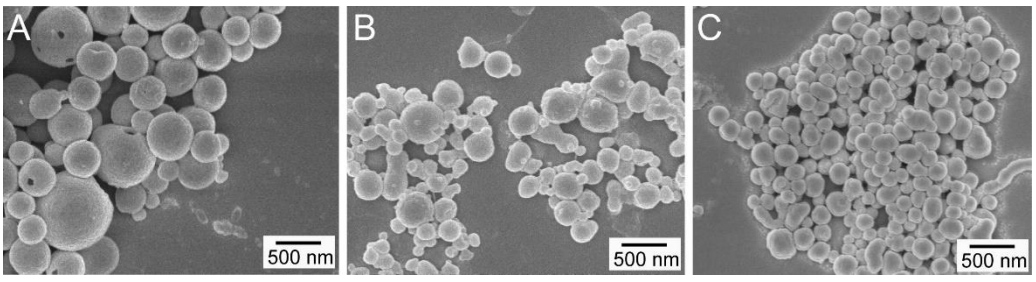

Figure 5.9 SEM images of the lipase-sensitive vesicles assembled without antibiotic (A), and with ratio of antibiotic: nanoparticle at 1:5 (B) and 2:5 (C).

It was revealed from SEM images that the size of empty vesicles (around 500 nm, Figure 5.9A) were larger than antibiotic loaded vesicles. During antibiotic loading process, we also found that the vesicle size decreases with higher antibiotic/nanoparticle ratio. At ratio of antibiotic:nanoparticle at 1:5 in Figure 5.9B, the vesicle size was around 400 nm while it reached 300 nm at 2:5 (Figure 5.9C). We believe that antibiotics can be intercalated into the nanoparticle film layer during hydration, which enhances the cohesion among apolar portions of the membrane and leads to the reduction in the vesicle size.[211]

5.3.3 Lipase degradation of the amphiphilic vesicles of $MnFe_2O_4$@PCL/PEG

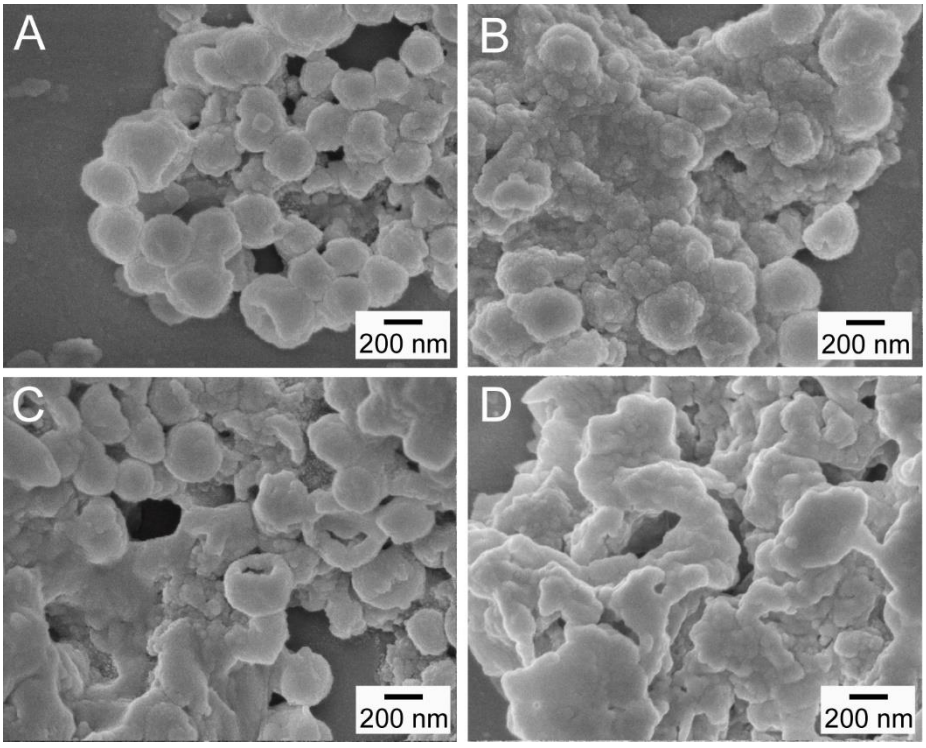

Figure 5.10 SEM images of the vesicles after incubating with lipase at 1 mg/ml for 5 h (A), 15 h (B), 25 h (C) and 48 h (D).

As PCL is biodegradable, the morphology of the vesicles should be changed at different time intervals with lipase. 1 mg/ml lipase (from *Pseudomonas cepacia*) was used to treat the vesicles as this enzyme concentration is high enough to degrade PCL quickly.[206] Figure 5.10 shows the vesicle morphology changes after the degradation of PCL. Small holes came out in the initially more intact vesicles after treatment with enzyme for 5 h, leading to hollow cavities exposure. More and more vesicles lost integrity and part of them lost original vesicle structures as the treatment time increases to 15 and 25 h. All vesicles almost lost their structures and clusters of nanoparticles were observed after 48 h. The degradation of PCL part changes the hydrophobic/hydrophilic ratio which is crucial to form vesicles.[212] To confirm that the structure destruction was caused by lipase degradation, control experiment was performed at the same condition without lipase addition, the vesicles retain their structures after 48 h (Figure 5.11).

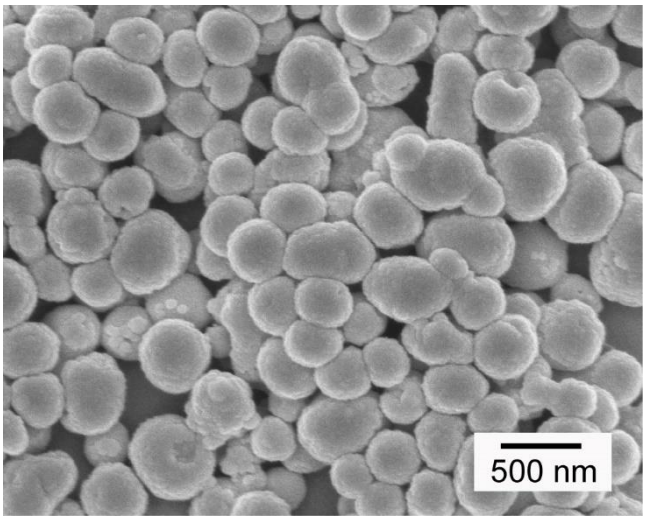

Figure 5.11 SEM image of vesicles without lipase treatment after 48 h.

5.3.4 Antibiotic encapsulation

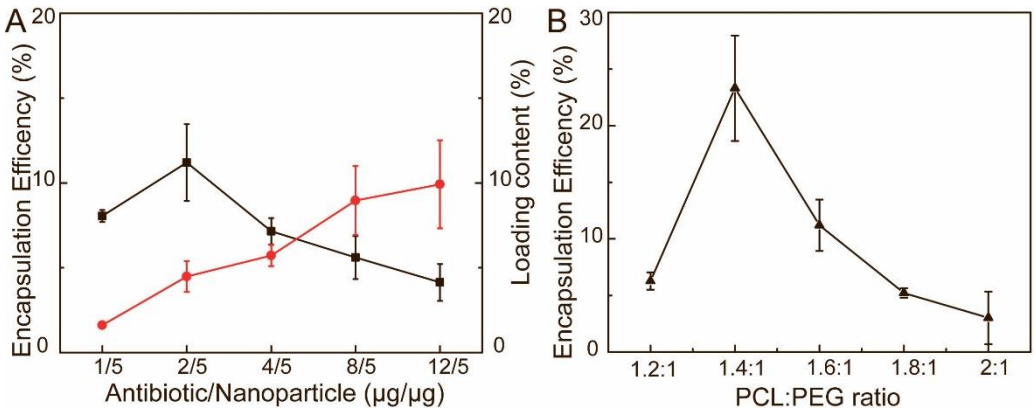

Figure 5.12 (A) Norfloxacin loading efficiency (black line) and loading content (red line) encapsulated in the vesicles against the ratio of antibiotic/nanoparticles. (B) Norfloxacin loading efficiency against ratio of PCL versus PEG during ligand exchange reaction.

Vesicular structures have been extensively reported to effectively deliver cancer drugs, protein, peptides and gene.[213] Here we investigated whether our vesicles could function as a carrier to encapsulate antibiotics for antibacterial application. Firstly, we encapsulated hydrophobic norfloxacin into the impact shell layer by mixing antibiotics with nanoparticles before forming the film layer at the weight ratio of 1.6:1 for PCL and PEG. As demonstrated in Figure 5.12A, the total loading content of norfloxacin elevates with the antibiotic/nanoparticle ratio increases and it reaches its maximal value (~10%) at a antibiotic/nanoparticle ratio of 12/5 based on the total norfloxacin feeding weight since higher loading content is expected with increasing amount of antibiotic available for loading. However, the highest antibiotic loading efficiency (11.2%) appeared at an antibiotic/nanoparticle ratio of 2/5 and the antibiotic loading content at this antibiotic/nanoparticle ratio was just about 5%. Interestingly, the

antibiotic loading efficiency decreased when further increasing the antibiotic/nanoparticle ratio. It is reasonable since non-covalent interaction is the basis for the nanoparticle antibiotic loading and much higher antibiotic/nanoparticle ratio decreases the interaction chance for the nanoparticle and antibiotic molecules, which leads to a lower antibiotic loading efficiency. Considering the efficiency and practicable, we further investigated the effect of PCL/PEG weight ratio on antibiotic loading efficiency with fixed antibiotic/nanoparticle ratio (2/5) as the interaction between hydrophobic PCL and the antibiotic is crucial for antibiotic loading. The antibiotic encapsulation efficiency, presented in Figure 5.12B, first increased from 6.3% (1.2:1) to 23.3% (1.4:1) but dropped to 11.2%, 5.2% and 3.0% at molar ratio 1.6:1, 1.8:1 and 2:1. PCL functions as a linkage to fill the gap between nanoparticles. Initially, increasing PCL content favors membrane integrity and enhances antibiotic loading though non-covalent interaction. However, decreased encapsulation efficiency for 1.6:1 to 2:1 raised from the further increased rigidity and lower free space for antibiotic to insert into the membrane at higher PCL content of the vesicles.[205]

5.3.5 Antibiotic release

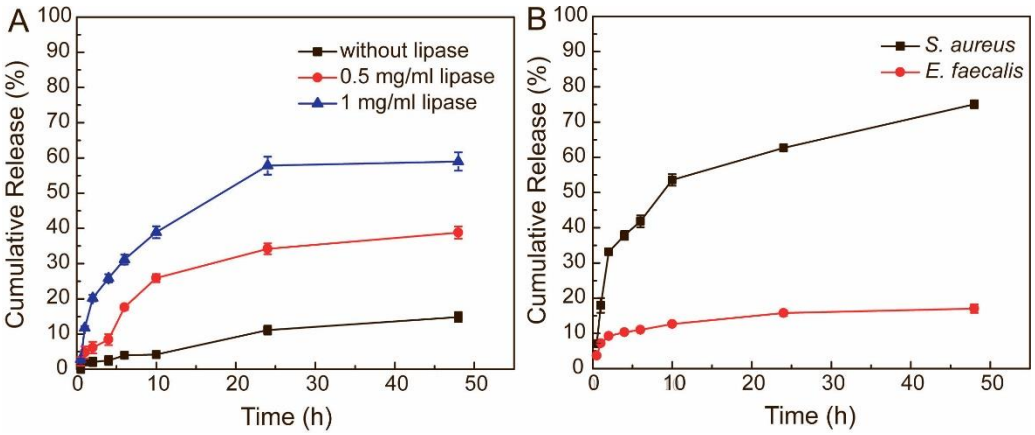

Figure 5.13 (A) Cumulative release of norfloxacin from vesicles without (black line) lipase or with 0.5 mg/ml (red line) or 1mg/ml lipase (blue line). (B) Cumulative release of norfloxacin from vesicles with *S. aureus* or *E. faecalis* at OD_{600} value of 1.0.

As mentioned above, we think that the shell of the vesicle was composed by the nanoparticle and PCL. The degradable PCL will be degraded once the lipase or lipase-secreting bacteria applied leading to the loading antibiotic leakage. Thus, we investigated the release behaviour of norfloxacin from the vesicles in the PBS at 37 °C with or without lipase. As illustrated in Figure 5.13A, the release of norfloxacin was the lowest in the plain PBS buffer without the presence of lipase at 14.1% release of encapsulated antibiotics after 48 h incubation. With lipase addition, faster release of antibiotic was demonstrated as the degradation of PCL disrupted vesicle structures. The release rate also dependends on the lipase concentration and higher lipase concentration favors faster and higher antibiotic release. At 1mg/ml lipase concentration, the cumulative release reached 59.0% of total encapsulated antibiotic while it only

arrived at 38.8% at lipase concentration of 0.5 mg/ml at 48 h. The release behaviour slowed down after 24 h of incubation.

To further understand the bacteria triggered antibiotic release behaviour, lipase-secreting bacteria *S. aureus* and control bacteria *E. faecalis* with low lipase secreting were selected to incubate with vesicles in appropriate mediums. The distinct properties in lipase production by different bacteria were accessed by tributyrin agar test. Tributyrin agar is the differential medium that differentiates between bacteria that produces lipase and the ones that does not. Since tributyrin oil, which is not soluble in water, forms opaque suspension in the agar. When the lipase is produced, the oil breaks down lipids into smaller fragments, such as glycerol and fatty acids, and a clear halo will appear around the area that produces lipases. Following this principle, *S. aureus*, with a clear halo around bacteria as shown in Figure 5.14A, produces lipases to break down lipids while *E. faecalis*, with opaque surroundings as shown in Figure 5.14B, does not secret lipases.

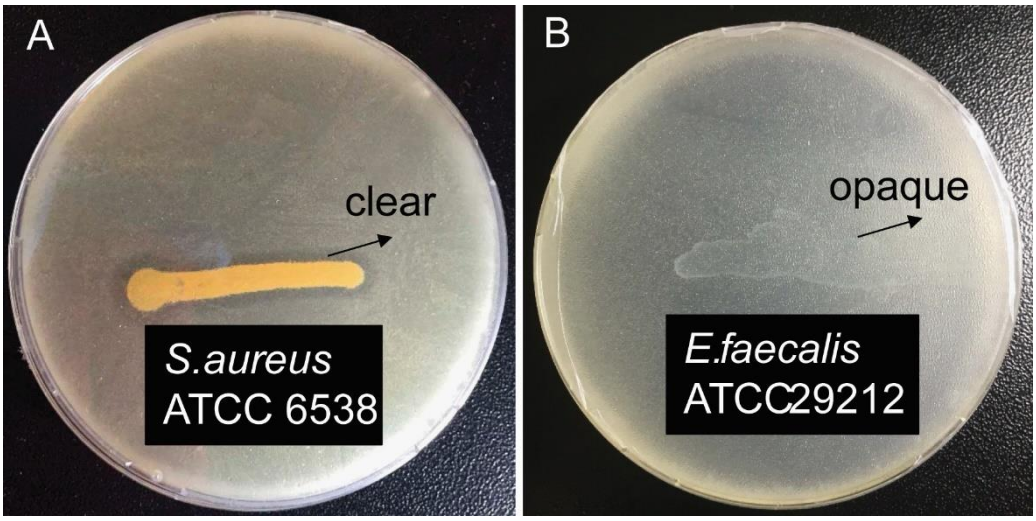

Figure 5.14 Tributyrin agar test of *S. aureus* (A) and *E. faecalis* (B).

Triggered by *S. aureus* at OD600nm value of 1 (8×10^8 CFU/ml), rapid antibiotic release from vesicles was observed with 53.6% cumulative release of total encapsulated antibiotic over 10 h as shown in Figure 5.13B. Steady release rate retains over time and the cumulative release of antibiotic reached 75.1% over 48 h incubation. The release behaviour, unlike for specific lipase concentration mentioned above, didn't slow down after 24 h since lipase was continuously produced by the bacteria instead of at a fixed concentration. To confirm the vesicle was destroyed by lipase, *E. faecalis* was used as the control bacteria. As expected, the cumulative release of antibiotic in the presence of *E. faecalis* was much lower than that in the condition of *S. aureus* (17.0% over 48 h incubation). This finding leads us to conclude that the controlled antibiotic release from the vesicles was triggered by lipase-secreting bacteria. Thus, our bio-inspired vesicles may find some particular application in medical related fields.

5.3.6 Bacteria growth inhibition

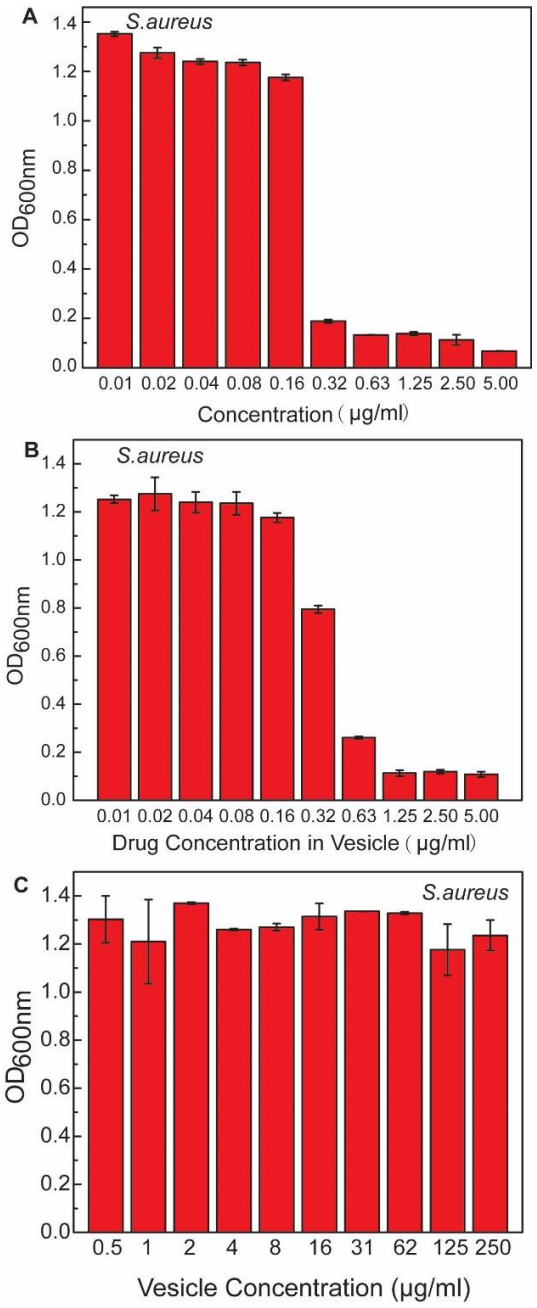

Figure 5.15 Growth inhibition of *S. aureus* at 24 h in the presence of free antibiotic (A) , antibiotic loaded vesicles (B) and blank vesicles (C). The antibiotic concentration in vesicle represents the amount of norfloxacin loaded into the vesicles.

A related issue concerns if the norfloxacin-loaded vesicles could inhibit the lipase-secreting bacteria (*S. aureus*) after confirming that lipase-secreting bacteria triggered antibiotic release from vesicle. Figure 5.15A and Figure 5.16A demonstrates the inhibition of *S. aureus* and *E. faecalis* of pure antibiotic alone while Figure 5.15B and Figure 5.16B demonstrates the inhibition of *S. aureus* and *E. faecalis* in the presence of norfloxacin loaded vesicles. From Figure 5.15A, the norfloxacin inhibits *S. aureus* growth at 0.32 μg/ml. The result was similar for norfloxacin-loaded vesicles with equivalent antibiotic concentration (Figure 5.15B) after 24 h incubation. The vesicles started to suppress *S. aureus* growth at 0.32 μg/ml and almost inhibit their growth at 0.64 μg/ml, indicating that antibiotic loading vesicles could inhibit the growth of lipase-secreting bacteria. On the other hand, although norfloxacin suppresses *E. faecalis* growth from concentration of 0.32 μg/ml, the norfloxaicn loaded vesicles inhibits *E. faecalis* growth from a much higher equivalent antibiotic concentration in vesicles without lipase addition, which was 1.25 μg/ml (red column in Figure 5.16B). We further investigated the antibiotic-loaded vesicles against *E. faecalis* with lipase addition of 1 mg/ml. The vesicles, in this case, starts to inhibit *E. faecalis* growth at a relatively lower concentration of 0.63 μg/ml since more antibiotics are released with lipase addition. We also examined bacteria growth with the blank vesicles and it shows no bacteria growth inhibition (Figure 5.15C and Figure 5.16C). These findings confirm that the vesicles are triggered to release antibiotics by lipase-secreting bacteria and the released antibiotics are capable to kill the bacteria, achieving the target for on-demand antibiotic release.

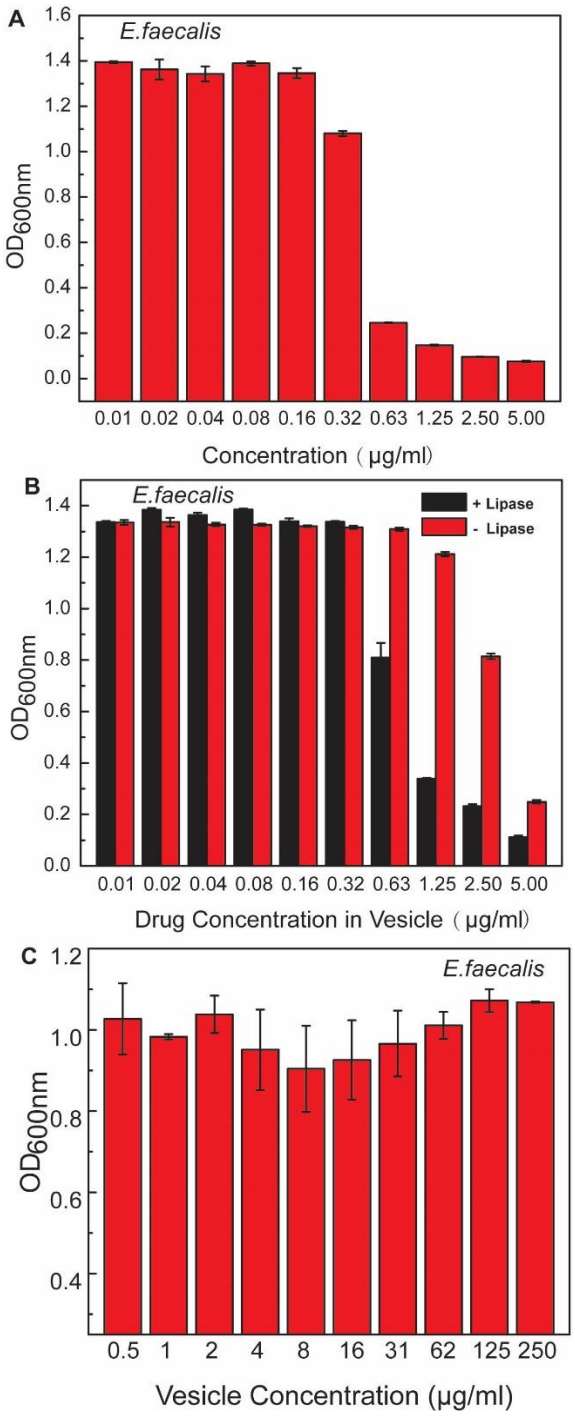

Figure 5.16 Growth inhibition of *E. faecalis* at 24 h in the presence of free antibiotic (A), antibiotic loaded vesicles (B) and blank vesicles (C). The antibiotic concentration in vesicle represents the amount of norfloxacin loaded into the vesicles.

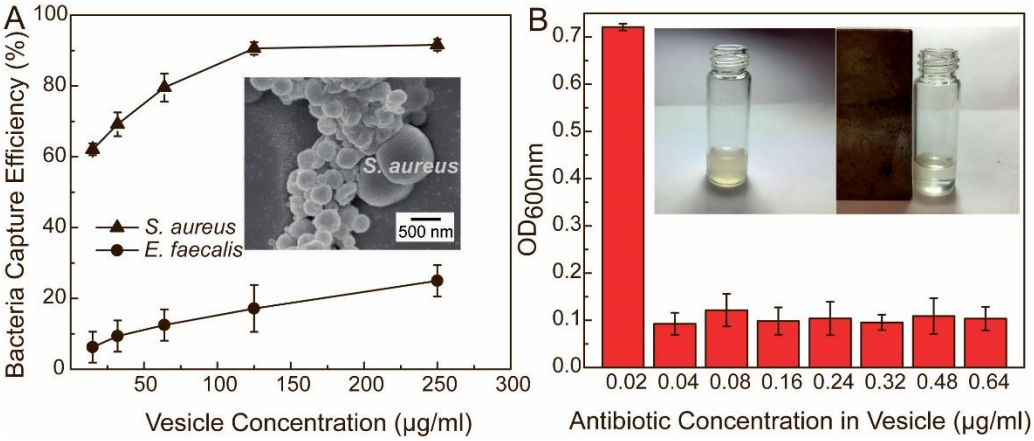

Figure 5.17 (A) Bacteria capture efficiency of *S. aureus* and *E. faecalis* by antibody-conjugated blank vesicles at different vesicle concentrations. Inset: SEM images of bacteria captured by vesicles. (B) Growth inhibition of *S. aureus* against antibiotic concentration in vesicle after enrichment process. Inset: Photo of vesicles solution before and after magnetic separation.

5.3.7 Magnetic enrichment

To selectively recognize and capture *S. aureus*, the vesicles were conjugated with anti-*S. aureus* antibody. As surface properties of vesicles changed after conjugation with antibody, the surface ζ potential (pH=6.6) was characterized by measuring their electrophoretic mobility using DLS. The ζ potential of the vesicles without antibody conjugation was 17.2 ± 1.1 mV, suggesting the presence of amine groups of PEG on the particle surface. After conjugation reactions, the ζ potential changes from positive to negative values (-18.5 ± 1.3 mV) due to the net negative charges carried by the antibody since the value of pI for antibody rabbit IgG was reported to be 6.1 - 6.5.[214] The change of ζ potential from positive to negative values indicates successful conjugation of antibody onto vesicle surfaces.

Besides, the vesicles demonstrate superparamagnetic properties with fast response in magnetic separation. After applying magnet for 5 min, the originally well-dispersed vesicles are mostly separated, as shown in Figure 5.17B. To prove that antibody conjugated vesicles could act as an effective probe to recognize and capture *S. aureus*, the blank vesicles were incubated with bacteria for 0.5 h and the amount of captured bacteria by vesicles was counted by subtracting free bacteria in the supernatant after magnetic separation (Figure 5.17A). A gradual enhancement in capture efficiency of *S. aureus* was observed with increasing concentration of anti-*S. aureus* antibody conjugated blank vesicles, with the efficiency of 62%, 70%, 79%, 90% and 91% for weight concentration of vesicles at 15, 32, 64, 125 and 250 μg/ml respectively. On the other hand, for the control bacteria *E. faecalis*, only 6%, 9%, 12%, 17% and 25% were lost by the same vesicle concentration during separation due to nonspecific adhesion of bacteria onto vesicle surfaces. The results further confirm the specific recognition properties of antibody conjugated vesicles. We then investigated the capture properties of antibody conjugated nanoparticles with SEM measurements. The vesicles, with the size of around 300 nm, come close to the surfaces of *S. aureus*, which has the size of around 800 nm.

We finally explored bacteria killing performance of the magnetic separation vesicles in LB medium with magnetic enrichment (Figure 5.17B). The antibiotic loaded vesicles with antibody conjugated, at predetermined concentrations, were shaken with a bacteria suspension containing *S. aureus* (10^5 CFU/ml) for 0.5 h at 37 °C. After magnetic separation and supernatant removal, the vesicles, with their captured bacteria, were redispersed in medium with 1/20 of original volume. The growth of bacteria were fully inhibited at 0.04 μg/ml

based on the initial applied antibiotic concentration in vesicles, which is 1/16 of the concentration (0.64 μg/ml) for vesicles before enrichment, achieving efficient antibacterial activity. In one word, our antibiotic-loaded nanoparticle shows excellent antibacterial by the magnetic enrichment.

Up to the stage, the experiment answers our hypothesis. The designed nanoparticle based vesicular system successfully encapsulated up to 11.2% weight percentage of drug. The biodegradable polymer in the system supports lipase responsive degradation of the vesicles, facilitating drug release while it gives no response without lipase presence. The drug release is also proportional to the lipase concentration as higher lipase level favors higher percentage of degradation process. As the fact that bacteria like *S.aureus* produce lipase while the other *E.faecalis* does not, the vesicles only release drugs in the presence of *S.aureus*, achieving our target of specific release purposes. This is important as selectivity killing of bacteria species may be preferred during treatment of disease. Taking advantage of antibody attached, the magnetic vesicles are able to collected attached selective bacteria and enriched themselves to reach a higher level of drug concentration and kill this special type of bacteria. This enrichment process reduces drug dosage requirement during treatment process and is beneficial to reduce drug resistance.

5.4 Conclusion

In summary, we have successfully developed antibody conjugated, antibiotic loaded and lipase-sensitive polymer based vesicles assembled from superparamagnetic nanoparticles. The results demonstrated that the vesicular

system not only delivered the antibiotic on demand to treat targeted bacteria, but also captured the bacteria and inhibited their growth at lower vesicle amount. The on-demand antibiotic release was triggered by bacteria lipase after degrading the PCL inside the vesicle shell while it was not achieved in the presence of low lipase-secreting bacteria. The extracellular growth of lipase-secreting bacteria was effectively controlled by the antibiotic released from the vesicle. Additionally, the vesicles, with antibody conjugated, accurately captured targeted bacteria and were separated by magnetic force. After enriching them in one twentieth amount of original medium, the bacteria killing efficiency was elevated up to sixteen times.

Chapter 6. Conclusions and future work

6.1 Conclusions

In this thesis, we depended on polymer functionalized nanostuctures to synthesize new materials or construct appropriate drug carriers for antimicrobial applications. The nanostructures not only provide platform for polymers due to their high surface to volume ratio, but also assist bacteria killing process by their own intrinsic chemical or physical properties such as hyperthermia effect.

Firstly, we prepared poly(4-vinylpyridine) functionalized GO and quaternized them by different alkyl chains. The nanosheet wrapped around the cells, where they were able to destroy bacteria cell membrane. The composites were not only effective in solution, but were facile to modify into paper form to execute toxicity.

In the second project, instead of using non-degradable poly(4-vinylpyridine), we synthesized biodegradable cationic polycarbonates and subsequently grafted them onto superparamagnetic nanoparticles. The materials display synergetic killing effect. On one hand, cationic polymers interacted with cell membrane and led to membrane destruction. On the other hand, the superparamagnetic core generated enough heat to kill bacteria under alternating magnetic field. The combined effect reached higher activity against bacteria.

Considering polymer based nanoparticles were able to be assembled into vesicles as antibiotic carriers, which will not only benefit antibiotics that existed in the market, but also those will be developed in future, we successfully

synthesized vesicles based on biodegradable polymer grafted superparamagnetic nanoparticles, encapsulating the antibiotic norfloxacin. The vesicles achieved on-demand antibiotic release to kill bacteria triggered by bacteria secreting lipase. Besides, functionalized with targeted antibody, the vesicles were able to capture the *S. aureus* and enriched in lower amount of medium, reducing the requirement of material dosage.

6.2 Future Research

Polymer functionalized nanomaterials have demonstrate their distinct advantages for loading abundant polymers on nanomaterials with high surface to volume ratio, incorporating special characteristics of nanomaterials into antibacterial applications, and assembling ability into drug carriers by polymers on nanomaterial surface. The strategies here enable us to develop more composites for effective microbial control.

The future researches may be explored in the following areas:

(1) It was reported that N-heterocycyle quaternized polycarbonates significantly enhanced antimicrobial activity of cationic polymers.[130] Different quaternization agents may be introduced to the polycarbonate grafted nanoparticles to investigate the biocidal activity. Additionally, since triblock copolymer containing two blocks of poly(trimethylene carbonate) and one block of cationic poly((3-chloropropyl 5-methyl-2-oxo-1,3-dioxane-5-carboxylate) were synthesized and illustrated efficient killing ability against bacteria at low doses with low toxicity towards human beings, copolymer structures instead of single polycarbonate

could be further explored by being grafted onto nanoparticles.[131] We believe that incorporating noncharged polycarbonate section may enhance hydrophobicity of materials, which could elevate the interaction between material and bacteria membrane. Apart from the biodegradable polymer we synthesized in the second project, other types of antibacterial biodegradable polymers, such as chitosan and peptide mimic polymers, can also be incorporated onto superparamagnetic nanoparticles to display synergistic antibacterial activity based on membrane destruction by polymers and hyperthermia mechanism by nanoparticles.[215]

(2) Gold nanorods, with an intense absorption in the near-infrared region, provide possibilities for photothermal therapy, which is an extensively studied technology for cancer and infectious organism treatment. Besides, gold nanorods are also facile for surface functionalization by covalent bonds such as Au-S bond. The superparamagnetic nanoparticles can thus be replaced by gold nanorods to generate localized heat for antibacterial applications.

(3) The vesicles, which may also encapsulate cationic polymers inside the shell apart from loading antibiotics, can achieve on-demand release of polymers to kill bacteria, preventing nonspecific binding of polymers onto mammalian cells or other non-targeted bacteria. Additionally, instead of using lipase sensitive polymers, pH-responsive or thermo-responsive polymers may be used to functionalize nanoparticles and prepare antibiotic-loaded vesicles. These types of vesicles are expected to

achieve on-demand release of antibiotics and targeted bacteria killing by varying the surrounding pH or temperature.

References

(1) Ouwehand, A. C.; Salminen, S.; Isolauri, E. *Antonie van Leeuwenhoek* **2002**, *82*, 279.

(2) Shah, N. P. *Bioscience and Microflora* **2000**, *19*, 99.

(3) Macpherson, A. J.; Harris, N. L. *Nature reviews. Immunology* **2004**, *4*, 478.

(4) Sandvig, K.; Torgersen, M. L.; Engedal, N.; Skotland, T.; Iversen, T.-G. *FEBS Letters* **2010**, *584*, 2626.

(5) Fuller, R. *Gut* **1991**, *32*, 439.

(6) Gram, L.; Ravn, L.; Rasch, M.; Bruhn, J. B.; Christensen, A. B.; Givskov, M. *International Journal of Food Microbiology* **2002**, *78*, 79.

(7) Siu, R. G. H.; Reese, E. T. *The Botanical Review* **1953**, *19*, 377.

(8) Eriksson, K. E. L.; Blanchette, R. A.; Ander, P. In *Microbial and Enzymatic Degradation of Wood and Wood Components*; Springer Berlin Heidelberg: Berlin, Heidelberg, 1990, p 1.

(9) Arancibia, F.; Bauer, T. T.; Ewig, S.; et al. *Archives of Internal Medicine* **2002**, *162*, 1849.

(10) Leib, S. L.; Täuber, M. G. *Infectious Disease Clinics of North America* **1999**, *13*, 527.

(11) Aktuğ, Ş. E.; Karapinar, M. *International Journal of Food Microbiology* **1986**, *3*, 349.

(12) Wilson, M. E. *Emerging Infectious Diseases* **1995**, *1*, 39.

(13) Ashbolt, N. J. *Toxicology* **2004**, *198*, 229.

(14) Glaser, C. A.; Angulo, F. J.; Rooney, J. A. *Clinical Infectious Diseases* **1994**, *18*, 14.

(15) Rasmussen, M. A.; Casey, T. A. *Critical Reviews in Microbiology* **2001**, *27*, 57.

(16) Evans, A. S.; Brachman, P. S. *Bacterial Infections of Humans: Epidemiology and Control*; Springer US, 2013.

(17) Gavazzi, G.; Herrmann, F.; Krause, K.-H. *Clinical Infectious Diseases* **2004**, *39*, 83.

(18) Slayton, R. B.; Toth, D.; Lee, B. Y.; Tanner, W.; Bartsch, S. M.; Khader, K.; Wong, K.; Brown, K.; McKinnell, J. A.; Ray, W.; Miller, L. G.; Rubin, M.; Kim, D. S.; Adler, F.; Cao, C.; Avery, L.; Stone, N. T. B.; Kallen, A.; Samore, M.; Huang, S. S.; Fridkin, S.; Jernigan, J. A. *MMWR. Morbidity and mortality weekly report* **2015**, *64*, 826.

(19) Cohen, M. L. *Nature* **2000**, *406*, 762.

(20) Wenzel , R. P.; Edmond , M. B. *New England Journal of Medicine* **2000**, *343*, 1961.

(21) Awad, S. S.; Palacio, C. H.; Subramanian, A.; Byers, P. A.; Abraham, P.; Lewis, D. A.; Young, E. J. *The American Journal of Surgery* **2009**, *198*, 607.

(22) Silhavy, T. J. *Journal of Bacteriology* **2016**, *198*, 201.

(23) Muñoz-Bonilla, A.; Cerrada, M.; Fernández-García, M.; Kenawy, E. R.; Lienkamp, K.; Xiao, H.; Nomiya, K.; Lagaron, J.; Piozzi, A.; Sun, G. *Polymeric Materials with Antimicrobial Activity: From Synthesis to Applications*; Royal Society of Chemistry, 2013.

(24) Cabeen, M. T.; Jacobs-Wagner, C. *Nature Reviews Microbiology* **2005**, *3*, 601.
(25) Vasanthakumari, R. *Textbook of Microbiology*; B.I. Publications Pvt. Limited, 2007.
(26) Rahn, O. *Bacteriological Reviews* **1945**, *9*, 1.
(27) McDonnell, G.; Russell, A. D. *Clinical Microbiology Reviews* **1999**, *12*, 147.
(28) Rutala, W. A.; Gergen, M. F.; Weber, D. J. *Infection Control & Hospital Epidemiology* **2010**, *31*, 1025.
(29) Sala, F. J.; Burgos, J.; Condón, S.; Lopez, P.; Raso, J. In *New Methods of Food Preservation*; Gould, G. W., Ed.; Springer US: Boston, MA, 1995, p 176.
(30) Waterhouse, S.; Hall, G. M. *Journal of Membrane Science* **1995**, *104*, 1.
(31) Wiseman, A. *Trends in Biochemical Sciences* **1989**, *14*, 510.
(32) Ascenzi, J. M. *Handbook of Disinfectants and Antiseptics*; Taylor & Francis, 1995.
(33) Russell, A. D. *Journal of Antimicrobial Chemotherapy* **2002**, *49*, 597.
(34) Gallo, G. G.; Lancini, G.; Parenti, F. *Antibiotics: A Multidisciplinary Approach*; Springer US, 2013.
(35) Bennett, J. W.; Chung, K.-T. In *Advances in Applied Microbiology*; Academic Press: 2001; Vol. Volume 49, p 163.
(36) Aminov, R. I. *Frontiers in Microbiology* **2010**, *1*, 134.
(37) Zaffiri, L.; Gardner, J.; Toledo-Pereyra, L. H. *Journal of Investigative Surgery* **2012**, *25*, 67.
(38) Fischbach, M. A.; Walsh, C. T. *Science* **2009**, *325*, 1089.
(39) Kohanski, M. A.; Dwyer, D. J.; Hayete, B.; Lawrence, C. A.; Collins, J. J. *Cell* **2007**, *130*, 797.
(40) Yim, G.; Wang, H. H.; Davies, J. *International Journal of Medical Microbiology* **2006**, *296*, 163.
(41) Armstrong, G. L.; Conn, L. A.; Pinner, R. W. *JAMA* **1999**, *281*, 61.
(42) Projan, S. J. *Current Opinion in Microbiology* **2003**, *6*, 427.
(43) Projan, S. J.; Shlaes, D. M. *Clinical Microbiology and Infection* **2004**, *10*, 18.
(44) Hall, R. M.; Collis, C. M. *Drug Resistance Updates* **1998**, *1*, 109.
(45) Blair, J. M. A.; Webber, M. A.; Baylay, A. J.; Ogbolu, D. O.; Piddock, L. J. V. *Nature Reviews Microbiology* **2015**, *13*, 42.
(46) Neu, H. C. *Science* **1992**, *257*, 1064.
(47) Davies, J.; Davies, D. *Microbiology and Molecular Biology Reviews* **2010**, *74*, 417.
(48) Wiegand, I.; Hilpert, K.; Hancock, R. E. W. *Nature Protocols* **2008**, *3*, 163.
(49) Spencer, J. F. T.; de Spencer, A. L. R. *Food Microbiology Protocols*; Humana Press, 2001.
(50) Goldman, E.; Green, L. H. *Practical Handbook of Microbiology, Third Edition*; CRC Press, 2015.

(51) Sabir, M. I.; Xu, X.; Li, L. *Journal of Materials Science* **2009**, *44*, 5713.

(52) Rao, C. N. R.; Cheetham, A. K. *Journal of Materials Chemistry* **2001**, *11*, 2887.

(53) Cioffi, N.; Rai, M. *Nano-Antimicrobials: Progress and Prospects*; Springer Berlin Heidelberg, 2012.

(54) Hajipour, M. J.; Fromm, K. M.; Ashkarran, A. A.; Jimenez de Aberasturi, D.; de Larramendi, I. R.; Rojo, T.; Serpooshan, V.; Parak, W. J.; Mahmoudi, M. *Trends in Biotechnology* **2012**, *30*, 499.

(55) Nel, A.; Xia, T.; Mädler, L.; Li, N. *Science* **2006**, *311*, 622.

(56) Kumar, S. K.; Jouault, N.; Benicewicz, B.; Neely, T. *Macromolecules* **2013**, *46*, 3199.

(57) Gu, H.; Ho, P. L.; Tong, E.; Wang, L.; Xu, B. *Nano Letters* **2003**, *3*, 1261.

(58) Yoshioka, Y.; Higashisaka, K.; Tsutsumi, Y. In *Nanomaterials in Pharmacology*; Lu, Z., Sakuma, S., Eds.; Springer New York: New York, NY, 2016, p 185.

(59) Seil, J. T.; Webster, T. J. *International Journal of Nanomedicine* **2012**, *7*, 2767.

(60) Sharifi, S.; Behzadi, S.; Laurent, S.; Laird Forrest, M.; Stroeve, P.; Mahmoudi, M. *Chemical Society Reviews* **2012**, *41*, 2323.

(61) Oberdörster, G.; Maynard, A.; Donaldson, K.; Castranova, V.; Fitzpatrick, J.; Ausman, K.; Carter, J.; Karn, B.; Kreyling, W.; Lai, D.; Olin, S.; Monteiro-Riviere, N.; Warheit, D.; Yang, H. *Particle and Fibre Toxicology* **2005**, *2*, 1.

(62) Warheit, D. B.; Borm, P. J. A.; Hennes, C.; Lademann, J. *Inhalation Toxicology* **2007**, *19*, 631.

(63) Guzman, M.; Dille, J.; Godet, S. *Nanomedicine: Nanotechnology, Biology and Medicine* **2012**, *8*, 37.

(64) Kim, J. S.; Kuk, E.; Yu, K. N.; Kim, J. H.; Park, S. J.; Lee, H. J.; Kim, S. H.; Park, Y. K.; Park, Y. H.; Hwang, C. Y.; Kim, Y. K.; Lee, Y. S.; Jeong, D. H.; Cho, M. H. *Nanomedicine: Nanotechnology, Biology and Medicine* **2007**, *3*, 95.

(65) Le Ouay, B.; Stellacci, F. *Nano Today* **2015**, *10*, 339.

(66) Jose Ruben, M.; Jose Luis, E.; Alejandra, C.; Katherine, H.; Juan, B. K.; Jose Tapia, R.; Miguel Jose, Y. *Nanotechnology* **2005**, *16*, 2346.

(67) Park, H. J.; Kim, J. Y.; Kim, J.; Lee, J. H.; Hahn, J. S.; Gu, M. B.; Yoon, J. *Water Research* **2009**, *43*, 1027.

(68) Chappel, J. B.; Greville, G. D. *Nature* **1954**, *174*, 930.

(69) Panáček, A.; Kvítek, L.; Prucek, R.; Kolář, M.; Večeřová, R.; Pizúrová, N.; Sharma, V. K.; Nevěčná, T. j.; Zbořil, R. *The Journal of Physical Chemistry B* **2006**, *110*, 16248.

(70) Pal, S.; Tak, Y. K.; Song, J. M. *Applied and Environmental Microbiology* **2007**, *73*, 1712.

(71) Rai, M. K.; Deshmukh, S. D.; Ingle, A. P.; Gade, A. K. *Journal of Applied Microbiology* **2012**, *112*, 841.

(72) Percival, S. L.; Bowler, P. G.; Dolman, J. *International Wound Journal* **2007**, *4*, 186.

(73) Ayala-Núñez, N. V.; Lara Villegas, H. H.; del Carmen Ixtepan Turrent, L.; Rodríguez Padilla, C. *NanoBiotechnology* **2009**, *5*, 2.

(74) Fan, Z.; Lu, J. G. *Journal of Nanoscience and Nanotechnology* **2005**, *5*, 1561.

(75) Mishra, Y. K.; Chakravadhanula, V. S. K.; Hrkac, V.; Jebril, S.; Agarwal, D. C.; Mohapatra, S.; Avasthi, D. K.; Kienle, L.; Adelung, R. *Journal of Applied Physics* **2012**, *112*, 064308.

(76) Song, Z.; Kelf, T. A.; Sanchez, W. H.; Roberts, M. S.; Rička, J.; Frenz, M.; Zvyagin, A. V. *Biomedical Optics Express* **2011**, *2*, 3321.

(77) Jide, Z. In *Electronics and Optoelectronics (ICEOE), 2011 International Conference on* 2011; Vol. 3, p V3.

(78) Lakshmi Prasanna, V.; Vijayaraghavan, R. *Langmuir* **2015**, *31*, 9155.

(79) Zhang, H.; Chen, B.; Jiang, H.; Wang, C.; Wang, H.; Wang, X. *Biomaterials* **2011**, *32*, 1906.

(80) Seven, O.; Dindar, B.; Aydemir, S.; Metin, D.; Ozinel, M. A.; Icli, S. *Journal of Photochemistry and Photobiology A: Chemistry* **2004**, *165*, 103.

(81) Espitia, P. J. P.; Soares, d. N. F. F.; Coimbra, J. d. S. R.; de Andrade, N. J.; Cruz, R. S.; Medeiros, E. A. A. *Food and Bioprocess Technology* **2012**, *5*, 1447.

(82) Ahmed, S.; Rasul, M. G.; Martens, W. N.; Brown, R.; Hashib, M. A. *Desalination* **2010**, *261*, 3.

(83) Sirelkhatim, A.; Mahmud, S.; Seeni, A.; Kaus, N. H. M.; Ann, L. C.; Bakhori, S. K. M.; Hasan, H.; Mohamad, D. *Nano-Micro Letters* **2015**, *7*, 219.

(84) Messner, K. R.; Imlay, J. A. *Journal of Biological Chemistry* **1999**, *274*, 10119.

(85) Premanathan, M.; Karthikeyan, K.; Jeyasubramanian, K.; Manivannan, G. *Nanomedicine: Nanotechnology, Biology and Medicine* **2011**, *7*, 184.

(86) Li, M.; Zhu, L.; Lin, D. *Environmental Science & Technology* **2011**, *45*, 1977.

(87) Song, W.; Zhang, J.; Guo, J.; Zhang, J.; Ding, F.; Li, L.; Sun, Z. *Toxicology Letters* **2010**, *199*, 389.

(88) Heinlaan, M.; Ivask, A.; Blinova, I.; Dubourguier, H. C.; Kahru, A. *Chemosphere* **2008**, *71*, 1308.

(89) Aydin Sevinç, B.; Hanley, L. *Journal of Biomedical Materials Research Part B: Applied Biomaterials* **2010**, *94B*, 22.

(90) Méndez-Vilas, A. *Science Against Microbial Pathogens: Communicating Current Research and Technological Advances*; Formatex Research Center, 2011.

(91) Pedro, T.; María del Puerto, M.; Sabino, V. V.; Teresita, G. C.; Carlos, J. S. *Journal of Physics D: Applied Physics* **2003**, *36*, R182.

(92) Thomas, L. A.; Dekker, L.; Kallumadil, M.; Southern, P.; Wilson, M.; Nair, S. P.; Pankhurst, Q. A.; Parkin, I. P. *Journal of Materials Chemistry* **2009**, *19*, 6529.

(93) Pankhurst, Q. A.; Connolly, J.; Jones, S. K.; Dobson, J. *Journal of Physics D Applied Physics* **2003**, *36*, R167.

(94) Morrish, A. H. *The Physical Principles of Magnetism*; Wiley, 2001.

(95) Gu, H.; Ho, P. L.; Tsang, K. W. T.; Wang, L.; Xu, B. *Journal of the American Chemical Society* **2003**, *125*, 15702.

(96) Deatsch, A. E.; Evans, B. A. *Journal of Magnetism and Magnetic Materials* **2014**, *354*, 163.

(97) Jordan, A.; Scholz, R.; Wust, P.; Fähling, H.; Roland, F. *The Journal of Magnetism and Magnetic Materials* **1999**, *201*, 413.

(98) Rudolf, H.; Silvio, D.; Robert, M.; Matthias, Z. *Journal of Physics: Condensed Matter* **2006**, *18*, S2919.

(99) Li, Z.; Kawashita, M.; Araki, N.; Mitsumori, M.; Hiraoka, M.; Doi, M. *Materials Science and Engineering C* **2010**, *30*, 990.

(100) Hergt, R.; Andra, W.; d'Ambly, C. G.; Hilger, I.; Kaiser, W. A.; Richter, U.; Schmidt, H. G. *IEEE Transactions on Magnetics* **1998**, *34*, 3745.

(101) Singh, V.; Joung, D.; Zhai, L.; Das, S.; Khondaker, S. I.; Seal, S. *Progress in Materials Science* **2011**, *56*, 1178.

(102) Zhao, J.; Deng, B.; Lv, M.; Li, J.; Zhang, Y.; Jiang, H.; Peng, C.; Li, J.; Shi, J.; Huang, Q.; Fan, C. *Advanced Healthcare Materials* **2013**, *2*, 1259.

(103) Stankovich, S.; Dikin, D. A.; Dommett, G. H. B.; Kohlhaas, K. M.; Zimney, E. J.; Stach, E. A.; Piner, R. D.; Nguyen, S. T.; Ruoff, R. S. *Nature* **2006**, *442*, 282.

(104) Dreyer, D. R.; Park, S.; Bielawski, C. W.; Ruoff, R. S. *Chemical Society Reviews* **2010**, *39*, 228.

(105) Dikin, D. A.; Stankovich, S.; Zimney, E. J.; Piner, R. D.; Dommett, G. H. B.; Evmenenko, G.; Nguyen, S. T.; Ruoff, R. S. *Nature* **2007**, *448*, 457.

(106) Zhu, Y.; Murali, S.; Cai, W.; Li, X.; Suk, J. W.; Potts, J. R.; Ruoff, R. S. *Advanced materials* **2010**, *22*, 3906.

(107) Mao, H. Y.; Laurent, S.; Chen, W.; Akhavan, O.; Imani, M.; Ashkarran, A. A.; Mahmoudi, M. *Chemical Reviews* **2013**, *113*, 3407.

(108) Hu, W.; Peng, C.; Luo, W.; Lv, M.; Li, X.; Li, D.; Huang, Q.; Fang, C. *ACS Nano* **2010**, *4*, 4317.

(109) Perreault, F.; de Faria, A. F.; Nejati, S.; Elimelech, M. *ACS Nano* **2015**.

(110) Chen, J.; Peng, H.; Wang, X.; Shao, F.; Yuan, Z.; Han, H. *Nanoscale* **2014**, *6*, 1879.

(111) Romero-Vargas Castrillón, S.; Perreault, F.; de Faria, A. F.; Elimelech, M. *Environmental Science & Technology Letters* **2015**, *2*, 112.

(112) Liu, S.; Hu, M.; Zeng, T. H.; Wu, R.; Jiang, R.; Wei, J.; Wang, L.; Kong, J.; Chen, Y. *Langmuir* **2012**, *28*, 12364.

(113) Liu, S.; Zeng, T. H.; Hofmann, M. H.; Burcombe, E. B.; Wei, J.; Jiang, R.; Kong, J.; Chen, Y. *ACS Nano* **2011**, *5*, 6971.

(114) Cai, X.; Tan, S.; Lin, M.; Xie, A.; Mai, W.; Zhang, X.; Lin, Z.; Wu, T.; Liu, Y. *Langmuir* **2011**, *27*, 7828.

(115) Cornell, R. J.; Donaruma, L. G. *The Journal of Medicinal Chemistry* **1965**, *8*, 388.

(116) Timofeeva, L.; Kleshcheva, N. *Applied Microbiology and Biotechnology* **2011**, *89*, 475.

(117) Muñoz-Bonilla, A.; Fernández-García, M. *Progress in Polymer Science* **2012**, *37*, 281.

(118) Xue, Y.; Xiao, H.; Zhang, Y. *International Journal of Molecular Sciences* **2015**, *16*, 3626.

(119) Kenawy, E. R.; Abdel Hay, F. I.; El Shanshoury, A. E. R. R.; El Newehy, M. H. *Journal of Polymer Science Part A: Polymer Chemistry* **2002**, *40*, 2384.

(120) Tiller, J. C.; Lee, S. B.; Lewis, K.; Klibanov, A. M. *Biotechnology and Bioengineering* **2002**, *79*, 465.

(121) Sambhy, V.; Peterson, B. R.; Sen, A. *Angewandte Chemie International Edition* **2008**, *47*, 1250.

(122) Tiller, J. C.; Liao, C. J.; Lewis, K.; Klibanov, A. M. *The Proceedings of the National Academy of Sciences USA* **2001**, *98*, 5981.

(123) Li, G.; Shen, J.; Zhu, Y. *Journal of Applied Polymer Science* **1998**, *67*, 1761.

(124) Sharma, S. K.; Chauhan, G. S.; Gupta, R.; Ahn, J.-H. *Journal of Materials Science: Materials in Medicine* **2010**, *21*, 717.

(125) Anderson, E. B.; Long, T. E. *Polymer* **2010**, *51*, 2447.

(126) Geng, F.; Zheng, L.; Yu, L.; Li, G.; Tung, C. *Process Biochemistry* **2010**, *45*, 306.

(127) Mizerska, U.; Fortuniak, W.; Chojnowski, J.; Hałasa, R.; Konopacka, A.; Werel, W. *European Polymer Journal* **2009**, *45*, 779.

(128) Ding, X.; Yang, C.; Lim, T. P.; Hsu, L. Y.; Engler, A. C.; Hedrick, J. L.; Yang, Y. Y. *Biomaterials* **2012**, *33*, 6593.

(129) Qiao, Y.; Yang, C.; Coady, D. J.; Ong, Z. Y.; Hedrick, J. L.; Yang, Y. Y. *Biomaterials* **2012**, *33*, 1146.

(130) Ng, V. W. L.; Tan, J. P. K.; Leong, J.; Voo, Z. X.; Hedrick, J. L.; Yang, Y. Y. *Macromolecules* **2014**, *47*, 1285.

(131) Nederberg, F.; Zhang, Y.; Tan, J. P. K.; Xu, K.; Wang, H.; Yang, C.; Gao, S.; Guo, X. D.; Fukushima, K.; Li, L.; Hedrick, J. L.; Yang, Y.-Y. *Nature Chemistry* **2011**, *3*, 409.

(132) Lu, G.; Wu, D.; Fu, R. *Reactive and Functional Polymers* **2007**, *67*, 355.

(133) Lenoir, S.; Pagnoulle, C.; Detrembleur, C.; Galleni, M.; Jérôme, R. *Journal of Polymer Science Part A: Polymer Chemistry* **2006**, *44*, 1214.

(134) Dizman, B.; Elasri, M. O.; Mathias, L. J. *Journal of Applied Polymer Science* **2004**, *94*, 635.

(135) Tamami, M.; Salas-de la Cruz, D.; Winey, K. I.; Long, T. E. *Macromolecular Chemistry and Physics* **2012**, *213*, 965.

(136) Rodič, P.; Bratuša, M.; Lukšič, M.; Vlachy, V.; Hribar-Lee, B. *Colloids and Surfaces A: Physicochemical and Engineering Aspects* **2013**, *424*, 18.

(137) Williams, S. R.; Long, T. E. *Progress in Polymer Science* **2009**, *34*, 762.

(138) Laschewsky, A. *Current Opinion in Colloid & Interface Science* **2012**, *17*, 56.

(139) Zheng, A.; Xu, X.; Xiao, H.; Guan, Y.; Li, S.; Wei, D. *Journal of Materials Science* **2012**, *47*, 7201.

(140) Xu, X.; Xiao, H.; Ziaee, Z.; Wang, H.; Guan, Y.; Zheng, A. *Journal of Materials Science* **2013**, *48*, 1162.

(141) Yudovin-Farber, I.; Beyth, N.; Nyska, A.; Weiss, E. I.; Golenser, J.; Domb, A. J. *Biomacromolecules* **2008**, *9*, 3044.

(142) Beyth, N.; Yudovin-Farber, I.; Bahir, R.; Domb, A. J.; Weiss, E. I. *Biomaterials* **2006**, *27*, 3995.

(143) Rembaum, A.; Senyei, A. E.; Rajaraman, R. *Journal of Biomedical Materials Research* **1977**, *11*, 101.

(144) Ikeda, T.; Yamaguchi, H.; Tazuke, S. *Biochimica et Biophysica Acta (BBA) - Biomembranes* **1990**, *1026*, 105.

(145) Meyers, S. R.; Juhn, F. S.; Griset, A. P.; Luman, N. R.; Grinstaff, M. W. *Journal of the American Chemical Society* **2008**, *130*, 14444.

(146) Strydom, S. J.; Rose, W. E.; Otto, D. P.; Liebenberg, W.; de Villiers, M. M. *Nanomedicine: Nanotechnology, Biology and Medicine* **2016**, *9*, 85.

(147) Zarena, A. S.; Shubha, G. *Mini-Reviews in Medicinal Chemistry* **2013**, *13*, 1448.

(148) Chen, K.; Zhou, X.; Wang, X. *Journal of Surfactants and Detergents* **2014**, *17*, 1081.

(149) Worley, B. V.; Slomberg, D. L.; Schoenfisch, M. H. *Bioconjugate Chemistry* **2014**, *25*, 918.

(150) Song, J.; Jang, J. *Advances in Colloid and Interface Science* **2014**, *203*, 37.

(151) Dong, H.; Huang, J.; Koepsel, R. R.; Ye, P.; Russell, A. J.; Matyjaszewski, K. *Biomacromolecules* **2011**, *12*, 1305.

(152) Kong, H.; Song, J.; Jang, J. *Environmental Science & Technology* **2010**, *44*, 5672.

(153) Joo, Y. T.; Jung, K. H.; Kim, M. J.; Kim, Y. *Journal of Applied Polymer Science* **2013**, *127*, 1508.

(154) Wu, F.; Meng, G.; He, J.; Wu, Y.; Wu, F.; Gu, Z. *ACS Applied Materials & Interfaces* **2014**, *6*, 10005.

(155) Du, J.; O'Reilly, R. K. *Soft Matter* **2009**, *5*, 3544.

(156) Kim, J. K.; Kim, H. J.; Chung, J. Y.; Lee, J. H.; Young, S. B.; Kim, Y. H. *Archives of Pharmacal Research* **2014**, *37*, 60.

(157) Soppimath, K. S.; Aminabhavi, T. M.; Kulkarni, A. R.; Rudzinski, W. E. *Journal of Controlled Release* **2001**, *70*, 1.

(158) Pornpattananangkul, D.; Zhang, L.; Olson, S.; Aryal, S.; Obonyo, M.; Vecchio, K.; Huang, C. M.; Zhang, L. *Journal of the American Chemical Society* **2011**, *133*, 4132.

(159) Xiong, M. H.; Bao, Y.; Yang, X. Z.; Wang, Y. C.; Sun, B.; Wang, J. *Journal of the American Chemical Society* **2012**, *134*, 4355.

(160) Radovic-Moreno, A. F.; Lu, T. K.; Puscasu, V. A.; Yoon, C. J.; Langer, R.; Farokhzad, O. C. *ACS Nano* **2012**, *6*, 4279.

(161) Abed, N.; Couvreur, P. *International Journal of Antimicrobial Agents* **2014**, *43*, 485.

(162) Murata, H.; Koepsel, R. R.; Matyjaszewski, K.; Russell, A. J. *Biomaterials* **2007**, *28*, 4870.

(163) Lee, S. H.; Dreyer, D. R.; An, J.; Velamakanni, A.; Piner, R. D.; Park, S.; Zhu, Y.; Kim, S. O.; Bielawski, C. W.; Ruoff, R. S. *Macromolecular Rapid Communications* **2010**, *31*, 281.

(164) Hummers, W. S.; Offeman, R. E. *Journal of the American Chemical Society* **1958**, *80*, 1339.

(165) Basirun, W. J.; Sookhakian, M.; Baradaran, S.; Mahmoudian, M. R.; Ebadi, M. *Nanoscale Research Letters* **2013**, *8*, 1.

(166) Roghani-Mamaqani, H. *RSC Advances* **2015**, *5*, 53357.

(167) Shen, J.; Hu, Y.; Shi, M.; Lu, X.; Qin, C.; Li, C.; Ye, M. *Chemistry of Materials* **2009**, *21*, 3514.

(168) Stankovich, S.; Dikin, D. A.; Piner, R. D.; Kohlhaas, K. A.; Kleinhammes, A.; Jia, Y.; Wu, Y.; Nguyen, S. T.; Ruoff, R. S. *Carbon* **2007**, *45*, 1558.

(169) Zhang, Y.; Chen, C.; Wu, G.; Guan, N.; Li, L.; Zhang, J. *Chemical Communications* **2014**, *50*, 4305.

(170) Compton, O. C.; Dikin, D. A.; Putz, K. W.; Brinson, L. C.; Nguyen, S. T. *Advanced Materials* **2010**, *22*, 892.

(171) Jasim, D. A.; Menard Moyon, C.; Begin, D.; Bianco, A.; Kostarelos, K. *Chemical Science* **2015**, *6*, 3952.

(172) Mizutani, M.; Palermo, E. F.; Thoma, L. M.; Satoh, K.; Kamigaito, M.; Kuroda, K. *Biomacromolecules* **2012**, *13*, 1554.

(173) Gao, P.; Nie, X.; Zou, M.; Shi, Y.; Cheng, G. *The Journal of Antibiotics* **2011**, *64*, 625.

(174) Malhotra, B.; Keshwani, A.; Kharkwal, H. *Frontiers in microbiology* **2015**, *6*, 611.

(175) Pothayee, N.; Balasubramaniamb, S.; Davis, R. M.; Riffle, J. S.; Carroll, M. R.; Woodwardb, R. C.; Pierre, T. G. *Polymer* **2011**, *52*, 1356.

(176) Eckhardt, S.; Brunetto, P. S.; Gagnon, J.; Priebe, M.; Giese, B.; Fromm, K. M. *Chemical Reviews* **2013**, *113*, 4708.

(177) Holt, K. B.; Bard, A. J. *Biochemistry* **2005**, *44*, 13214.

(178) Ingle, A. P.; Duran, N.; Rai, M. *Applied Microbiology and Biotechnology* **2014**, *98*, 1001.

(179) Fasciani, C.; Silvero, M. J.; Anghel, M. A.; Arguello, G. A.; Becerra, M. C.; Scaiano, J. C. *Journal of the American Chemical Society* **2014**, *136*, 17394.

(180) Wu, M. C.; Deokar, A. R.; Liao, J. H.; Shih, P. Y.; Ling, Y. C. *ACS Nano* **2013**, *7*, 1281.

(181) Lin, D.; Qin, T.; Wang, Y.; Sun, X.; Chen, L. *ACS Applied Materials & Interfaces* **2014**, *6*, 1320.

(182) Khan, S. A.; Singh, A. K.; Fan, Z.; Senapati, D.; Ray, P. C. *Chemical Communications* **2012**, *48*, 11091.

(183) Lal, S.; Clare, S. E.; Halas, N. J. *Accounts of Chemical Research* **2008**, *41*, 1842.

(184) Lee, J. H.; Jang, J. T.; Choi, J. S.; Moon, S. H.; Noh, S. H.; Kim, J. W.; Kim, J. G.; Kim, I. S.; Park, K. I.; Cheon, J. *Nature Nanotechnology* **2011**, *6*, 418.

(185) Laurent, S.; Dutz, S.; Hafeli, U. O.; Mahmoudi, M. *Advances in Colloid and Interface Science* **2011**, *166*, 8.

(186) Chertok, B.; Moffat, B. A.; David, A. E.; Yu, F.; Bergemann, C.; Ross, B. D.; Yang, V. C. *Biomaterials* **2008**, *29*, 487.

(187) Jiang, T.; He, F.; Zhuo, R. X. *Polymer Degradation and Stability* **2013**, *98*, 325.

(188) Pratt, R. C.; Nederberg, F.; Waymouth, R. M.; Hedrick, J. L. *Chemical Communications* **2008**, 114.

(189) Sun, S.; Zeng, H.; Robinson, D. B.; Raoux, S.; Rice, P. M.; Wang, S. X.; Li, G. *Journal of the American Chemical Society* **2004**, *126*, 273.

(190) Yang, C.; Ong, Z. Y.; Yang, Y. Y.; Ee, P. L.; Hedrick, J. L. *Macromolecular Rapid Communications* **2011**, *32*, 1826.

(191) Bao, N.; Shen, L.; Wang, Y.; Padhan, P.; Gupta, A. *Journal of the American Chemical Society* **2007**, *129*, 12374.

(192) Sahoo, Y.; Pizem, H.; Fried, T.; Golodnitsky, D.; Burstein, L.; Sukenik, N. C.; Markovich, G. *Langmuir* **2001**, *17*, 7907.

(193) Kim, M. H.; Yamayoshi, I.; Mathew, S.; Lin, H.; Nayfach, J.; Simon, S. I. *Annals of Biomedical Engineering* **2013**, *41*, 598.

(194) Levy, S. B.; Marshall, B. *Nature Medicine* **2004**, *10*, S122.

(195) Wright, G. D. *Advanced Drug Delivery Reviews* **2005**, *57*, 1451.

(196) Walsh, C. T.; Fisher, S. L.; Park, I. S.; Prohalad, M.; Wu, Z. *Chemistry & Biology* **1996**, *3*, 21.

(197) Armstead, A. L.; Li, B. *International journal of nanomedicine* **2011**, *6*, 3281.

(198) Proctor, R. A.; von Eiff, C.; Kahl, B. C.; Becker, K.; McNamara, P.; Herrmann, M.; Peters, G. *Nature Reviews Microbiology* **2006**, *4*, 295.

(199) Tulkens, P. M. *European Journal of Clinical Microbiology and Infectious Diseases* **1991**, *10*, 100.

(200) Maurin, M.; Mersali, N. F.; Raoult, D. *Antimicrobial Agents and Chemotherapy* **2000**, *44*, 3428.

(201) Astruc, D.; Boisselier, E.; Ornelas, C. *Chemical Reviews* **2010**, *110*, 1857.

(202) Zaru, M.; Sinico, C.; De Logu, A.; Caddeo, C.; Lai, F.; Manca, M. L.; Fadda, A. M. *Journal of Liposome Research* **2009**, *19*, 68.

(203) Muppidi, K.; Wang, J.; Betageri, G.; Pumerantz, A. S. *Antimicrobial Agents and Chemotherapy* **2011**, *55*, 4537.

(204) Forier, K.; Raemdonck, K.; De Smedt, S. C.; Demeester, J.; Coenye, T.; Braeckmans, K. *Journal of Controlled Release* **2014**, *190*, 607.

(205) Pradhan, P.; Giri, J.; Banerjee, R.; Bellare, J.; Bahadur, D. *Journal of Magnetism and Magnetic Materials* **2007**, *311*, 208.

(206) Gan, Z.; Liang, Q.; Zhang, J.; Jing, X. *Polymer Degradation and Stability* **1997**, *56*, 209.

(207) Jaeger, K. E.; Dijkstra, B. W.; Reetz, M. T. *Annual Review of Microbiology* **1999**, *53*, 315.

(208) Whatley, J. D.; Spolnik, K. J.; Vail, M. M.; Adams, B. H.; Huang, R.; Gregory, R. L.; Ehrlich, Y. *Quintessence International* **2014**, *45*, 647.

(209) Palma, E.; Oliveira, B. L.; Correia, J. D.; Gano, L.; Maria, L.; Santos, I. C.; Santos, I. *Journal of Biological Inorganic Chemistry* **2007**, *12*, 667.

(210) Song, J.; Cheng, L.; Liu, A.; Yin, J.; Kuang, M.; Duan, H. *Journal of the American Chemical Society* **2011**, *133*, 10760.

(211) Manconi, M.; Sinico, C.; Valenti, D.; Loy, G.; Fadda, A. M. *International Journal of Pharmaceutics* **2002**, *234*, 237.

(212) Discher, D. E.; Eisenberg, A. *Science* **2002**, *297*, 967.

(213) Torchilin, V. P. *Nature Reviews Drug Discovery* **2005**, *4*, 145.

(214) Wu, X. Z.; Huang, T.; Mullett, W. M.; Yeung, J. M.; Pawliszyn, J. *Journal of Microcolumn Separations* **2001**, *13*, 322.

(215) Kong, M.; Chen, X. G.; Xing, K.; Park, H. J. *International Journal of Food Microbiology* **2010**, *144*, 51.

Appendix

Table A. 1 Statistical analysis of Figure 3.8

Two samples	*p-values*
E.coli (10ug/ml)	
GO versus GO-PVP	0.0497
GO-PVP versus C_2PVP	0.0009
C_2PVP versus GO-C_2PVP	0.0009
GO versus GO-C_2PVP	0.0001
GO-C_2PVP versus GO-C_4PVP	0.0043
GO-C_4PVP versus GO-C_6PVP	0.0005
GO-C_6PVP versus GO-C_8PVP	0.0002
S.aureus (1ug/ml)	
GO versus GO-PVP	0.0002
GO-PVP versus C_2PVP	<0.0001
C_2PVP versus GO-C_2PVP	<0.0001
GO versus GO-C_2PVP	<0.0001
GO-C_2PVP versus GO-C_4PVP	0.0007
GO-C_4PVP versus GO-C_6PVP	0.0004
GO-C_6PVP versus GO-C_8PVP	<0.0001
Paper Form	
E.coli	
GO versus GO-C_2PVP	0.0003
GO-C_2PVP versus GO-C_4PVP	0.0023
GO-C_4PVP versus GO-C_6PVP	<0.0001
GO-C_6PVP versus GO-C_8PVP	0.0376
S.aureus	
GO versus GO-C_2PVP	0.002
GO-C_2PVP versus GO-C_4PVP	0.0264
GO-C_4PVP versus GO-C_6PVP	0.0038
GO-C_6PVP versus GO-C_8PVP	0.0008

Table A. 2 Statistical analysis in Figure 4.13

(-heating)vs (+ heating) (Figure 4.13)	Concentration	p values
A	8	<0.0001
	15	<0.0001
	30	0.0023
	60	0.0089
	120	0.0208
B	8	0.0018
	15	0.0004
	30	0.0008
	60	0.0006
	120	0.16667
C	8	0.5689
	15	0.9438
	30	0.6572
	60	0.2184
	120	0.4266
D	8	0.1726
	15	0.0643
	30	0.9766
	60	0.1132
	120	0.5269

Table A. 3 Statistical analysis in Figure 4.16

	p values	
	PBS versus material	material versus bacteria-bound-material
380A	0.0415	0.0003
	0.0377	<0.0001
	0.0078	0.0003
	0.0078	<0.0001
	0.0116	<0.0001
410A	0.0426	<0.0001
	0.0444	0.0006
	0.0045	<0.0001
	0.0045	<0.0001
	0.0204	0.0004

Table A. 4 Statistical analysis of Figure 5.16

two sample t test of +lipase and -lipase for E.faecalis test	
antibiotic concentration in the vesicle (μg/ml)	p values
0.63	0.0042
1.25	<0.0001
2.5	<0.0001
5	<0.0001

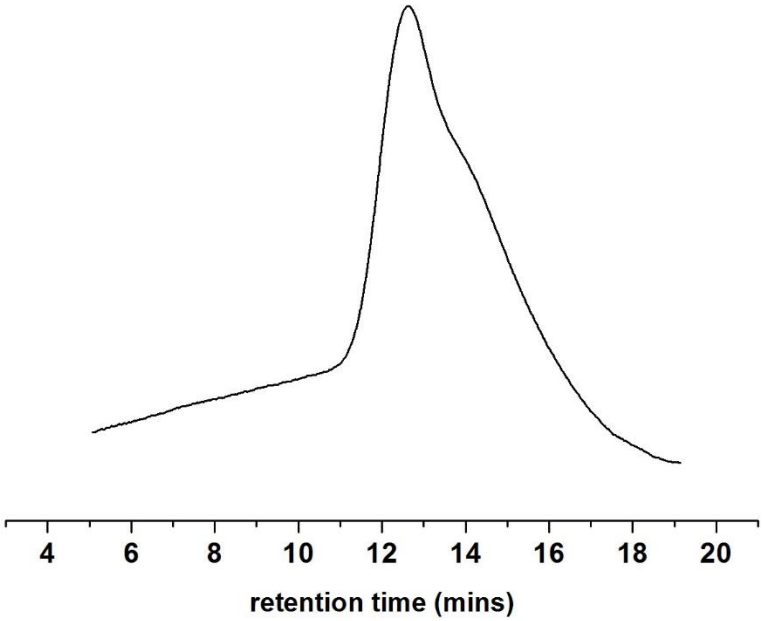

Figure A. 1 Molecular weight analysis of free polymer during polymerization process

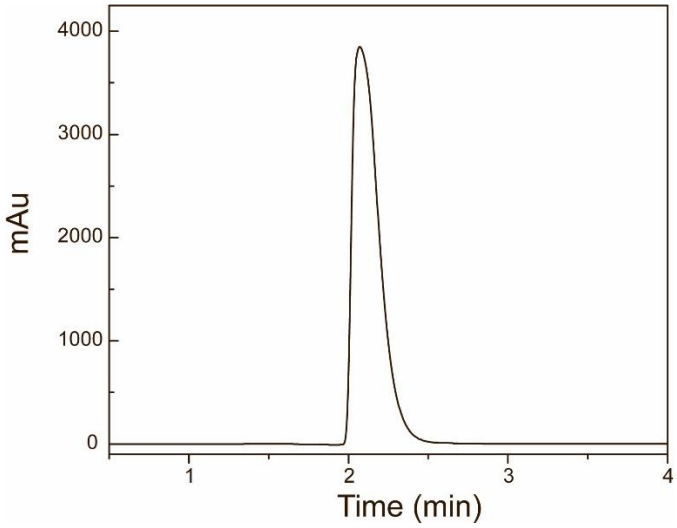

Figure A. 2 Characteristic HPLC curve for norfloxacin.